FHWA/IN/JTRP-2007/27

Final Report

RELATING MATERIAL PROPERTIES TO EXPOSURE CONDITIONS FOR PREDICTING SERVICE LIFE OF CONCRETE BRIDGE DECKS IN INDIANA

Vinit Barde
Aleksandra Radlinska
Menashi Cohen
W. Jason Weiss

January 2009

INDOT Research

TECHNICAL *Summary*

Technology Transfer and Project Implementation Information

TRB Subject Code: 32-4 Concrete Durability *January 2009*
Publication No.: FHWA/IN/JTRP-2007/27, SPR-2941 *Final Report*

Relating Material Properties to Exposure Conditions for Predicting Service Life of Concrete Bridge Decks in Indiana

Introduction

Bridges in the US are deteriorating at an alarming rate. It has been estimated that transportation agencies across the US invest more than 5 billion dollars on concrete bridge repair and renovation annually [Tikalsky, 2000]. To meet the needs of transportation industry, high performance concrete (HPC) has been developed for the construction of bridges. However, to date, the link between material properties and field performance is not completely established. Goodspeed et al. [1996] defined the performance of concrete using four material parameters that describe durability and four material parameters that describe mechanical properties. It should be noted however, that material properties alone can not entirely define field performance. Rather, some consideration is needed to quantify the conditions to which the concrete will be exposed. The exposure conditions vary based on the geographical location. This work attempts to relate material properties with the exposure conditions typical of those in the state of Indiana to estimate the performance of concrete bridge decks.

The exposure conditions in the state of Indiana have been assessed, specifically, temperature, rainfall, wetting events, freeze thaw cycles, and relative humidity. To assess the variation in these parameters across the state, contour maps were developed using information from cities in the state of Indiana and surrounding states. The eight parameters suggested by Goodspeed et al. [1996] have been reviewed. Three key distress behaviors (chloride ingress, freezing and thawing, and shrinkage cracking) have been investigated in depth. Relationships have been developed to relate measured material properties (from the results of AASHTO/ASTM tests) with the predicted performance of the concrete structure.

Findings

Three prediction models of service life were developed using a combination of material properties and exposure conditions.

First, a service life prediction model for the chloride induced corrosion deterioration has been described in this work. The diffusion coefficient was estimated using the Rapid Chloride Permeability test (RCPT). A model was developed that accounts for two geometries of bridge decks: a bridge deck with plain concrete, and a bridge deck where latex modified concrete is used as an overlay on plain concrete. In case of plain concrete bridge deck, four cases with different combinations of cement, silica fume and fly ash has been considered in this model. The results of this model were observed to be in reasonable agreement with the results observed in the literature.

Second, service life prediction model for concrete exposed to freezing and thawing has been described in this work. The service life was predicted in two parts. First, the time to damage initiation or time to reach critical saturation was predicted ($Life_{init}$). Second, the time to proceed to a defined level of damage from damage initiation ($Life_{sec}$) was assessed. It was observed that two exposure parameters

influence the service life in freezing and thawing: the cumulative duration of wetting events and the number of annual freeze thaw cycles. It was observed that the modeling approach could predict the relative dynamic modulus with some agreement to the measured values.

Third, a service life prediction model relating shrinkage in concrete with probability of cracking has been described in this work. Shrinkage-based model was used to assess concrete bridge decks' susceptibility to cracking. A diagram relating the magnitude of shrinkage to the probability of cracking was developed for a sample concrete mixture.

Additionally, the temperatures, annual number of freeze thaw cycles, rainfall, relative humidity, and wetting events have been classified for the state of Indiana. A variation was observed in time to corrosion and based on the observed variation it was possible to divide the state of Indiana into two exposure zones. The first zone may include northern four districts (Laporte, Fort Wayne, Crawfordsville and Greenfield district), and the second zone may include remaining two districts (Vincennes and Seymour district).

Implementation

Goodspeed et al. [1996] used four material parameters that describe durability and four material parameters that describe mechanical properties to specify the performance of High Performance Concrete (HPC). These material parameters were reviewed in this work as they apply to bridge decks in Indiana. Applying Indiana's experience for concrete bridge decks, three key distresses (chloride ingress, freezing and thawing, and shrinkage cracking) have been further investigated. It should be noted that the material properties alone can not entirely define the performance in the field conditions. Rather some consideration is required to quantify the conditions to which the concrete will be exposed. Therefore, the exposure conditions typical of those in the state of Indiana have been assessed. Maps were developed to describe the exposure conditions that will enable INDOT to evaluate the possibility of dividing the state of Indiana into different exposure zones for determining the material that should be specified in these zones.

The information in this report can be used in developing new specifications for concrete at various locations in Indiana. In addition, these results can be used by failed materials committee to evaluate the impact of materials that are outside specific acceptance ranges on the performance of these facilities.

Contacts

For more information:

Prof. W. Jason Weiss
Co-Principal Investigator
School of Civil Engineering
Purdue University
West Lafayette, IN 47907-2051
Phone: (765) 494-2215
Fax: (765) 496-1364
E-mail: wjweiss@ecn.purdue.edu

Prof. Menashi Cohen
Principal Investigator
School of Civil Engineering
Purdue University
West Lafayette, IN 47907-2051
Phone: (765) 494-5015
Fax: (765) 496-1364
E-mail: mcohen@ecn.purdue.edu

Indiana Department of Transportation
Office of Research & Development
1205 Montgomery Street
West Lafayette, IN 47906
Phone: (765) 463-1521
Fax: (765) 497-1665
E-mail: tnantung@indot.in.gov

Purdue University
Joint Transportation Research Program
School of Civil Engineering
West Lafayette, IN 47907-1284
Phone: (765) 494-9310
Fax: (765) 496-7996
E:mail: jtrp@ecn.purdue.edu

Final Report

FHWA/IN/JTRP-2007/27

RELATING MATERIAL PROPERTIES TO EXPOSURE CONDITIONS FOR PREDICTING SERVICE LIFE OF CONCRETE BRIDGE DECKS IN INDIANA

By

Vinit Barde
Graduate Research Assistant

Aleksandra Radlinska
Graduate Research Assistant

Menashi Cohen
Principal Investigator
Emeritus Professor

W. Jason Weiss
Professor of Civil Engineering

School of Civil Engineering
Purdue University

Joint Transportation Research Program
Project No. C-36-56ZZZ
File No. 7-4-77
SPR-2941

Conducted in Cooperation with the Indiana Department
of Transportation and the Federal Highway Administration
U.S. Department of Transportation

Purdue University
West Lafayette, Indiana
January 2009

TECHNICAL REPORT STANDARD TITLE PAGE

1. Report No.	2. Government Accession No.	3. Recipient's Catalog No.
FHWA/IN/JTRP-2007/27		

4. Title and Subtitle	5. Report Date
Relating Material Properties to Exposure Conditions for Predicting Service Life in Concrete Bridge Decks in Indiana	January 2009
	6. Performing Organization Code

7. Author(s)	8. Performing Organization Report No.
Vinit Barde, Aleksandra Radlinska, Menashi Cohen, and Jason Weiss	FHWA/IN/JTRP-2007/27

9. Performing Organization Name and Address	10. Work Unit No.
Joint Transportation Research Program 550 Stadium Mall Drive Purdue University West Lafayette, IN 47907-2051	
	11. Contract or Grant No. SPR-2941

12. Sponsoring Agency Name and Address	13. Type of Report and Period Covered
Indiana Department of Transportation State Office Building 100 North Senate Avenue Indianapolis, IN 46204	Final Report
	14. Sponsoring Agency Code

15. Supplementary Notes

Prepared in cooperation with the Indiana Department of Transportation and Federal Highway Administration.

16. Abstract

Bridges in the US are deteriorating at an alarming rate. It has been estimated that transportation agencies across the US invest more than 5 billion dollars on concrete bridge repair and renovation annually. To meet the needs of transportation industry, high performance concrete (HPC) has been developed for the construction of bridges. However, to date, the link between material properties and field performance is not completely established. Goodspeed et al. [1996] defined the performance of concrete using four material parameters that describe durability and four material parameters that describe mechanical properties. It should be noted however that material properties alone can not entirely define field performance. Rather some consideration is needed to quantify the conditions to which the concrete will be exposed. The exposure conditions vary based on the geographical location. This work relates material properties with the exposure conditions typical of those in the state of Indiana to estimate the performance of concrete bridge decks.

The exposure conditions in the state of Indiana have been assessed. Specifically, temperature, rainfall, wetting events, freeze thaw cycles, and relative humidity have been classified. To assess the variation in these parameters across the state, contour maps were developed using information from cities in the state of Indiana as well as cities in surrounding states. The eight parameters suggested by Goodspeed et al. [1996] have been reviewed. Three key distresses behavior (chloride ingress, freezing and thawing, and shrinkage cracking) have been investigated in depth. Relationships have been developed to relate measured material properties (from the results of AASHTO/ASTM tests) with the predicted performance of the concrete structure under different exposure condition.

First, a model is presented that relates the results of Rapid Chloride Permeability Test (RCPT) with the anticipated service life of bridge deck against corrosion due to chloride ingress. Second, a model is presented that relates results of sorptivity, porosity, and critical saturation with the anticipated service life of concrete exposed to freezing and thawing. Third, a model is presented that relates the shrinkage of concrete with the potential for premature cracking. The results of each of the models have been presented for conditions that are typical of the state of Indiana.

17. Key Words	18. Distribution Statement
bridge deck, concrete, cracking, early-age, performance specification	No restrictions. This document is available to the public through the National Technical Information Service, Springfield, VA 22161

19. Security Classif. (of this report)	20. Security Classif. (of this page)	21. No. of Pages	22. Price
Unclassified	Unclassified	214	

Form DOT F 1700.7 (8-69)

TABLE OF CONTENTS

LIST OF TABLES

LIST OF FIGURES

ABSTRACT

Bridges in the US are deteriorating at an alarming rate. It has been estimated that transportation agencies across the US invest more than 5 billion dollars on concrete bridge repair and renovation annually [Tikalsky, 2000]. To meet the needs of transportation industry, high performance concrete (HPC) has been developed for the construction of bridges. However, the link between material properties and field performance is not completely established. Goodspeed et al. [1996] defined the performance of concrete using four material parameters that describe durability and four material parameters that describe mechanical properties. It should be noted however that material properties alone can not entirely define field performance. Rather, some consideration is needed to quantify the conditions to which the concrete will be exposed. The exposure conditions vary based on the geographical location and to some extent on the geometry of the facility. This work attempts to relate material properties with the exposure conditions typical of those in the state of Indiana to estimate the performance of concrete bridge decks.

The exposure conditions in the state of Indiana have been assessed. Specifically, temperature, rainfall, wetting events, freeze thaw cycles, and relative humidity have been classified. To assess the variation in these parameters across the state, contour maps were developed using information from cities in the state of Indiana and surrounding states. The eight parameters suggested by Goodspeed et al. [1996] have been reviewed. Three key distress behaviors (chloride ingress, freezing and thawing, and shrinkage cracking) have been investigated in depth. Relationships have been developed to relate measured

material properties (from the results of AASHTO/ASTM tests) with the predicted performance of the concrete structure.

First, a model is presented that relates the results of Rapid Chloride Permeability Test (RCPT) with the anticipated service life of bridge deck against corrosion due to chloride ingress. Second, a model is presented that relates results of sorptivity, porosity, and critical saturation with the anticipated service life of concrete exposed to freezing and thawing. Third, a model is presented that relates the shrinkage of concrete with the potential for premature cracking. The results of each of the models have been presented for conditions that are typical of the state of Indiana.

CHAPTER 1. INTRODUCTION

1.1. Background

In 2000, the Federal Highway Administration (FHWA) estimated that approximately 90 billion dollars would be needed for the rehabilitation of existing bridges in the US [Kirkpatrick et al., 2002b]. While it is widely understood that chloride ingress, freezing and thawing, and volumetric instability can have a detrimental effect on the performance of concrete, engineers have had difficulties in translating this knowledge into specifications [Tikalsky, 2000]. Public agencies have begun to shift from prescription specifications to specifications which were based on anticipated long-term performance [Graveen, 2000]. To make this change transportation agencies would benefit greatly from models that can simulate the performance of a structure in the field.

This work aims to establish relationships between service life performance and properties conventionally measured by the Indiana Department of Transportation. This work begin with a review of a paper by Goodspeed et al. [1996], in which they proposed to evaluate concrete based on a series of material parameters (properties) which they denoted as performance characteristics. Furthermore, Goodspeed et al. [1996] suggested ASTM or AASHTO tests to evaluate each of the performance characteristics (material properties). Based on these performance characteristics Goodspeed et al. [1996] proposed performance grades for concrete. However, in order to use these performance grades in Indiana these performance grades need to be reviewed based on the conditions that the concrete is exposed to in Indiana.

It is known that the performance of building material is influenced by the exposure conditions. However, currently INDOT uses the same concrete mixture design for all locations throughout the state of Indiana. Although the current method is simple, it limits the options for the contractor to develop innovative and cost effective materials. As a result, this project was developed to determine where modification to the INDOT approach may be in order. However, before modifying the mixture selection process, the variation in exposure conditions across state of Indiana should be evaluated. Using the variation in exposure conditions and assessing its impact on service life prediction models, this work aims to provide recommendations that will enable INDOT to evaluate the possibility of different exposure conditions in the state of Indiana to assist material selection process.

1.2. Objectives

- The first objective of this work was to review deterioration mechanisms with respect to performance characteristics as described by Goodspeed et al. [1996].
- The second objective of this work was to prepare climatic maps to assist the INDOT in evaluating the possibility of dividing the state of Indiana into different exposure zones.
- The third objective of this work was to use service life models which relate climate and material properties to the performance of bridge decks in Indiana.
- The forth objective of this work was to relate material properties and exposure conditions to performance.

1.3. Organization of the Report

This report consists of eight chapters. The first chapter describes the objectives of this work. Chapter two consists of a literature review that is related to damage mechanisms. A brief review of ASTM/AASHTO tests prescribed by Goodspeed et al. [1996] is presented for each performance characteristics. Chapter three evaluates each performance characteristic separately and describes the relevance of each characteristic. The performance characteristics which require more detailed evaluation for the state of Indiana are identified in this chapter. The weather conditions for the state of Indiana have been reviewed in chapter four. Chapter five describes the development of a corrosion model that relates the measured RCPT response with the service life of reinforced concrete bridge decks with respect to corrosion caused by chloride ingress in concrete. Chapter six presents the development and results of service life prediction model accounting the freeze thaw damage. Chapter seven describes how information about magnitude of shrinkage experienced by concrete can be related to the probability of cracking in restrained concrete elements. The eight chapter presents the summary and conclusions of this study.

CHAPTER 2. LITERATURE REVIEW

2.1. Introduction

Almost two decades ago the FHWA proposed to define HPC using long-term performance criteria. At that time Goodspeed et al. [1996] provided guidelines to define HPC using material properties and performance grades. This chapter focuses on reviewing literature related to these material properties and performance grades.

In the first section of this chapter a brief review of the ASTM/AASHTO tests recommended by Goodspeed et al. [1996], is presented. The test procedures are explained for each test. Recommendations by Goodspeed et al. [1996] for each characteristics as measured by ASTM/AASHTO test has been also presented in this section.

In the second section a review of literature related to corrosion deterioration is presented. Literature related to transport of chlorides, chloride induced corrosion, and service life modeling for corrosion deterioration is presented.

In third section a literature review has been presented for freeze thaw deterioration. Initially, a short assessment of damage and resistance mechanisms related to freeze thaw has been presented. Considering that saturation of concrete is a most important parameter, a review of literature related to saturation of concrete and sorptivity of concrete is presented. The ASTM test [ASTM C 1585, 2004] is discussed as a measure of the rate of

absorption. A computer model is described which was used to calculate the surface temperature and wetting events for bridge decks.

2.2. Review of ASTM/AASHTO Tests Related to Performance Characteristics

2.2.1. Grades of Performance Characteristics for High Performance Structural Concrete

Goodspeed et al. [1996] defined performance for High Performance structural concrete using four material parameters that describe durability and four material parameters that describe mechanical properties. He also described performance of concrete with four performance grades. Each grade was defined for an anticipated range of performance in the field. An ASTM/AASHTO test has been suggested by Goodspeed et al. [1996] to measure the material parameter, and based on the results of the test, limiting values for each material parameter have been defined to describe each performance grade. Grade 4, which is the superior grade, defines the highest level of performance and grade 1 defines the lowest level of performance for the high performance concrete. Table 2-1 shows the performance parameters, test methods suggested for each parameter and performance grades for each parameter.

Table 2-1 Grades of performance characteristics for high performance structural concrete [Goodspeed *et al.*, 1996].

Performance Characteristics	Standard test method	FHWA HPC Performance Grade			
		1	2	3	4
Freeze/Thaw Durability (x= relative dynamic modulus of elasticity after 300 cycles)	AASHTO T 161 ASTM C 666 Proc. A	60%≤ x ≤ 80%	80%≤ x	___	___
Scaling Resistance (x= visual rating of the surface after 50 cycles)	ASTM C 672	X = 4,5	X = 2,3	X = 0,1	___
Abrasion Resistance (x= avg. depth of wear in mm)	ASTM C 944	2.0 > x ≥1.0	1.0 > x ≥ 0.5	0.5 > x	___
Chloride Permeability (x = Coulombs)	AASHTO T 277 ASTM C 1202	3000 ≥ x > 2000	2000 ≥ x > 800	800 ≥ x	___
Strength (x = compressive strength)	AASHTO T 22 ASTM C39	41 ≤ x < 55 MPa (6 ≤ x < 8 ksi)	55 ≤ x < 69 MPa (8 ≤ x < 10 ksi)	69 ≤ x < 97 MPa (10 ≤ x < 14 ksi)	x ≥ 97 MPa (x ≥ 14 ksi)
Elasticity (x = modulus of elasticity)	ASTM C 469	24 ≤ x < 40 GPa (4 ≤ x < $6x10^6$ psi)	40 ≤ x < 50 GPa (6 ≤ x < $7.5x10^6$ psi)	x ≥ 50 MPa (x ≥ $7.5x10^6$ psi)	___
Shrinkage (x = microstrain)	ASTM C 157	800 > x ≥ 600	600 > x ≥ 400	400 > x	___
Creep (x= microstrain/pressure unit)	ASTM C 512	___	___	___	___

2.2.2. Resistance of Concrete to Rapid Freezing and Thawing (AASHTO T 161-00/ASTM C 666-97)

This test is a standard laboratory test used to determine the resistance of concrete specimens to rapidly repeated cycles of freezing and thawing. It can be performed using two procedures, namely Procedure A and B. However, Goodspeed suggested to follow procedure A for determining the freeze thaw durability [Goodspeed *et al.*, 1996].

In Procedure A, a prism or cylindrical concrete specimen, that is made and cured in accordance with T 126 and M 210, is monitored for degradation under freeze thaw cycles. Freeze thaw cycles occur with the specimen in water while the temperature is varied between 4.4 to -17.8°C (40 to 0°F) within a period of 2-4 hours. The degradation can be measured by monitoring different parameters such as relative dynamic modulus, average length change, or change in mass. The freeze thaw cycles should be repeated until its relative dynamic modulus reaches a value 60 % of its initial dynamic modulus, or 300 cycles, whichever reached earlier. Using the values obtained from the measurements of relative dynamic modulus and number of cycles, durability factor can be calculated for specimens.

2.2.3. Standard Test Method for Scaling Resistance of Concrete Surfaces Exposed to Deicing Chemicals (ASTM C 672/C 672M-03)

This test is used to determine the scaling resistance of a horizontal concrete surface exposed to freezing and thawing cycles in presence of deicing chemicals. However, the relation between scaling resistance of concrete in the field and resistance of laboratory prepared specimen is not described in this test [ASTM C 672/C 672M, 2003] and has been questioned by many.

In this test method at least two concrete specimens each having minimum surface area of 0.045 m^2 (0.72 in^2) and 75 mm (3 in) depth are covered with approximately 6 mm layer of Calcium Chloride solution having a concentration such that each 100 ml of solution contains 4 g of anhydrous calcium chloride. The specimens are placed in the freezing environment for 16-18 hours, and followed by a 6-8 hours exposure to air at 23 $\pm$ 2°C [73.5 $\pm$ 3.5°F] with a 45-55% RH. The proper depth of solution is maintained by adding necessary water between each cycle. Such a cycle is repeated daily and at the end of 5 cycles the surface is flushed off for a visual examination. Generally, the scaled particles are collected and weighed each time the surface is flushed for visual examination although not required by standard test procedure. A visual rating, in accordance with the code, is provided for the surface after 5, 10, 15, 25, and every 25 cycles thereafter.

2.2.4. Standard Test for Abrasion Resistance of Concrete or Mortar Surfaces by the Rotating Cutter Method. (ASTM C944 – 99)

This test method determines the relative wear resistance of mortar and concrete. In this test a cored or fabricated concrete specimen is exposed to a rotating cutter using an abrasive device. The specimen should be placed in such a way that the shaft of abrasion device remains perpendicular to abrasion surface. The abrasion between the cutter and the abrasion surface of specimen should be continued for minimum of two minutes each on three separate representative areas of the specimen. The load for cutter can be varied as normal (98 N) or double (197 N) load. At the end of abrasion period loss in mass is recorded to the nearest 0.1 g.

2.2.5. Electrical Indication of Concrete's Ability to Resist Chloride Ion Penetration. (ASTM C 1202 – 94/AASHTO T 277-96)

This test provides a rapid indication of resistance to chloride ion penetrability of concrete specimen by measuring the electrical conductivity. This test method consists of monitoring the amount of electrical current passing through the concrete specimen using a 50 mm (2 in.) thick slice of 100 mm (4 in.) diameter cylinder. The current is passed through the specimen for six hours while a potential difference of 60 V DC is maintained across the ends. Both the ends are kept immersed in different solutions, namely sodium chloride and sodium hydroxide. The total charge passed, in coulombs, is then related with the resistance of the specimen to chloride ion penetration.

2.2.6. Standard Test Method for Compressive Strength of Cylindrical Concrete Specimen. (ASTM C 39/C39 M – 04)

This test is used to determine the compressive test of concrete specimen. In this test method a moist cured concrete specimen is loaded with a rate corresponding to a stress rate on the specimen of 35 $\pm$ 7 psi/s [30.25 $\pm$ 0.05 MPa/s]. The compressive load is applied until the indicator shows steadily decreasing load. Maximum load and fracture pattern are recorded for further corrections. Compressive strength is calculated by dividing the maximum load with cross sectional area of specimen.

2.2.7. Standard Test Method for Static Modulus of Elasticity and Poisson's Ratio of Concrete in Compression. (ASTM C469 – 02)

This test method is used to determine the chord modulus of elasticity (Young's) and Poisson's ratio of concrete specimen at desired age and designated curing condition. It should be noted that values obtained for modulus of elasticity in this test will usually be less than values derived from rapid load application (dynamic

or seismic rates). However, they will be higher than values under slow load application.

In this test method strain measurements are performed using a compressometer. Longitudinal strain measurements are taken especially at two points, first when longitudinal strain is 50 millionths and second, when applied load is 40% of the ultimate load. To locate the second point a companion specimen is tested for ultimate strength (ASTM 39) before testing for modulus of elasticity. If the Poisson's ratio is to be determined, transverse strain at the same points is recorded. Modulus of elasticity and Poison's ratio can be calculated using the above two measurements.

2.2.8. Standard Test Method for Length Change of Hardened Hydraulic-Cement Mortar and Concrete. (ASTM C 157/C 157M – 04)

This test method is used to determine the length changes that results due to causes other than applied forces and temperature changes. Concrete and mortar specimen are made in the laboratory with controlled conditions of temperature and relative humidity.

A concrete prism with a 4 in. [100 mm] square cross-section and 11 ¼ in. [285 mm] length should be used in the test when all aggregates pass 2 in. [50 mm] sieve. Whereas, a prism of 3 in [75 mm] square cross-section should be used when all of the aggregates pass 1 in [25 mm] sieve. In the case of mortar, a prism with a cross section of 1 in. [25 mm] square and 11 ¼ in. [285 mm] length should be used. This test method measures the length change as a difference between the comparator dial readings for a reference bar and the test specimen placed in comparator. The difference in comparator readings is expressed as a percentage of gauge length for the comparator.

2.2.9. Standard Test Method for Creep of Concrete in Compression (ASTM C 512)

This method is used for determining the creep of molded concrete cylinders subjected to sustained longitudinal compressive load. When the test is used to compare the creep potential of different concretes, the specimen are initially loaded at an age of 28 days. However, when the complete creep behavior of a concrete is required, the specimen can be loaded at variety of ages: 2, 7, 28, and 90 days, and 1 year, and the load and strain measurements are taken immediately before and right after loading, 2 to 6 hours later, then daily for 1 week, weekly until the end of first month, and monthly until the end of first year. Using these measurements the creep rate can be calculated as the slope of creep curve (total strain/pound force/in^2 verses time) on a semi log plot where time is plotted on logarithmic axis.

2.3. Review of Literature Related to Corrosion Model

2.3.1. Mechanism for Chloride Induced Corrosion and Associated Damage in Bridge Decks

More than half of the total bridge inventory of United States is reinforced concrete, which is degrading at an alarming rate. According to Cady and Weyers [Cady and Weyers, 1991] a major element of the this degradation involves chloride-induced corrosion of reinforcing steel in concrete bridge components. It is understood that reinforcement corrosion degrades a structure in several ways. First, as the reinforcement corrodes the cross sectional area of reinforcement contributing to load carrying capacity reduces and in severe cases may result in catastrophic failure. Secondly, the products of corrosion are expansive and can occupy 2 to 7 times more volume than the original steel. This volume increase can result in cracking and spalling of concrete. Finally, the stains resulting from corrosion may adversely affect the aesthetics of the structure. Altogether,

corrosion of reinforcement reduces the service life of structure. Therefore, in order to develop service life prediction models it is necessary to understand the mechanism of this deterioration.

It is well known that fresh concrete provides a highly alkaline environment for reinforcement steel and as long as the pH inside the concrete remains above 11.5, a passive layer is formed on the surface of steel. When the passive layer is intact, negligible corrosion occurs. However, this passive layer can be disrupted by two causes: carbonation or chloride intrusion. For a dense, high quality concrete due to the slow carbonation rate, loss of passivity owing to carbonation is generally not a concern within normal service life of bridge decks [Hartt, 2004]. However, Mindess et al. [2002] cited that chlorides deposited with deicing salt ingress concrete and cause the disruption of passive layer. This ability of disruption is more a function of ratio of chlorides-to-hydroxides ($[Cl^-]/[OH^-]$) than just the chlorides itself. Therefore, when $[Cl^-]/[OH^-]$ ratio is above certain level, chlorides initiate the corrosion by disrupting passive layer. The chloride concentration at which corrosion initiates is called as threshold concentration [Mindess *et al.*, 2002]. Considering this process, Tuutti's model explains corrosion-induced deterioration of reinforced concrete with three component steps: (1) time for corrosion initiation, T_i; (2) time, subsequent to corrosion initiation, for appearance of a crack on the external concrete surface (crack propagation), T_p; and (3) time for surface cracks to progress into further damage and develop into spalls, T_d, to the point where the functional service life, T_f, is reached [Hartt, 2004; Tuutti, 1982]. Fig. 2-1 shows the time periods and degradation due to chloride induced corrosion in concrete.

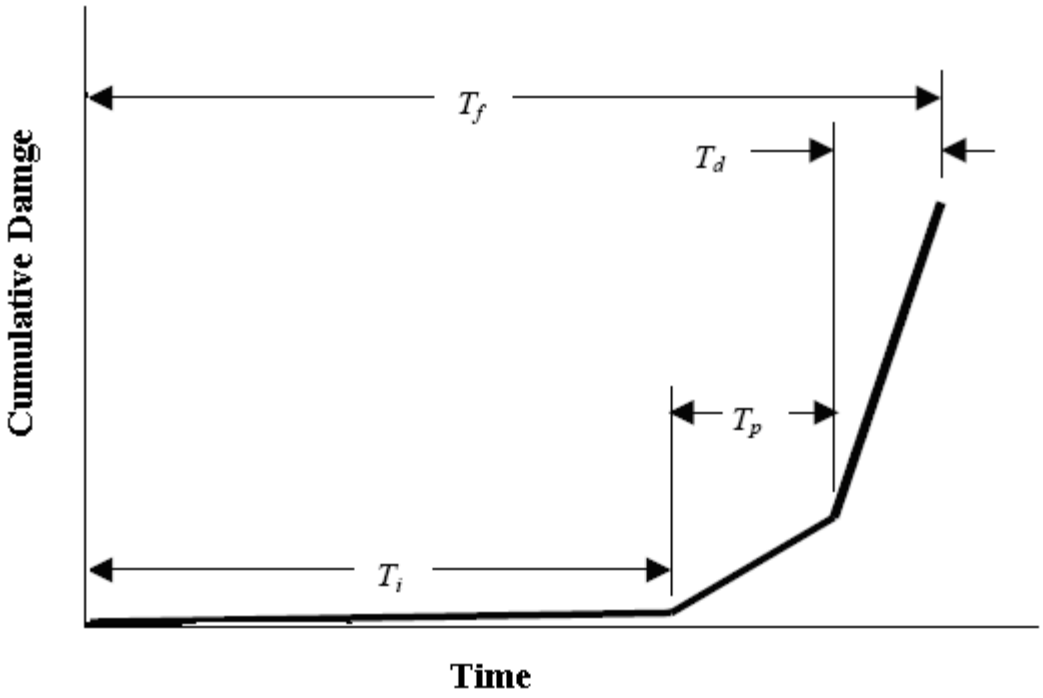

Fig. 2-1 Schematic illustration of various steps in deterioration of reinforced concrete due to chloride induced corrosion [Hartt, 2004; Tuutti, 1982].

2.3.2. Transport of Chlorides in Concrete

Capillary absorption, permeation, and diffusion are the means by which chloride ions can penetrate concrete [Stanish *et al.*, 1997]. Diffusion has been also used in various service life prediction models that model corrosion degradation [Stanish and Thomas, 2003].

Diffusion is the process by which matter is transported from one part of a system to another as a result of random molecular motions [Crank, 1956]. These molecular motions tend to transport matter from regions of higher concentration to those of lower concentration.

The transport of chlorides in concrete under the presence of concentration gradient can be described using Fick's second law [Crank, 1956],

$$\frac{\partial C}{\partial t} = D\frac{\partial^2 C}{\partial^2 x} \qquad \text{Eq. 2-1}$$

where D is the diffusion coefficient, t is the time, x is the depth from surface and C is the surface concentration of ions. Using the appropriate boundary conditions and assuming that the diffusion is occurring in a homogeneous, semi-infinite material, the solution of Fick's second law can be formulated as [Crank, 1956],

$$C(x,t) = C_S\left(1 - erf\left[\frac{x}{2\sqrt{D\cdot t}}\right]\right) \qquad \text{Eq. 2-2}$$

where, C_s is the surface concentration of ions uniformly distributed at the surface with a constant concentration and *erf* is the error function. Using equation 2-2, the concentration of ions (C) at any given time (t) and depth from surface (x) can be obtained. It should be noted here that D (m^2/s) is the material property of concrete.

2.3.3. Measurement of Diffusion Coefficient – Application of Nernst-Einstein Equation

As discussed in section 2.3.2 diffusion is the property used to model the transport of chloride ions in concrete. This property can be determined by using the diffusion cells or immersion in a salt solution. However, these methods require considerable time, often requiring months or years to obtain results [Feldman *et al.*, 1994]. Therefore, these methods are not suitable for rapid testing. Research has shown that diffusion coefficient can be related to electrical conductivity (i.e.,

the flow of current under an electrical potential is proportional to the reciprocal of resistivity) by the Nernst-Einstein equation [Mindess *et al.*, 2002]. It should be noted here that the rapid chloride permeability test (AASHTO T277/ASTM C1202) has been used as a quick and simple method which primarily measures conductivity [Hansen *et al.*, 1993; Liu and Beaudoin, 1999]. Therefore, RCPT measurements can be related to the diffusion coefficient by applying the Nernst-Einstein equation. In this study the Nernst-Einstein equation has been used to obtain the diffusion coefficient from the measurements of conductivity by RCPT.

2.3.4. Diffusion Coefficient for Latex Modified Concrete (LMC)

It has been observed in the past that of all the solutions proposed for rehabilitation, rigid overlays have certain advantages, including familiarity of technology, restoration of riding quality, and relatively low cost. Among the rigid overlays, LMC is one of the most popular form for bridge decks and studies in Indiana indicate a good performance of LMC [Whiting and Dziedzic, 1989].

The LMC used in the field is a modified portland cement concrete in which an admixture of styrene butadiene latex particles suspended in water is used to replace a portion of mixing water. Nonetheless, it is well understood that compared to concrete without latex, LMC is more resistant to the intrusion of chloride ions, have better tensile, compressive, and flexural strength [Kuhlmann, 1984; Lewis, 1990; Sprinkel, 1999; Weiss et al., 1998; Whiting and Dziedzic, 1989].

Chandra and Flodin [1987] proposed two theories for the action of polymers in concrete. The first theory maintains that there is no chemical interaction between the polymer and the concrete constituents. The improvement in properties is due to the formation of a three dimensional network by polymers. The other theory is that with reactive polymers, in addition to aforementioned benefit, chemical reaction between the polymer particles and the hydration products of the cement

takes place. However, the mechanism of the later theory is not fully understood and explained [Larbi and Bijen, 1990]. The first theory has been supported by many researchers [Ben-Dor *et al.*, 1985; Lewis, 1990; Ohama, 1995].

From the above discussion it can be concluded that LMC has improved material properties, particularly resistance to chloride ingress or lower diffusion coefficient [Whiting and Dziedzic, 1989]. However, as it is assumed that the diffusion coefficient for LMC would be similar to that of concrete without latex with respect to hydration reaction.

2.4. Review of Literature Related to Freeze Thaw Model

2.4.1. Mechanism of Freeze Thaw Induced Damage in Concrete

The damage of concrete in freezing and thawing is a combination of different processes, which makes it very difficult to explain. However, several theories have been developed to explain the behavior of concrete in freeze thaw environment.

Hydraulic Pressure Theory

One of the process that contribute to the damage in freezing and thawing is hydraulic pressure [Mindess et al., 2002]. It is understood that a 9 % increase in volume occurs as water becomes ice and the accompanying volume increase causes extra water to expel from the freezing site into the matrix. The resistance to water movement away from freezing site creates a hydraulic pressure that can be released only if water can escape through capillary to a free space by diffusing through unfrozen pores [ACI committee 201, 1992; Mindess et al., 2002]. The magnitude of this pressure depends on rate of freezing, degree of saturation, pore structure, and the length of flow path to the nearest void for the water escape [ACI committee 201, 1992]. When the water has to travel too far to

escape, the capillaries tend to dilate and the surrounding material will come under stress, eventually causing a tensile failure [Mindess et al., 2002].

Osmotic Pressure Theory

Later, Powers demonstrated that hydraulic pressure could not be the only source of damage [Powers, 1975]. It was observed by Powers [1975] that most of the effects of freezing in cement pastes were due to the movement of unfrozen water to the freezing sites. The initial production of ice in cavities produce a relatively concentrated alkali solution. This creates an osmotic potential that drives water from the nearby unfrozen pores to begin diffusing into the solution of the frozen cavities like osmosis, and generates pressure (osmotic pressure). When the cavity becomes full of ice and solution, any further ice-accretion produces dilative pressure, which can cause the paste to fail [ACI committee 201, 1992; Powers, 1975].

Microscopic Ice Length Growth

The water in concrete does not freeze uniformly, as water in the large pores freeze first, whereas, due to high surface forces, the water in small pores freezes at lower temperatures than that in large pores [ACI committee 201, 1992]. Because of this behavior, at the same time, some large pores contain ice bodies while unfrozen water remains in smaller pores. This co-existence of water and ice makes the damage mechanism possible that is similar to the mechanism that causes frost heave in the ground When water in large pores freezes, the unfrozen water migrates to freezing sites. This results in the growth of the ice bodies in large pores and thereby expose the pore walls to pressure [Fagerlund, 2001]. When pressure high enough builds up, concrete experiences failure.

2.4.2. Resistance to Freeze Thaw Damage – Air Entrainment

One of the major disadvantage of concrete is its susceptibility to damage during freezing and thawing cycles when it is in saturated or near saturated condition

[Mindess *et al.*, 2002]. Fortunately, concrete can be improved against the frost attack by air entrainment and this protection is widely used in practice. The main function of air bubbles is to prevent the development of osmotic pressure. It provides extra empty space where water can diffuse in instead of going to capillary and thus avoiding the development of osmotic pressure [Powers, 1975]. INDOT requires 6.5 $\pm$ 1.5 % air in concrete for structural purposes [INDOT, 2006]. However, it should be noted here that even the entrained air can provide protection against the frost only up to certain saturation level and after that freeze thaw damage starts with the freezing cycles. Therefore, in order to study the freeze thaw damage, it is required to understand the concept of critical saturation and actual saturation of concrete with time.

2.4.3. Critical Saturation of Concrete (Scr)

The damage mechanisms as explained in section 2.4.1 predicts the existence of maximum distance (D) between freezing site and the nearest air-filled space. In a more general way, this can be defined as critical flow distance (Dcr) which is a measure of the biggest distance that water can flow from freezing site to the surrounding nearest air filled space, without causing damage. At values lower than and up to the critical water content (Wcr), no damage in concrete is observed. However, even a very small increase after critical water content results in damage of concrete. The Fig. 2-2 illustrates the relation between critical flow distance and critical water content [Fagerlund, 2004]. The critical water content in concrete can be also expressed as degree of saturation (S) by dividing volume of water by volume of total pores. When critical water content is expressed as the degree of saturation, it is called as critical degree of saturation [equation 2-3].

.

$$S_{CR} = \frac{Vcr}{V_v} \qquad \text{Eq. 2-3}$$

where, Vcr is the volume of all evaporable water at critical water content and Vv is the total volume of voids in concrete.

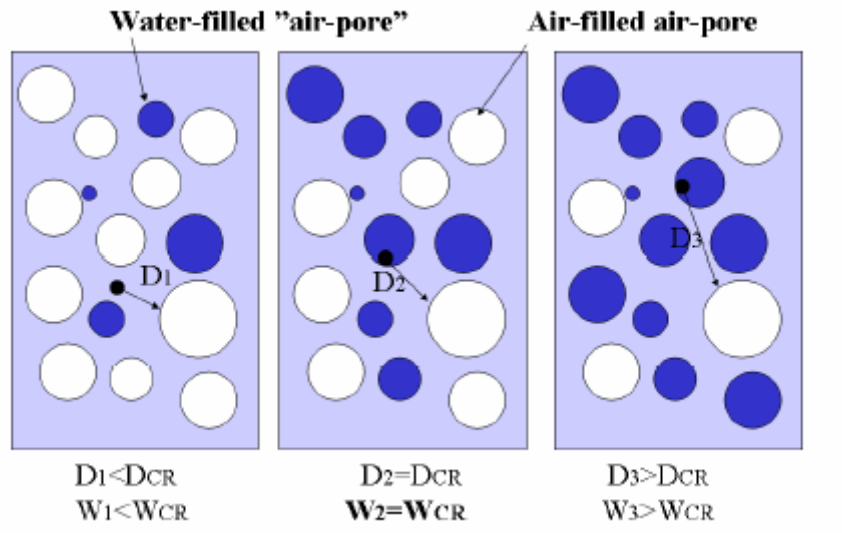

Fig. 2-2 An illustration of the concept of critical water content and distance [Fagerlund, 2004]

The critical degree of saturation for a concrete can be explained in simple words as the maximum degree of saturation a concrete can sustain before damage initiates due to freeze thaw cycles. It is understood that the critical saturation is unique for each concrete, and therefore, it is required that the value of Scr should be determined for each concrete [Fagerlund, 1997]. Scr can be determined experimentally by a freeze thaw testing of sealed specimens. The individual water contents in a specimen are adjusted before the test. The sealed specimens are exposed to a low number of freeze thaw cycles and a material property like strength or dynamic modulus is determined before and after the test [Yang, 2004]. The saturation at which the damage as determined based on material property initiates, is called the critical saturation.

As Scr is a crucial property in the analysis of freeze thaw damage, it is necessary to review the effect of other parameters on the value of Scr. It has been demonstrated with freeze thaw testing that the value of Scr does not change with number of freeze thaw cycles [Fagerlund, 2004]. This implies that, in the field, the number of freeze thaw cycles per year does not affect the value of Scr. Fagerlund [1977] showed that for a given concrete the value of Scr is almost completely independent of the rate of freezing. Nonetheless, using the theoretical calculations it has been shown that Scr is dependent on the air pore system along with the specific surface of air pores and air content. The smaller the volume of small pores, the smaller the allowable water filling and lower the value of Scr [Fagerlund, 2004]. From the above discussion it can be determined that Scr is almost independent of exposure conditions. Therefore, it can be considered as a true material property that can be used to develop the service life prediction model for freeze thaw damage.

2.4.4. Actual Saturation of Concrete (S_{Act})

The actual saturation of concrete fluctuates with time. It increases with a wetting event and decreases with drying. The increase in saturation with time depends on the rate of absorption and duration of exposure to water. The rate of absorption is called sorptivity, and is unique for each concrete. The sorptivity has been separately discussed later in section 2.4.6. In this section the process of saturation of concrete with time is discussed.

The actual saturation of concrete can be divided into three parts. The first part is the initial saturation, which is the degree of saturation before concrete undergoes its first wetting event. The saturation due to wetting events is divided into two remaining parts, saturation of capillary pores and saturation of air void system. It should be noted that there is no exact distinction between these two parts. However, for the purpose of explaining the saturation process, it is reasonable to assume this division. Similarly, Fagerlund explained the moisture level in

concrete with dividing into hygroscopic range, capillary range, and over-capillary range [Fagerlund, 2004]. Fig. 2-3 shows the different moisture levels as described by Fagerlund.

The initial saturation is normally in the hygroscopic range and within this level the moisture level is a function of relative humidity. Furthermore, the amount of water taken up by concrete at given relative humidity can be obtained from sorption isotherms. Therefore, using the absorption isotherms the initial water content or initial saturation can be obtained. Within the capillary range, the water absorption normally takes place from a free water surface. It is observed that by the time concrete reaches the upper limit of this range, capillary and gel pores of the concrete are saturated, and it can not take any more water by capillary forces. At this point concrete is supposed to reach capillary saturation. It should be noted that the sorptivity after this point is significantly lower than the sorptivity up to this point. This stage of saturation is also called as breaking point or nick point and time to reach this stage is called breaking point time or nick point time [Fagerlund, 2004]. It is observed that the saturation of the air void system starts after concrete has reach to breaking point [Fagerlund, 1999]. Normally, the saturation of air voids takes place within the over capillary moisture range and it is observed that this saturation is driven by the dissolution of enclosed air in pore water surrounding the air pores, gradual diffusion of the dissolved air to the surface, and replacement of dissolved air by water from outside [Fagerlund, 2004]. It should be noted here that, normally the critical water content is within the over capillary range. This implies that, at the time of critical saturation, for an air-entrained concrete, some part of air pore system is water filled.

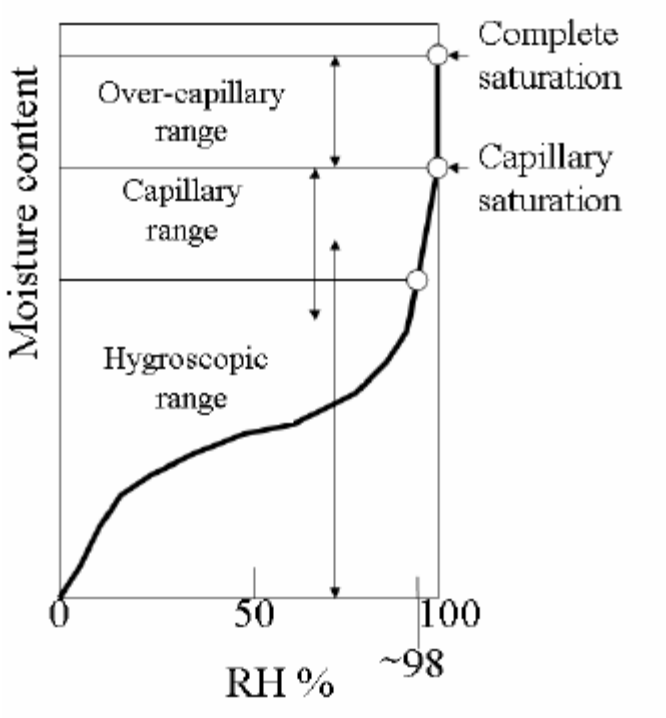

Fig. 2-3 Different moisture levels as regards the basic absorption mechanism [Fagerlund, 2004].

2.4.5. Damage Initiation in Concrete Exposed to Frost

As discussed before, the saturation in concrete changes with time and in the case of a wetting event it increases. When the saturation is below Scr concrete can sustain freeze thaw cycles. However, when concrete is saturated above the Scr and experience freezing, the damage is initiated in the concrete. If concrete is saturated above Scr level, but it does not experience freezing, then damage would not initiate. Fig. 2-4 shows a schematic presentation of damage initiation in concrete. However, it should be noted that this is just a hypothetical case and saturation profiles shown in the Fig. 2-4 are assumed profiles. From Fig. 2-4 it can be clearly observed that concrete lost its serviceability only when it was saturated above critical level and experience freezing, i.e., point B in the profile.

Furthermore, damage increases with increasing number of FT cycles. When this damage proceeds to the acceptable damage level, it is said to reach the service life.

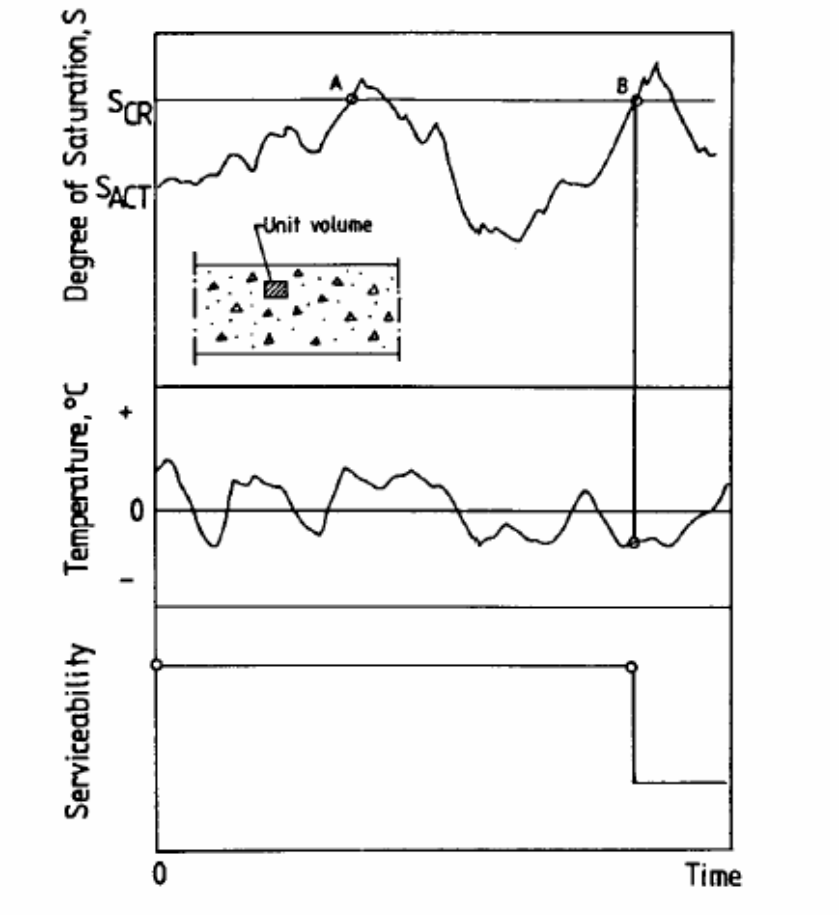

Fig. 2-4 Schematic presentation of damage initiation in concrete [Fagerlund, 2001].

2.4.6. Sorptivity

Sorptivity can be defined as an easily measured material property which characterizes the tendency of a porous material to absorb and transmit water by

capillarity [Hall, 1989]. As in unsaturated concrete the rate of ingress of liquid is controlled by absorption due to capillary rise, sorptivity is considered to be an important material property for calculating the water uptake in concrete. It is observed that this material property depends on:

(a) concrete mixture proportions;

(b) the presence of chemical admixtures and supplementary cementitious materials;

(c) the composition and physical characteristics of the cementitious component and of the aggregates;

(d) the entrained air content;

(e) the type and duration of curing;

(f) the degree of hydration or age;

(g) the presence of microcracks;

(h) the presence of surface treatments such as sealers or form oil;

(i) placement method including consolidation and finishing;

(j) moisture condition of the concrete at the time of testing [ASTM C 1585, 2004; Hall, 1989; Kelham, 1988; Nokken, 2002; Yang, 2004].

The sorptivity have been observed to change after nick point time [ASTM C 1585, 2004]. The sorptivity before nick point time is called as initial sorptivity, and after nick point time, as secondary sorptivity.

2.4.7. Measurement of Rate of Absorption (Sorptivity)

Rate of absorption is a key material property in the freeze thaw model and as discussed before in section 2.4.6 it depends on number of parameters. This makes it unique for each concrete and needs be measured with a standard ASTM test. In this section a brief review of standard test method for measurement of rate of absorption of water by hydraulic cement concretes – ASTM C 1585 -04 have been presented.

This test method measures the rate of absorption for unsaturated concrete with one surface exposed to water. The background work for the development of this test method can be found elsewhere in the literature [Hall, 1989].

In this test, a specimen of 100 ± 6 mm diameter disc with a length of 50 ± 3 mm is used. It should be noted here that the specimens are conditioned at 80 ± 3 % RH and 50 ± 2 °C for 3 days before storing them inside a sealable container at 23 ± 2 °C for 15 days. The specimen is exposed to water as shown in Fig. 2-5. The increase in the mass is measured with an accuracy of 0.01 g for 7 days at certain intervals.

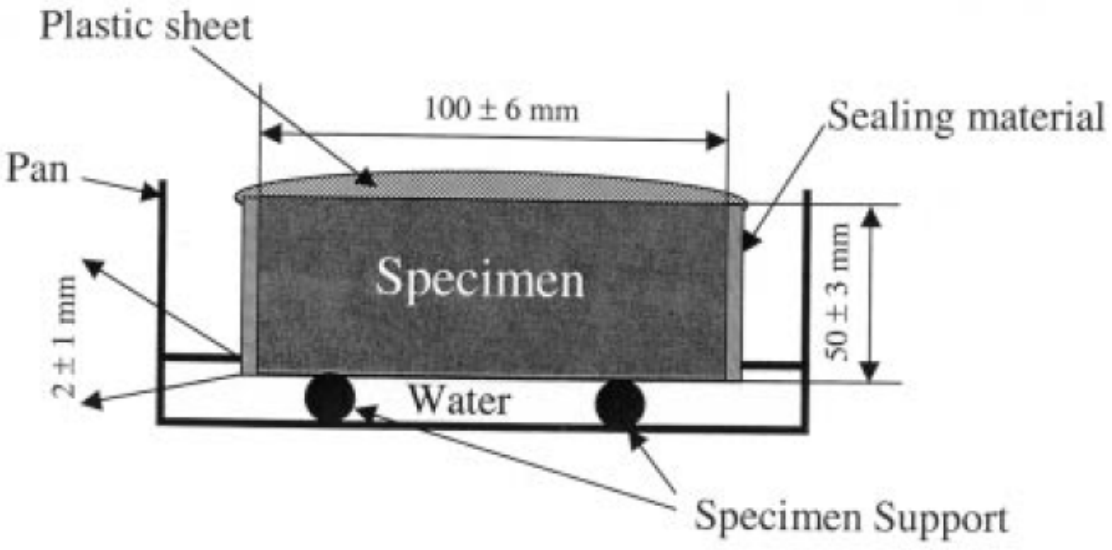

Fig. 2-5 Schematic of procedure for ASTM C 1585 [ASTM C 1585, 2004].

Based in the observations, the initial rate of water absorption or initial sorptivity ($mm/s^{0.5}$) is defined as the slope of the line that is the best fit to *I* plotted against the square root of time ($s^{0.5}$). Where *I,* the absorption, can be calculated as increase in the mass (m_t) at the time t per unit area (a) divided by density (ρ) [equation 2-3] .

$$I = \frac{m_t}{a/\rho}$$ Eq. 2-4

It should be noted here that for calculating initial rate of absorption readings from 1 minute to 6 hours are used. Whereas, for secondary rate of absorption or secondary sorptivity, the reading from 1 day to 7 days are considered. Fig. 2-6 shows a example plot as obtained in a test [ASTM C 1585, 2004]. In order to calculate the rate of absorption or sorptivity, the data obtained from test is fitted to following relation [equation 2-5],

$$I = S\sqrt{t} + b$$ Eq. 2-5

where, S (mm/√s) is the sorptivity which can be initial or secondary depending the selected data. t (seconds) is the time and b is the intercept on Y axis.

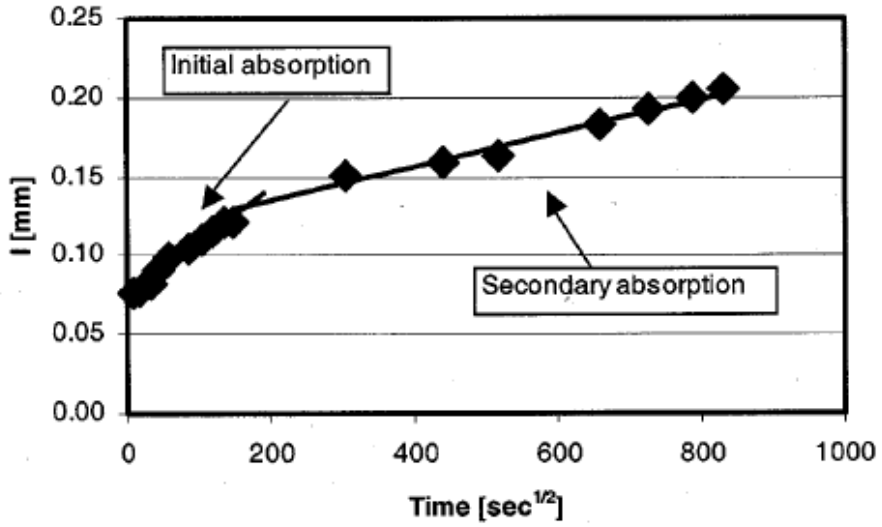

Fig. 2-6 Example plot of absorption against square root of time [ASTM C 1585, 2004].

2.4.8. Computer Model to Predict Surface Temperature and Time of Wetness for Bridge Decks

It is well known that the surface temperature of bridge decks is different than the temperature of air. However the surface temperature and time of wetness is of particular interest to this study and therefore it is required that we calculate these variables for bridge decks. A computer model developed by NIST under a FHWA project, CONCTEMP [Bentz, 2000], was used in this study to calculate the surface temperature and time of wetness. This section provides a brief review of the CONCTEMP model and explains some of the aspects of the model which are used in this study. Detailed calculations and code for the program can be found elsewhere in the literature [Bentz, 2000].

This model is based on a one-dimensional finite difference scheme and it accounts for heat transfer due to conduction, convection, and radiation. Fig. 2-7 shows a basic representation of heat transfer model used for bridge decks. For calculations related to weather, this model uses typical meteorological years weather data (TMY2DATA) provided by the National Renewable Energy Laboratory [(NREL), 1961-1990]. This program uses the material properties and convection coefficient as observed in the literature. Table 2-2 shows material properties that are used in the model as default values.

Table 2-2 Generic material properties for heat transfer/time of wetness model [Bentz, 2002].

Material	Heat Capacity	Thermal conductivity	Density	Emissivity	Solar Absorptivity
	(J/(kg-°C))	(W/(m-°C))	Kg/m^3		
Concrete	1000	1.5	2350	0.9	0.65

This model provides the output for entire year in the form of time-of-wetness events, surface temperature, and freezing events. For time-of-wetness it provides details regarding start time, duration, minimum surface temperature achieved, and exterior relative humidity prior to event. It should be noted that for wetting events this model considers two possibilities. First, an event is registered in case of precipitation event (rain, drizzle, sleet, or hail) and second, when surface temperature of concrete falls below the dew point temperature (but still above 0 °C). In case of freezing events, this model registers a freezing event when concrete surface temperature is below 0 °C.

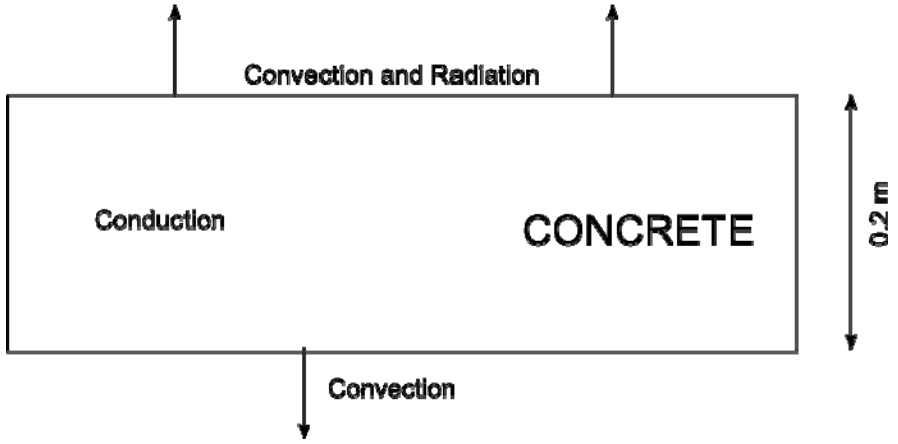

Fig. 2-7 Basic configurations of one dimensional heat transfer model for bridge deck [Bentz, 2000].

2.5. Summary and Conclusions

A brief review have been presented for the ASTM/AASHTO tests related to eight material parameters as suggested by Goodspeed et al. [1996]. The literature related to damage mechanisms for chloride induced corrosion and freezing and thawing have been reviewed in this chapter.

Based on the literature review it was observed that:

- From the review of ASTM/AASHTO test it was observed that, in the case of the standard test to measure creep of concrete in compression, a comparatively very long period is required to obtain the measurements. In addition, Goodspeed et al. [1996] does not define any performance grades for the creep of concrete.
- The material property, diffusion coefficient, plays an important role in the chloride ingress. Therefore, it is recommended that diffusion coefficient should be used in the corrosion model.
- The role of saturation of concrete in the damage mechanism in freezing and thawing have been explained in this chapter. Based on this review, it is recommended that further relationships should be developed between saturation and performance of concrete in freezing and thawing.

CHAPTER 3. REVIEW OF PERFORMANCE PARAMETERS

The FHWA defined HPC using eight parameters [Table 2-1] that are related to durability and mechanical performance as described in chapter two [Goodspeed et al., 1996]. This chapter presents a brief review of each parameter along with the discussion as to how these parameters are related to the Indiana's experience for concrete bridge decks. In addition, the results of a survey conducted by the FHWA High Performance Concrete Technology Delivery Team [Napier and Maruri, 2003] is presented in this chapter. Based on the review and survey, important deterioration mechanisms for Indiana has been short listed for further investigations.

3.1. Scaling

Internal cracking and surface scaling are two distinct distresses that occur during freezing and thawing [Foy et al., 1988]. Internal cracking caused by freezing and thawing is discussed in chapter six. This section focuses on the discussion concerned with salt scaling.

Scaling has been defined as the local flaking or peeling away of the near-surface portion of hardened concrete or mortar [ACI committee 116, 2005]. In spite of the considerable amount of research devoted to scaling, researchers have not fully understood the exact mechanism responsible for scaling [Ghafoori and Mathis, 1997]. However, it is expected that more than one process is responsible for scaling in concrete [Mindess et al., 2002]. It is believed that the primary cause for scaling is the development of hydraulic and osmotic pressure [ACI committee 201, 1992; Foy et al., 1988]. These pressures lead to the

development of stresses which, if high enough can exceed the tensile strength of aggregates or cement paste, which results in scaling. The use of deicing salt increases the potential for this deterioration. Moreover, it has been generally agreed in literature that amount of water or saturation of concrete is a driving force behind scaling [Browne, 1975; Foy et al., 1988; Ghafoori and Mathis, 1997].

Deicing chemicals influence the development of pressure in various ways. Salt reduces the ice forming temperature. This results in a decreased rate of freezing, which in turn results in reduced magnitude of hydraulic pressure. However, this initial reduction eventually turns into freezing of water with a higher crystallization velocity as temperature decreases. Consequently, it generates a greater magnitude of hydraulic pressure as temperature decreases. It has been also suggested that the consumption of heat required to melt ice when a deicer is applied causes a rapid drop in temperature of concrete just below the surface, which may cause damage either from the effects of rapid freezing or stress caused by differential thermal strains [Mindess et al., 2002].

It is generally accepted that, the use of air entrainment with adequate spacing factor increases the scaling resistance of concrete [Kurtz and Constantiner, 2004; Persson, 2003; Powers, 1975]. Therefore, the use of an adequately air entrained, low w/c, low permeability concrete is the best protection against salt scaling [ACI committee 201, 1992; Mindess et al., 2002]. In addition, Powers has also shown that, in the absence of improper finishing procedures, adequate entrained air prevents scaling in concrete [Powers, 1975].

Based on the discussion above, it can be concluded that an adequate air entrained would provide sufficient scaling resistance. Furthermore, it has been shown that, well cured concretes show sufficient resistance to scaling [Krishnan, 2002]. Therefore, considering the scope of this study it was decided that scaling would not be considered for further examinations in this study.

3.2. Abrasion

Wear of concrete can be divided into three categories, namely, abrasion, erosion, and cavitation [Mindess et al., 2002]. Out of these, abrasion is of particular interest to this study. Abrasion is caused by the wear due to the repeated rubbing or frictional processes resulting from traffic on the pavements. The abrasion of concrete reduces the thickness of the concrete slab and increases dusting on the road surface due to fractioned particles of concrete. This reduction in concrete thickness causes an increase in tensile stresses, which may lead to tensile cracking that shortens service life [Atis, 2002].

It is understood that abrasion resistance is affected by various factors such as compressive strength, aggregate properties, finishing method, and curing [Naik et al., 1994]. However, compressive strength is the single most important factor that is related to the abrasion resistance of concrete. It has been shown that, doubling the compressive strength, reduces the abrasion of concrete by approximately 50 % [Gjorv et al., 1990].

It has been observed that mechanical abrasion is the dominant abrasion for bridge decks exposed to studded tires, and conventional concrete can not withstand the abrasion caused by studded tires [ACI committee 201, 1992; Gjorv et al., 1990]. However, the normal abrasion caused by rubber tires does not induce an alarming damage to well cured concrete surfaces [Goodspeed et al., 1996]. Therefore, for bridge decks exposed to normal traffic throughout the year, abrasion wear is not a major concern of deterioration. Therefore, since studded tires are not permitted in the state of Indiana, this parameter is not further examined in this study.

3.3. Mechanical Property Parameters

Goodspeed et al. [1996] used mechanical properties such as compressive strength, modulus of elasticity, and creep to define the long-term performance of

HPC. It is understood that compressive strength, modulus of elasticity, and creep contribute towards the resistance of concrete to early-age cracking. The contribution of these properties is discussed later in this report. The creep of concrete is influenced by applied stress and duration of load [Mindess et al., 2002].

The measurement of creep is a very difficult and expensive. As discussed in the literature review [section 2.2.9], the measurement of creep requires extensive long-term measurements. Therefore, creep of concrete is not considered as an acceptance parameter.

3.4. FHWA Survey

During the fall of 2003 and winter of 2004, the FHWA High Performance Concrete (HPC) Technology Delivery Team conducted a survey and compiled results on the status of HPC implementation nationwide [Napier and Maruri, 2003]. In this survey each state DOT was asked 14 questions. One question was to rank the type of distress observed in the respective state [Napier and Maruri, 2003]. The response to this question is of particular interest to this study as the predominant type of distress can be short listed from this response for the further investigations. It should be noted that all 50 states, the District of Columbia, Puerto Rico and the FHWA Federal Lands Highway Division Bridge Office participated in this survey. Fig. 3-1 shows the results of the response from the states. The rank provided to particular types of distress was considered as the weight of that distress. The weighted value for each rank was calculated as the sum of the product of the rank provided to the distress and the number of states that provided similar rank to that particular distress. The weighted sum for each type of distress was calculated by adding the weighted value of each rank for the particular type of distress. It can be clearly observed from the weighted sum of the response from various states [Fig. 3-2] that early age cracking,

corrosion of reinforcing steel, and freezing and thawing are the predominant types of distressed observed.

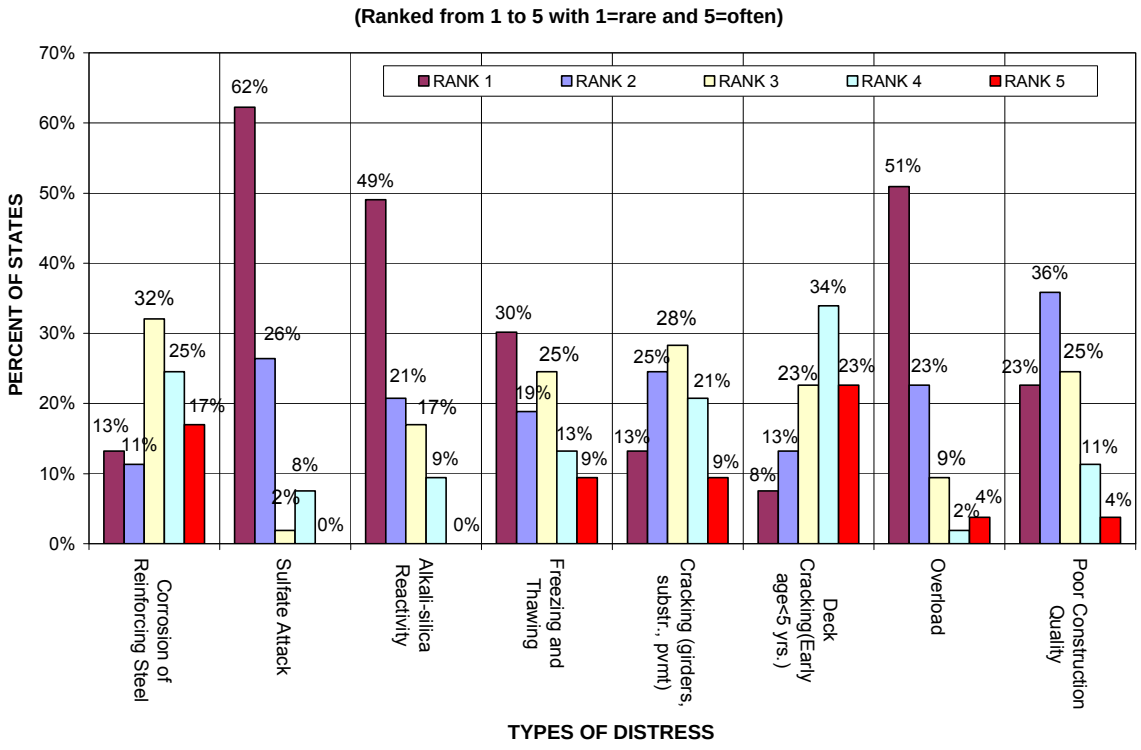

Fig. 3-1 Summary of rankings provided in the response of survey (% of states) [Napier and Maruri, 2003]

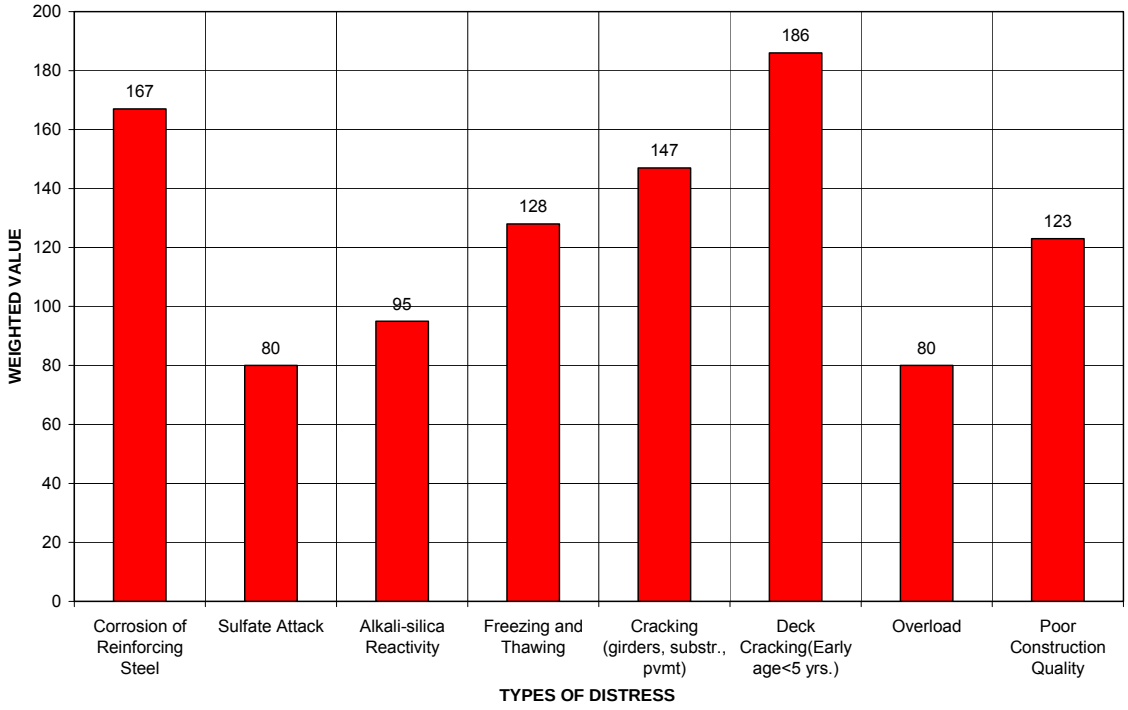

Fig. 3-2 Weighted average for type of distress (based on results of survey) [Napier and Maruri, 2003]

3.5. Conclusions

This chapter reviews the eight performance parameters that have been used to define long-term performance of HPC [Table 2-1]. Based on the evaluation it was observed that:

- Chloride permeability, freeze thaw durability, and early-age cracking are three parameters that require further investigation. It is understood that these parameters are related to chloride induced corrosion, freeze thaw damage, and early-age shrinkage cracking distress, respectively.
- As compressive strength and modulus of elasticity were generally determined based on the structural requirements, these are not explicitly examined in this study. However, it is understood that these parameters

contribute to resistance against early-age shrinkage cracking and are studied with respect to shrinkage cracking in chapter 7.

- It is well known that testing for creep is a very difficult, time consuming and expensive. Furthermore, it was observed that FHWA does not provide any grades for this performance parameter. Therefore, considering the scope of this study, it was decided not to examine this parameter further in the study.
- Since studded/chain tires are not used in the state of Indiana, the abrasion observed in the state would not warrant the limits for abrasion. Therefore, considering the scope of this study this performance parameter is not further examined in this study.
- It was observed from the literature, air entrainment has proven to provide sufficient resistance against scaling. The state of Indiana has outlined the requirement for air entrainment as 6 $\pm$ 1.5 % air. Krishnan [2002] observed that the concrete with air entrainment within these limits provide sufficient scaling resistance. Therefore, considering the scope of this study, it was decided that scaling would not be considered for further examination in this study.

CHAPTER 4. ASSESSMENT OF VARIATION IN EXPOSURE CONDITIONS ACROSS STATE OF INDIANA

4.1. Introduction

Currently, only one class of concrete exists for INDOT structures. This class of concrete is applied to the entire state of Indiana and does not consider variations related to exposure conditions which may include weather, traffic, or salt application. Exposure conditions however can play a critical role in determining the performance of concrete. As INDOT shifts from prescriptive specifications to performance specifications, the effect of exposure conditions needs to be incorporated along with material property selection. For example, INDOT needs to ascertain whether a bridge deck in Gary (IN) which has heavy traffic loading and heavy salt application, should be composed of the same material for a bridge deck in Evansville (IN) which has less traffic, and lower salt application. Said another way, should INDOT consider using a different material on the basis of geographical location, weather conditions, and the function of the structure. In this chapter, the weather conditions for the state of Indiana are developed based on geographical location. Profile maps of temperature, time to corrosion, relative humidity, rainfall, freeze thaw cycles and wetting events are presented.

4.2. Objective of Map Profile

One of the major objectives of this study is to analyze whether different concrete mixtures could, or should, be specified for concrete bridge decks on the basis of geographical location in the state of Indiana. However, prior to performing

service life simulations, the variation in the exposure conditions that can be expected in the state of Indiana must be assessed. In order to evaluate this variation, maps were developed based on rainfall, wetting events, temperature, time to corrosion for bridge decks, freeze thaw cycles, duration of wetting events and relative humidity.

4.3. Map Profiles for State of Indiana

To develop map profiles for the state of Indiana, four major cities in Indiana were chosen along with cities in the surrounding states. Table 4-1 shows the cities used in this assessment. Fig. 4-1 shows the states and cities in each state that were used for the development of maps. The district boundaries currently used by Indiana Department of Transportation are also shown in the map [Fig. 4-1].

Table 4-1 List of Cities

Illinois	Indiana	Kentucky	Ohio	Michigan	Wisconsin
Chicago	Evansville	Louisville	Akron	Alpena	Green Bay
Moline	Fort Wayne		Cincinnati	Detroit	La Crosse
Peoria	Indianapolis		Cleveland	Marquette	Madison
Rockford	South Bend		Columbus	Sault ste. Marie	Milwaukee
Springfield			Dayton		
			Toledo		
			Youngstown		

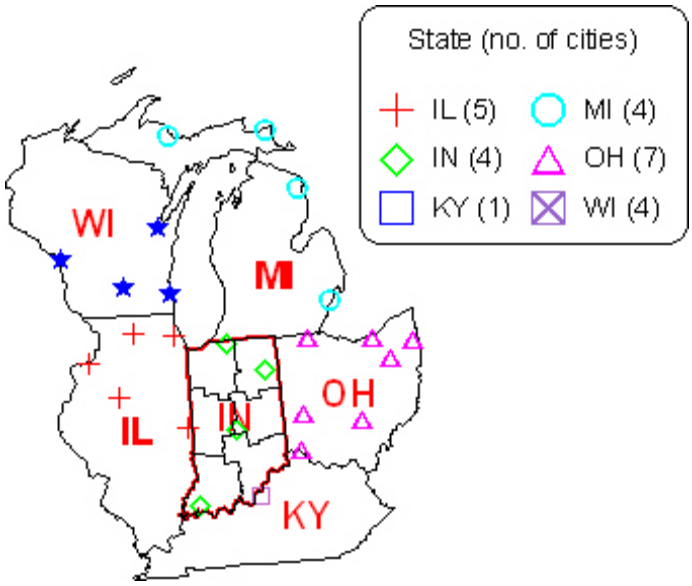

Fig. 4-1 States and cities used for the development of maps

Data for each weather parameter, that has been assessed in this study, was obtained for the cities used to develop the map profiles. Each city was identified by latitude and longitude. Gradient maps were developed for temperature, time to corrosion, relative humidity, rainfall, freeze thaw cycles and wetting events. The development of the gradient maps is greatly affected by the interpolation method used between the points. In this study, a Radial Basis Function was used as a gridding method. Equation 4-1 defines the set of weights to apply to the data points when interpolating a grid node in this method.

$$B(h) = \sqrt{h^2 + R^2} \qquad \text{Eq. 4-1}$$

where, h is the anisotropically rescaled distance from the point to the node and R^2 is the smoothing factor. The larger the R^2 parameter, the smoother the results. However, based on the data, the MapViewer software suggests a default value for R^2 parameter which was used in this study. In the gridding process the anisotropically rescaled distance (h) accounts for any trends that may be present

in the data. Its setting includes a ratio and an angle. Different gradient map profiles were developed based on the gridding method described above. The gradient in each map is marked by contour lines. The maps developed for different parameters of exposure are discussed separately further in this section.

4.3.1. Time to Corrosion

Application of this work is aimed at performing an assessment of the variation in the predicted service life performance of concrete for different geographical locations. To begin, simple simulations were performed using Life365^{TM} to obtain the time to corrosion for bridge decks at each city listed in Table 4-1. The Life365^{TM} simulations were performed considering a bridge deck with 8 in thickness, 2.5 in clear cover over reinforcement, a water to cement ratio (w/c) of 0.4, no entrained air and 1.2 % epoxy coated steel. The salt application and exposure conditions were varied based on geographic location. Life365^{TM} provides default values for salt application (chloride build up) and temperature profiles based on geographic location. Therefore, considering the scope of this study, the default values provided by Life365^{TM} (Version 1.1) were used in this assessment.

Fig. 4-2 shows the developed contour map profile for time to corrosion. It can be observed from this map profile (Fig. 4-2) that a variation exists in the performance of the same material based on its location in Indiana. Therefore, it seems that it may be possible to divide Indiana into different zones. The bridge decks in southern end of Indiana may be expected to have longer time to corrosion of reinforcement than the same bridge deck in the northern part of Indiana. It can be observed from the Fig. 4-2 that, for the case of bridge decks in district 1 and 2 the predicted time to corrosion is between 10 to 11 years. Whereas the predicted time to corrosion is between 11 to 13 years for district 3 and 4, and 13 to 19 years for district 5 and 6. Finally, a difference of

approximately 9 years can be observed in predicted time to corrosion across the state.

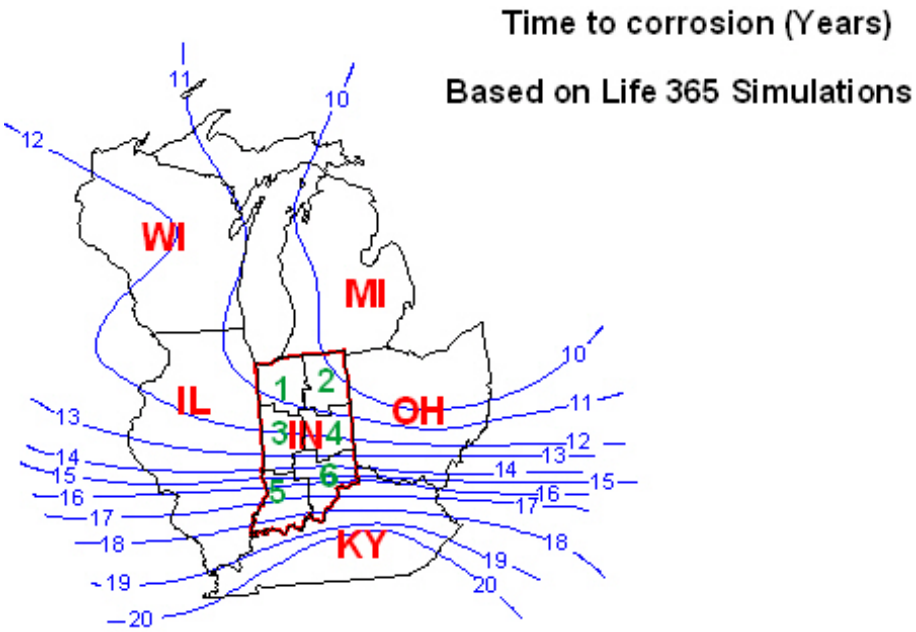

Fig. 4-2 Variation in time to corrosion (Years)

4.3.2. Temperature

Temperature affects the rate of strength development and therefore the length of curing that would be necessary [Mindess et al., 2002]. Therefore it is necessary to study the variation in temperature observed across the state of Indiana.

Due to a concern of slow strength gain, current Indiana Department of Transportation (INDOT) specifications restrict the use of blended cements, fly ash, and ground granulated blast furnace slag during a period of April 1st to October 15th of the same calendar year [INDOT, 2006]. As a result, it appears to be appropriate to evaluate the temperature across the state for two time periods.

The first time period exists between the 1st of April and the 15th of October and second period from the 15th of October and the 1st of April. Contour maps of mean maximum and mean minimum temperature were developed for these periods. The data used for the development of these maps was obtained from National Climatic Data Center, Climate Services Division. This data was compiled by Air Force Climatology Center (AFCCC) under the name of Engineering Weather Data (EWD). The measurements for different weather parameters from 1967 to 1996 were compiled in this data set [(AFCCC), 1967-1996]. It should be noted that since the database had the temperatures recorded for the 14th October, the maps were developed for data till 14th October instead of the 15th October.

Based on the available data, the variation in temperature across state of Indiana was assessed in three ways. First, the mean daily range (difference between daily maximum and daily minimum temperatures) for dry-bulb temperature was evaluated. Second, the mean maximum dry bulb temperature for both the time periods. Finally, the mean minimum dry bulb temperature for both the periods across the state of Indiana was assessed. It should be noted here that the mean of measurements from 1967 to 1996 was considered for the assessment [(AFCCC), 1967-1996].

Table 4-2 shows the mean daily range of temperature for four cities in Indiana. It can be observed from Table 4-2 that there is not much variation in the mean daily range across the state of Indiana, and for all practical purposes the mean daily variation can be taken as 18°F.

Table 4-2 Mean daily range of temperature for cities in Indiana (°F)

City	Mean daily range of temperature (°F)
Indianapolis	18
Evansville	19
South Bend	17
Fort Wayne	18

It can be observed from Fig. 4-3 and Fig. 4-4 that from the 1st of April to the 14th of October the mean maximum temperature fluctuates across the state by approximately 6°F, between 71 to 77°F and for second period by 7°F between approximately 39 to 46°F. The mean minimum temperature in first period fluctuates between 51 to 57°F (approximately 6°F (Fig. 4-5)). Whereas, in second period it fluctuates between 23 to 29 °F (approximately 6°F (Fig. 4-6)).

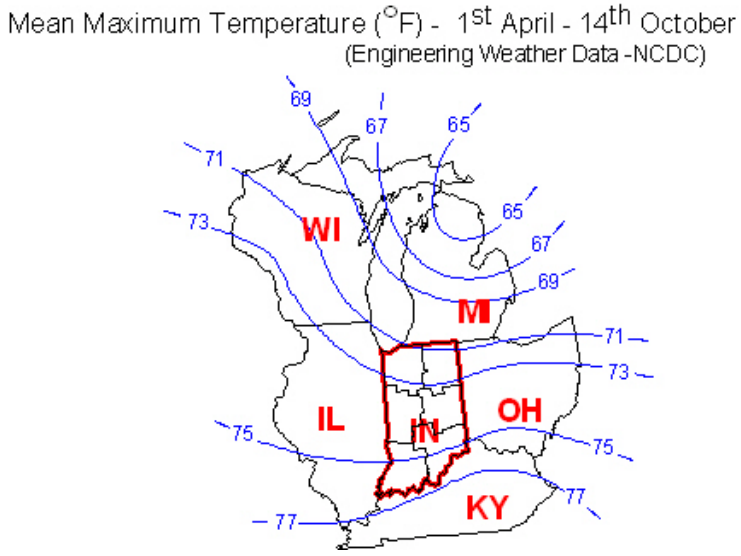

Fig. 4-3 Mean maximum temperature - 1st of April – 14th of October

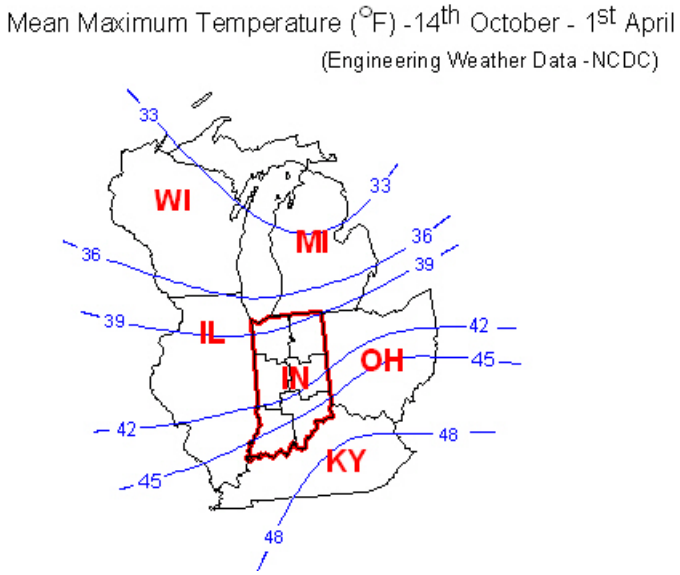

Fig. 4-4 Mean maximum temperature - 14th of October – 1st of April

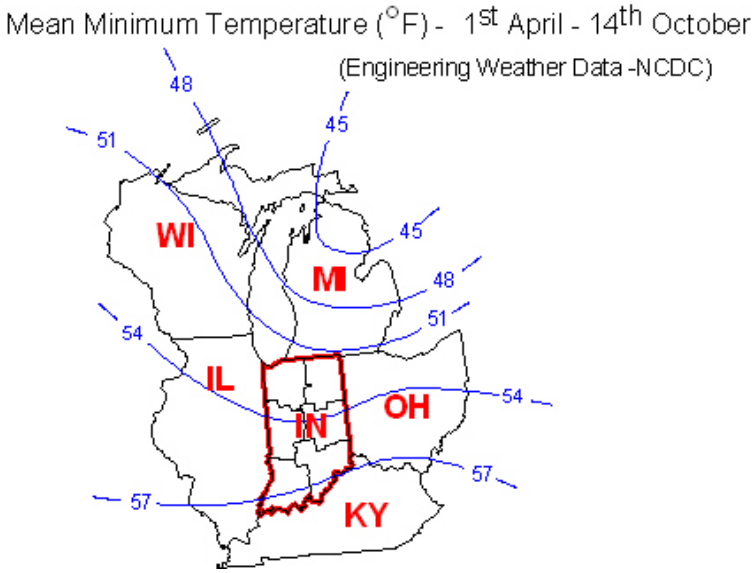

Fig. 4-5 Mean minimum temperature - 1st of April – 14th of October

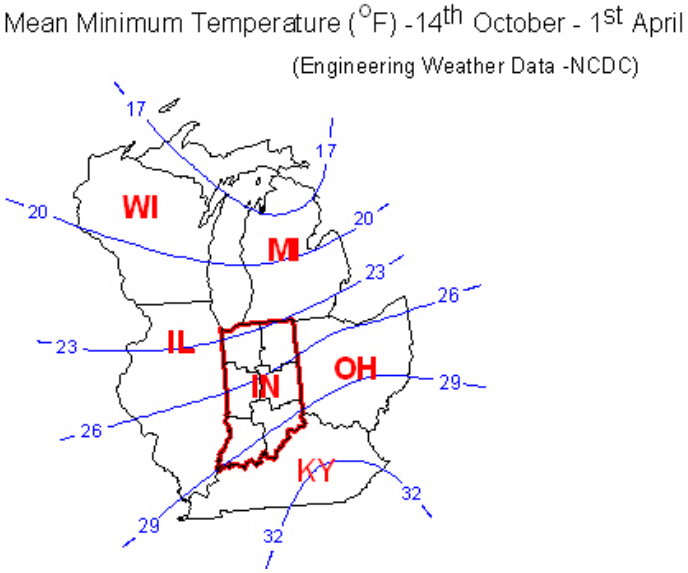

Fig. 4-6 Mean minimum temperature - 14th of October – 1st of April

4.3.3. Freeze Thaw Cycles

The annual number of freeze thaw cycles is an important factor that is related to the freeze thaw deterioration of concrete [Fagerlund, 2004]. A contour map was developed for the annual number of freeze thaw cycles in Indiana. The number of annual freeze thaw cycles data was obtained from engineering weather data [(AFCCC), 1967-1996]. It should be noted here that the engineering weather data counts a freeze thaw cycle when the air temperature drops below freezing (31 °F [-0.5 °C] or colder) and then rises above freezing (33 °F [0.5 °C] or warmer). Fig. 4-7 shows the freeze thaw cycle contour map. The variation in the number of freeze thaw cycles is relatively small from the north of the state to the south (i.e., ten freeze thaw cycles (48 – 58)). It would be difficult to divide Indiana into zones based solely on number of freeze thaw cycles. However, the freeze thaw damage is not a function of just temperature. The freeze thaw damage is also affected by the moisture saturation of concrete. Therefore,

variation in other weather parameters which affect the moisture saturation of concrete (rainfall and wetting events) should be assessed.

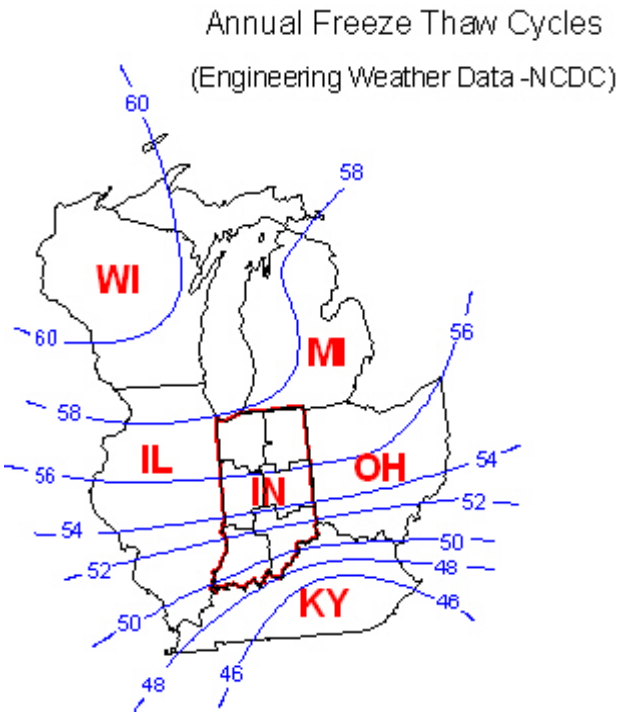

Fig. 4-7 Annual Freeze thaw cycles

4.3.4. Rainfall

Rainfall in any given area is a major source of water for the saturation of concrete. As saturation is an important parameter in the freeze thaw deterioration process, it was necessary to understand the possible variation observed across the Indiana for saturation of concrete. However, the saturation varies continuously as the water content in concrete changes with time. Obtaining the measurements of water content as a function of time is a difficult task. The variation in the rainfall is considered to be a major cause responsible for the variation in water content and consequently saturation. The average

monthly rainfall for each city was obtained [(AFCCC), 1967-1996]. However, considering that the contribution of rain towards saturation in the freezing period would be more critical, the contour map was developed for mean rainfall from September to April for each city. It can be observed from Fig. 4-8 that the mean rainfall for this period differs across the state by about 1.0 in, where northern part of Indiana has about 2.5 in and southern part of Indiana has approximately 3.3 in of mean rain.

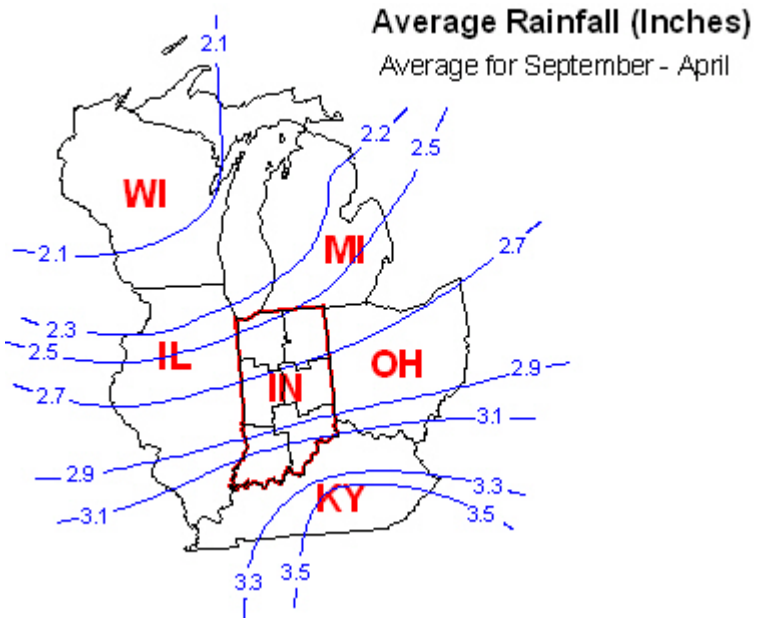

Fig. 4-8 Mean rainfall for September through April

4.3.5. Wetting Events

One of the crucial parameters used to define the freeze thaw damage is degree of saturation of concrete. The saturation of concrete depends on the total volume of voids and volume of water present in concrete. The amount of water present in concrete depends on the rate of absorption (sorptivity) of concrete and the time concrete is exposed to water. The time concrete is exposed to water (wetting event) is calculated under two possibilities. First, is in case of precipitation event (rain, drizzle, sleet, or hail) and second, when surface temperature of concrete falls below the dew point temperature (but still above 0 °C). As discussed in the literature review, the sorptivity of concrete changes after it has been exposed to water for a given period of time. This response contains a point that is described as nick point time [section 2.4.6]. The amount of water absorbed after the nick point time (i.e., after sorptivity changes) contributes toward the saturation of air void system, and is of particular interest to this study. Therefore, the wetting events that last longer than the time to reach the nick point time are considered in this assessment. As ASTM C 1585 defines 6 hours as the nick point duration, in this section a contour map has been presented for cumulative duration of wetting events that lasted more than 6 hours [Fig. 4-9]. The duration of wetting events used in this assessment was calculated using the CONCTEMP program for bridge decks and yearly events are considered while preparing the map profile [Bentz, 2000]. It can be observed from Fig. 4-9 that the wetting duration varies by approximately 100 hours across state of Indiana. Furthermore, a greater variation can be observed in the southern part of Indiana. A variation of approximately 35% of the total variation can be observed in district number 1 to 4) and remaining 65% of the total variation can be observed in district number 5 and 6.

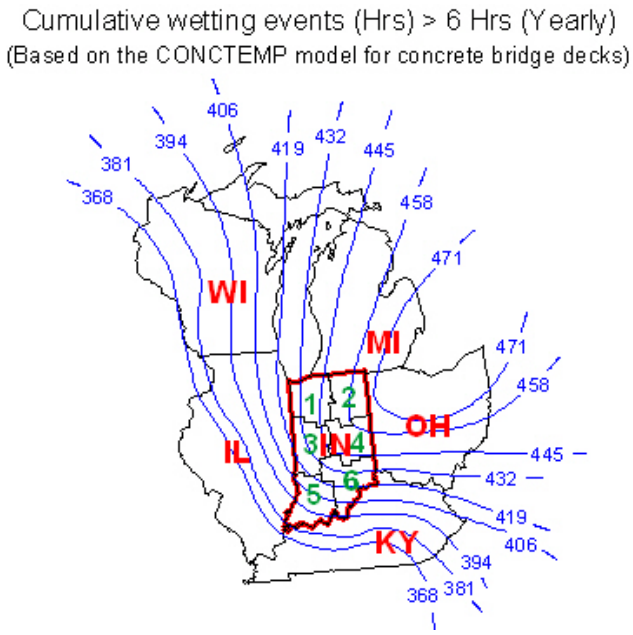

Fig. 4-9 Cumulative duration of wetting greater than 6 hours considered over a year

4.3.6. Relative Humidity

Relative humidity is a very important weather parameter for both freeze thaw and shrinkage. Therefore, the variation of relative humidity across the state was studied. Similar to the temperature profile, mean maximum and minimum relative humidity profiles were developed for two time periods same as those considered in the development of temperature contour map. The Engineering Weather Data (EWD) was obtained as the humidity ratio (grains/pound) for selected locations [(AFCCC), 1967-1996]. As the humidity ratio is not widely used with reference to concrete, this data was converted to percentage relative humidity using psychrometric calculations as performed by envirotex [Envirochex, 2001]. It can be observed from Fig. 4-10 and Fig. 4-11 the mean maximum %RH fluctuate across the state by approximately 4% (84 to 80) in the summer and 6% (87 to 80) in the winter. The mean minimum % RH around summer fluctuates

between 60 and 58% (i.e., just 2%) (Fig. 4-12). Whereas, in winter fluctuates between 78 and 70% (i.e., approximately 8%) (Fig. 4-13).

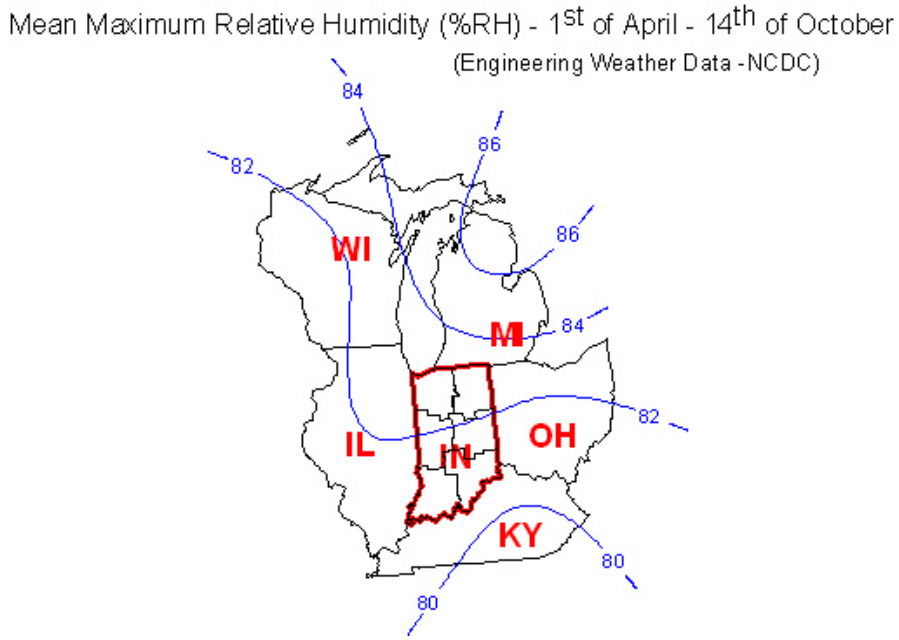

Fig. 4-10 Mean Maximum Relative Humidity 1st of April – 14th of October

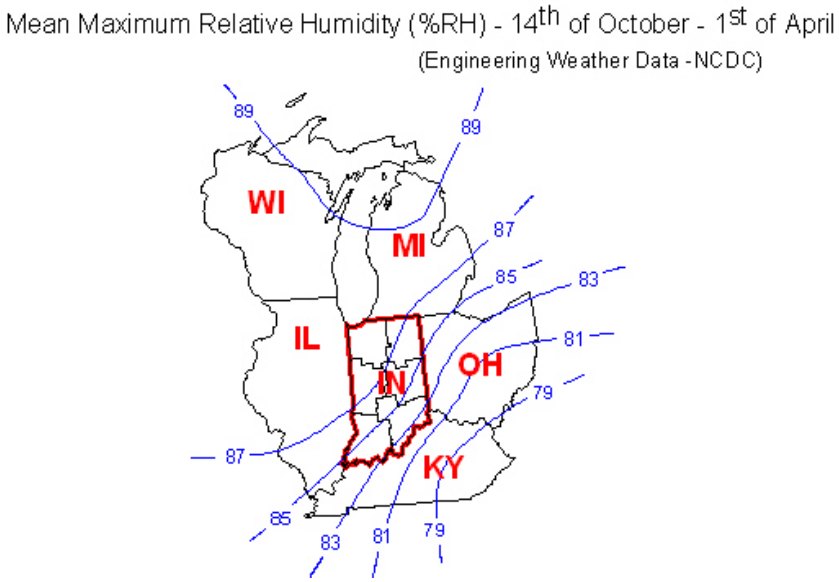

Fig. 4-11 Mean Maximum Relative Humidity 14th of October – 1st of April

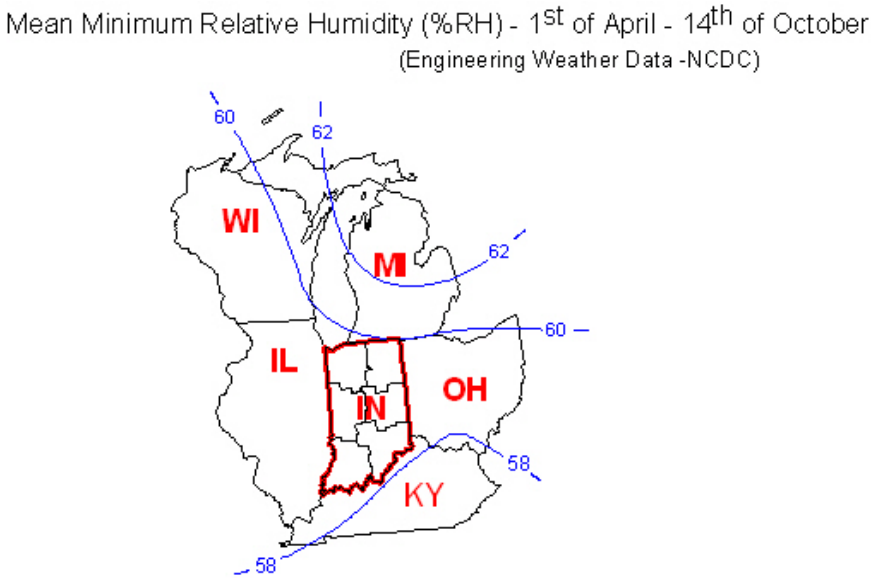

Fig. 4-12 Mean Minimum Relative Humidity 1st of April – 14th of October

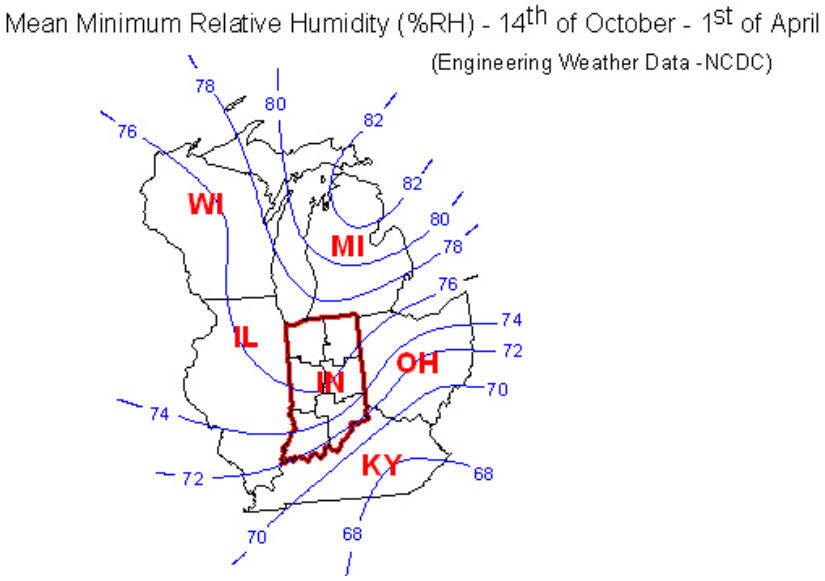

Fig. 4-13 Mean Minimum Relative Humidity 14th of October – 1st of April

4.4. Conclusions

The objective of this chapter was to review weather patterns in Indiana and to prepare maps to assist the INDOT in evaluating the possibility of dividing the state of Indiana into different exposure conditions. Based on the contour maps developed in this chapter, it was observed that

- The time to corrosion, as simulated with Life365™, varies by a small amount in the northern part of Indiana (i.e., 20% of the total variation across the state). However, the variation in southern part is much higher and 80 % of the total variation takes place in this region. Based on this variation it could be suggested that the state of Indiana should be divided in to two zones. First zone should consist districts 1 to 4 (Laporte, Fort Wayne, Crawfordsville and Greenfield district), and second zone should have district 5 and 6 (Vincennes and Seymour district).

- Small variations in temperature were observed for both the time periods under consideration. The mean maximum or minimum temperature was observed to vary by approximately 6 to 8°F across the state. The average mean maximum temperature observed in the summer was approximately 74°F while the temperature in winter was 42°F. The average mean minimum temperature observed in summer was approximately 54°F. whereas, in winter the temperature was 26°F Furthermore, the daily fluctuation for cities across Indiana was observed to be approximately same (i.e., 18°F).
- The variation in the number of annual freeze thaw cycles was observed to be approximately 10 cycles across the state. Furthermore, this variation was observed to be more or less evenly spaced across the state. The average number of annual freeze thaw cycles for the state of Indiana was observed to be 52 cycles.
- The average rainfall for the time period under consideration was observed to be approximately 2.8 in while the variation was 0.6 in which was evenly spaced across the state. However, it is understood that the amount of rainfall does not represent the saturation events for freeze thaw cycles completely. Therefore, the variation of wetting events was evaluated across the state of Indiana, and variation in total duration of wetting events under consideration was observed to be about 100 hrs (Approximately 20 % of the maximum cumulative wetting duration). This variation was more in the southern part of state (i.e., approximately 65 % of total variation). Based on this variation it could be suggested that the state of Indiana should be divided in to two zones similar to that suggested for time to corrosion. The first zone should consist district 1 to 4 (Laporte, Fort Wayne, Crawfordsville and Greenfield district), and second zone should have district 5 and 6 (Vincennes and Seymour district).
- The variation in the relative humidity across the state was less than 5 % RH in case of mean maximum and mean minimum RH of period under

consideration. The average mean maximum RH observed in summer was approximately 82%, whereas in winter 85%. The average mean minimum RH observed in summer was approximately 61%, whereas in winter 75%.

CHAPTER 5. DETERIORATION MODELS - CORROSION MODEL

The purpose of this chapter is to describe the development of the model that is used to relate material property with corrosion damage. In this chapter section 5.1 emphasizes the importance and need of corrosion model. Section 5.2 illustrates the approach used for model development. Section 5.3 illustrates a test that INDOT can use to rapidly assess the concrete resistance to chloride ingress. The background of the Rapid Chloride Permeability Test is discussed along with it's limitations and strengths and their impact on the model. Section 5.4 describes the development of the relationship between results of the RCPT test and the material property that is used for service life prediction, the diffusion coefficient. Section 5.5 compares the results for the relationship between RCPT results and diffusion coefficient with the results of other studies. The differences observed in the results are discussed in Section 5.6. Section 5.7 evaluates the effect of diffusion coefficient and exposure on service life prediction for bridge decks. Section 5.8, describes the development of the relationship between service life prediction and diffusion coefficient. Two specimen geometries are considered. First, a concrete bridge deck with a 2.5 in (from the surface) clear cover over the reinforcement. Second, a bridge deck with a latex modified concrete overlay (1.5 in) above a concrete layer. The clear cover over the reinforcement in the concrete layer is 1 in (from the interface of LMC and concrete). The results of the developed model are discussed in Section 5.9. Section 5.10 end this chapter with the summary and conclusions.

5.1. Introduction to Corrosion Model

The deterioration of nation's highway infrastructure is proceeding at an alarming rate. These rehabilitation projects consume large financial resources and result in traffic delays as well. In 2000, maintenance expenditures had increased 47.6 % (after accounting for inflation) above the 1970 expenditures [FHWA, 2000]. It is known that chloride-induced corrosion of the reinforcing steel is a major cause of premature rehabilitation of bridge structures. The annual direct cost of corrosion to bridges is estimated to be between 5.9-9.7 billion dollars [William *et al.*, 2004]. As a result, it would be valuable to have a method to relate properties of concrete to corrosion and service life.

There are two main causes of corrosion: carbonation and chloride ingress. Chloride ingress occurs as a result of deicing salts which are spread on decks in the winter to avoid icing. A fraction of the chlorides , along with water penetrates inside the concrete. Fig. 5-1 shows a typical chloride profile in concrete, which describes the concentration of chlorides at different time and depths from surface of a structure.

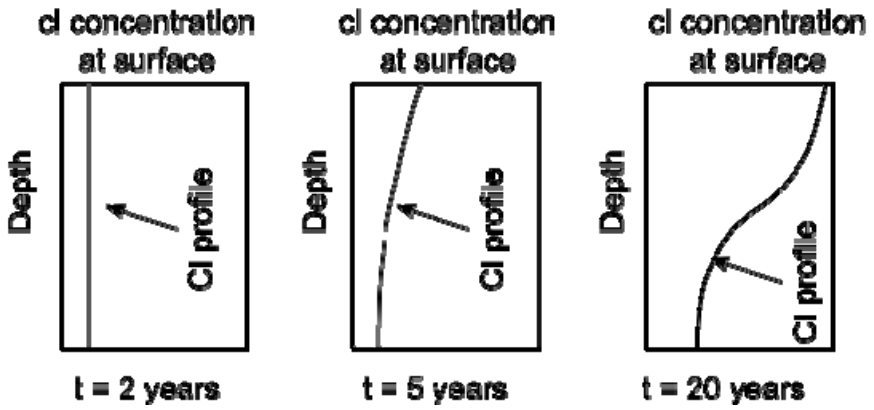

Fig. 5-1 Typical chloride profile in concrete at different time and depths

When the chloride concentration at the level of the reinforcement exceeds a specific limit, corrosion of reinforcement can be thought to have initiated. This corrosion, with time, becomes the reason for ending service life of bridge decks. A model has been used which can estimate the service life of bridges deck in Indiana with respect to corrosion failure. This chapter describes this model.

5.2. Development of the Service Life Model for Corrosion in the Presence of Chlorides

One of the main objectives of this research was to relate the properties of concrete to the service life of bridge decks in the state of Indiana.

To accomplish this objective a four step model was used. Fig. 5-2 shows the flow chart of the four steps. In step one, an approach is used to measure chloride ingress in concrete. There are various tests available to perform this measurement and details about these tests can be found elsewhere in literature [Stanish et al., 1997]. However, since the FHWA suggested that the Rapid Chloride Permeability Test (RCPT) should be used to measure the chloride permeability of concrete and as this equipment is readily available in the INDOT, RCPT was selected as a test method [Goodspeed et al., 1996]. In step two, results from the RCPT were related with a fundamental material property, Diffusion coefficient (D). The Nernst Einstein equation was used to transform the RCPT results to the diffusion coefficient. The details of this transformation are explained in section 5.4. In step three, the diffusion coefficient was used to estimate the service life of reinforced concrete element. Life 365^{TM} was used to development this relationship as described in section 5.8. Finally, in step 4 the service life is related back to measurable properties from the RCPT test results.

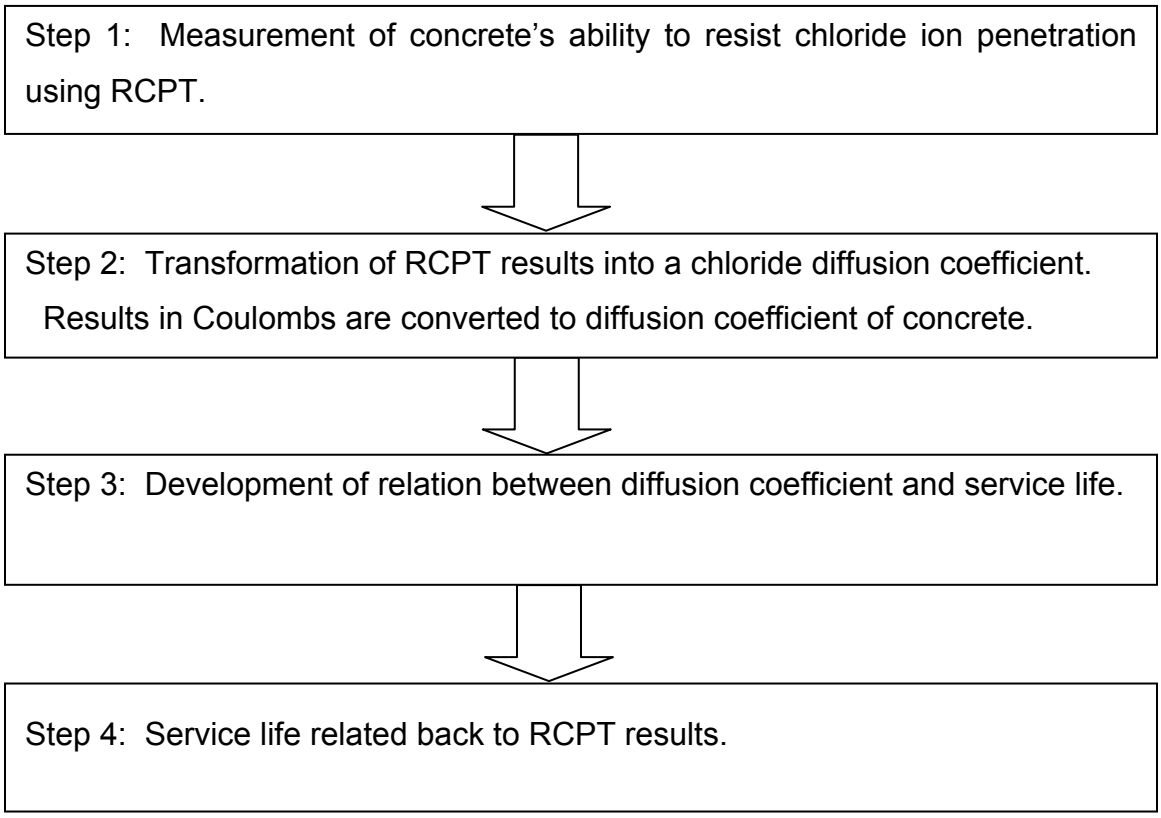

Fig. 5-2 Flow chart for corrosion model

5.3. Measurements of Resistance to Chlorides ion Penetration Using Rapid Chloride Permeability Test (RCPT)

According to FHWA, the RCPT (ASTM C 1202/ AASHTO T 277) should be used to measure the chloride permeability of bridge decks [Goodspeed *et al.*, 1996]. Details about the RCPT procedure have been already discussed in chapter 2. The RCPT test was developed to rapidly measure permeability of concrete to chloride ions [Feldman et al., 1994]. Although this test has been adopted as a standard test and widely used in literature, there has been also criticism [Andrade, 1993; Hansen et al., 1993; Stanish et al., 1997]. As the results of the RCPT are used as the primary input for the modeling application, it was

necessary to understand and evaluate the limitations of this test. The main limitations of the RCPT are:

- When the electric field is applied, migration of all the ions in the solution occurs rather than just chloride ions. Thus the current passed is related to all ions than just chloride [Andrade, 1993],
- The measurements are made before steady state migration is achieved,
- The high voltage applied leads to increase in temperature,
- The high voltage is applied to the specimen. This high voltage can result in irreversible changes in the microstructure of the specimen, effectively making it impossible to know if a representative sample is being tested [Aldea et al., 1999; Alonso et al., 2000; Jaiswal et al., 1998].

These limitations impose certain errors in the results of the test; and even in the interpretation of the results obtained. Therefore, these errors should be accounted while developing the model.

The heating effect known as the joule effect has been described by many researchers [Aldea et al., 1999; Julio-Betancourt and Hooton, 2004; Snyder, 2000]. This generated heat (J) is expressed as,

$$J = EIt \qquad \text{Eq. 5-1}$$

where, J is the heat (joules), E is the potential (volts), I is the current (amperes) and t is the time (seconds). As the voltage and time are fixed for a RCPT, electric current is the only variable in equation 5-1. For the RCPT an incremental increase in temperature will increase the mobility of all ions that carry the current, which raises the total current flow producing more heat [Julio-Betancourt and Hooton, 2004]. The total charge passed in RCPT is calculated by integrating the electric current passed during 6 hours.

These effects result in the fact that the total charge passed in the RCPT does not represent the actual properties of tested concrete. Therefore, appropriate measures or corrections should be made to these results. It is important to calculate this correction factor in this model because the diffusion coefficient of concrete used in this model is calculated based on the total charge passed in RCPT and any error in RCPT results affects the diffusion coefficient. Furthermore, as this model uses diffusion coefficient for service life prediction, such variation in diffusion coefficient affects the service life prediction of this model.

Many authors have suggested initial current from impedance spectroscopy or RCPT as a better indicator of specimen properties than total charge passed [Aldea *et al.*, 1999; Feldman *et al.*, 1994; Hansen *et al.*, 1993; Jaiswal *et al.*, 1998; Snyder, 2000]. Therefore, it was decided to use the initial current for calculating diffusion coefficient in the model. However, the results of RCPT test, which are in the form of total charge passed, were used as the inputs to this model. Therefore, it was required that the initial current to be calculated from the total charge passed in the RCPT test.

Many researchers have made the measurements of initial current and total charge at the end of test [Aldea *et al.*, 1999; Feldman *et al.*, 1994; Hansen *et al.*, 1993; Jaiswal *et al.*, 1998; Snyder, 2000] . Based on these results available in the literature, a linear relation was formulated between initial charge and total charge passed as,

$$Q_i = CF \cdot Q_t \qquad \text{Eq. 5-2}$$

where, Q_i is the initial charge passed, Q_t is the total charge passed in the RCPT test, and CF is the correction factor. Fig. 5-3 shows the predicted RCPT value

assuming the initial charge remains constant for 6 hours and the total charge that was experimentally measured at the end of 6 hours in RCPT test.

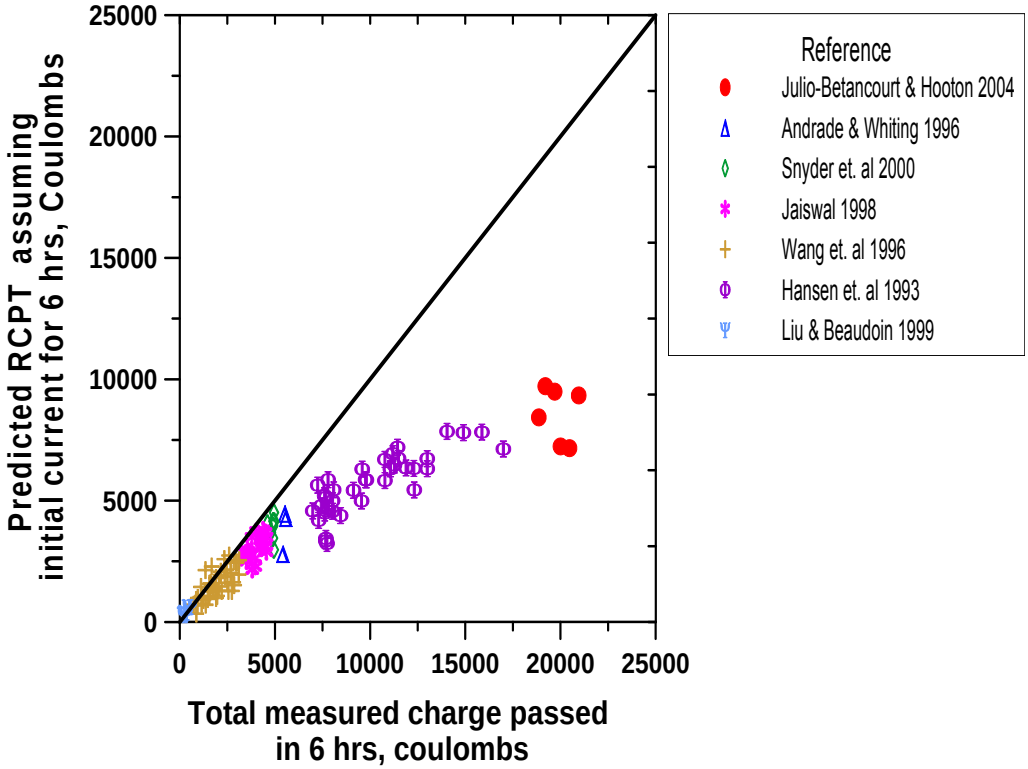

Fig. 5-3 Measurements of initial charge against total charge passed in RCPT

It was observed from Fig. 5-3 that this data set contains several very high values of total charge passed. However, RCPT defines concrete with greater than 4000 coulombs as high chloride ion permeability. Therefore any specimen with a RCPT value higher than 4000 is not likely to be used in the field. To calculate the correction factor, the measurements of the total charge passed obtained from the different researchers were restricted to the value of 5000 coulombs. Fig. 5-4 shows the restricted measurements from Fig. 5-3. In order to show the trend of measurements the results up to 8000 coulombs are shown in Fig. 5-4. Furthermore, it was observed that for the calculation of correction factor, the linear fit appears appropriate for measurements up to 5000 coulombs, which is

the range of interest to this study. This correction factor of 0.75 was used to calculate the initial charge from the total charge passed in RCPT; and further the initial charge was used for calculating diffusion coefficient.

$$Q_i = 0.75 \cdot Q_t \qquad \text{Eq. 5-3}$$

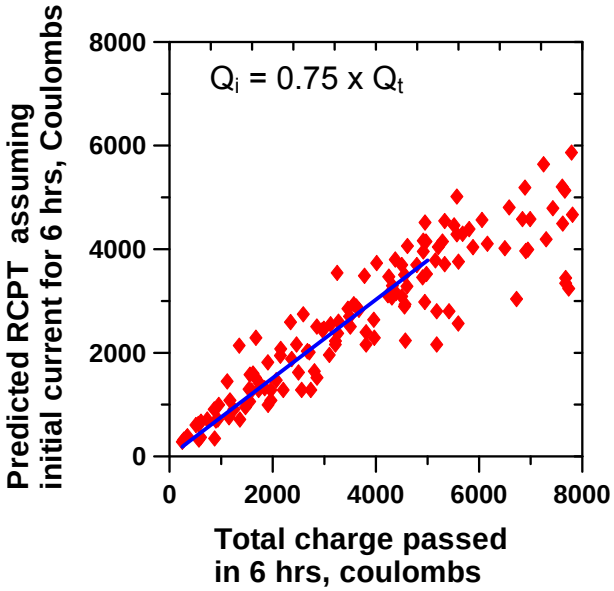

Fig. 5-4 Measurements of initial charge again total charge, where total charge passed was restricted to 8000 coulombs.

5.4. Development of the Relation Between RCPT and Diffusion Coefficient

Transport in concrete is very complicated and more than one transport mechanism such as permeation, absorption, and convection are involved [Yang, 2004]. Generally, four transport mechanisms (diffusion, permeation, capillary absorption, and convection) are used to describe the fluid flow in concrete [Yang, 2004]. Among the four mechanisms, diffusion is the process that occurs as a result of a concentration gradient and assumed to be the basic phenomenon for chloride ion ingress through concrete when concrete is in moist condition

[Andrade, 1993; Yang, 2004]. It has been also observed by many other researchers that main mechanism for transport of chloride ions through crack free concrete is diffusion [Feldman et al., 1994]. As diffusion was observed to be the basic phenomenon, diffusion coefficient was selected as the material property to be related with the results of RCPT. Therefore a relation was developed between diffusion coefficient and total charge passed through specimen (in coulombs).

The transformation of the results from RCPT to diffusion coefficient was done in two steps. In the first step the partial conductivity of the concrete was calculated using the current (I). Where current was calculated from the total charge passed in the RCPT as,

$$I = 0.75 \cdot \frac{Q_t}{t} \qquad \text{Eq. 5-4}$$

where, I is the current (ampere), which can also be expressed as coulombs/second, Q_t is the total charge passed through the specimen tested for rapid chloride permeability (coulombs). The time taken (6 hours or 21600 seconds) to pass charge Q_t is expressed as t and 0.75 is the correction factor obtained from Fig. 5-4. Therefore substituting this time as *t* and charge passed in RCPT as Q in Equation 4-1 current *I* was calculated. Furthermore, this current (*I)* was converted into conductivity using the Equation 5-5 [Snyder, 2000],

$$\sigma = \frac{I \cdot L}{V \cdot A} \qquad \text{Eq. 5-5}$$

where, σ is the conductivity (Siemens per millimeter, S/mm). The current, I can be calculated from Equation 5-4 and the voltage (V = 60 volts) applied across the specimen in the test, where L is the specimen length (50 mm) and A is the area of specimen (7865 mm^2).

In the second step, the conductivity was related to diffusion coefficient. It was observed in the literature that when concrete is considered as a solid electrolyte, the diffusivity of charged species *i* in concrete is related to its partial conductivity σ_i, and this relation [Equation 5-6] is called the Nernst-Einstein equation [Andrade, 1993; Lu, 1997]

$$D_i = \frac{R \cdot T \cdot \sigma_i}{Z_i^2 \cdot F^2 \cdot C_i} \qquad \text{Eq. 5-6}$$

where, D_i is the Diffusivity (cm^2/s) of the species i, R is the universal gas constant expressed in j/mol-K, T is temperature is expressed as in Kelvin (293 K), Z_i is the charge of the species i, and *F* is the Faraday's constant, 96500 coulombs/mo, C_i is the concentration of species i, expressed as mol/cm^3, σ_i is the partial conductivity of species i, expressed as S/cm. The partial conductivity σ_i of concrete is defined as [Lu, 1997],

$$\sigma_i = n_i \cdot \sigma \qquad \text{Eq. 5-7}$$

where, σ is the conductivity of concrete and n_i is the transference number of species i. The transference number is defined as the proportion of the current carried by the ion in proportion to the current carried by the rest of the ions [Andrade, 1993]. It is formulated as,

$$n_i = \frac{Q_i}{Q} = \frac{I_i}{I} \qquad \text{Eq. 5-8}$$

where, Q_i, I_i are the electric quantity and current contribution of species *i* to the total electric quantity Q and current I, respectively. When the diffusivity of an ion is to be determined by the Nernst-Einstein equation, the transference number of

this ion should be known. However, a simple approach is to make the transference number approximately equal to 1.0 [Andrade, 1993; Lu, 1997]. Therefore, using n_i as 1.0, conductivity can be calculated by Equation 5-5. This was used in equation 5-6 for calculating diffusion coefficient. Combing the Equation 5-5 and 5-6 results in a relation between total charged passed through specimen in RCPT and diffusion coefficient , which can be formulated as,

$$D = \frac{R \cdot T \cdot L \cdot (0.75)}{Z^2 \cdot F^2 \cdot C_i \cdot V \cdot A \cdot t} \cdot Q_t \qquad \text{Eq. 5.9}$$

where D is the diffusion coefficient and Q_t is the total charged passed in RCPT, which is expressed in coulombs. Using equation 5-6 the results of RCPT were converted to diffusion coefficient of concrete.

5.5. Comparison of Results for the Relation Between RCPT & Diffusion Coefficient

In order to develop a realistic model, it was necessary to confirm that the relationship developed between total charge passed in RCPT and diffusion coefficient gives realistic results. The results obtained with this relationship were verified with the results of testing observed in the literature [Lu, 2001]. Lu [2001] tested different concrete mixtures and recorded the total charge passed in RCPT for 28 days. Table 5-1 shows the results obtained by Lu [2001].

Table 5-1 Test results for 10 concrete mixtures, performed by Lu [2001].

Mix No.	W/B	Binder			RCPT-28 days
		FA (%)	SF (%)	Slag (%)	(coulombs)
1	0.40	0	6	0	1987
2	0.40	25	6	0	1851
3	0.40	40	6	0	1651
4	0.40	25	0	0	4313
5	0.35	40	0	0	3041
6	0.40	0	6	25	1278
7	0.35	0	0	0	3491
8	0.40	0	0	0	3561
9	0.35	0	0	25	1873
10	0.35	25	0	25	2025

In order to validate the diffusion coefficient calculated with the developed relation, diffusion coefficient obtained from Life365^{TM} was compared with calculated diffusion coefficient. Table 5-2 shows the comparison of the diffusion coefficients. It should be noted that the age of concrete was 28 days at time of comparison.

Table 5-2 Comparison of diffusion coefficient calculated with Life365™ and developed model using Lu's [2001] results.

Mix No.	W/B	RCPT-28 days	Diffusion Coefficient	Diffusion Coefficient	Difference
		(coulombs)	Life365 (m^2/s)	Eq. 5-9 (m^2/s)	% $D_{life365}$
1	0.40	1987	2.96E-12	3.17E-12	26.09
2	0.40	1851	2.96E-12	3.48E-12	17.46
3	0.40	1651	2.96E-12	3.10E-12	4.77
4	0.40	4313	7.94E-12	8.10E-12	2.03
5	0.35	3041	6.03E-12	5.71E-12	5.27
6	0.40	1278	2.96E-12	2.40E-12	18.90
7	0.35	3491	6.03E-12	6.56E-12	8.74
8	0.40	3561	2.96E-12	6.69E-12	15.76
9	0.35	1873	6.03E-12	3.52E-12	41.66
10	0.35	2025	6.03E-12	3.80E-12	36.92

5.6. Discussion of Results for Diffusion Coefficient

After comparing the results from Table 5-2, some difference in the diffusion coefficient was observed. This difference may be explained as:

- The Life365 software uses a relation to calculate diffusion coefficient which is based on the test results of bulk diffusion tests. The curing conditions used for the concrete in diffusion tests were different than the curing conditions used by Lu while testing concrete for RCPT. The curing conditions have an impact on the diffusion coefficient [Hooton et al., 2002].

- Life 365 calculates diffusion coefficient for 28 days based on w/b and amount of silica fume. It accounts for changes due to replacement of fly ash or slag after 28 days time. For instance, in Table 5-2, mix no. 7 and 10 has same w/b although they have different mixture proportions; and based on W/B ratio they have same diffusion coefficient for 28 days time. However in the case of developed model, it uses RCPT value to calculate diffusion coefficient, which is different in case of mixture number 7 and 10. Therefore, another possible explanation for the observed difference might be that, as RCPT is measuring material property at 28 days, it may be accounting for the hydration effects of fly ash or slag on the diffusion coefficient at 28 days, whereas in case of Life365^{TM} no such effect is accounted for the diffusion coefficient at 28 days period. Furthermore, it should be noted that in cases where slag is used, the diffusion coefficients differ more. However, in the absence of any other widely accepted model developed for diffusion calculations, Life365 results has been compared here. Considering the scope of this study the comparison is limited to one set of results obtained by one author only.
- The limitations of the RCPT tests can influence the results. It should be noted that although some of the effect of these limitations are accounted by the correction factor, it does not account for all discrepancies. Furthermore, the single operator coefficient of variation for RCPT test is 12.3% [ASTM C 1202, 1997]. The variation in the RCPT result itself introduces variation in the determination of diffusion coefficient.

Considering the above discussion it can be suggested that more intensive research is required to get more accurate model. The difference in determination of diffusion coefficient was significant in case of concretes with slag. However, for other cases the difference observed was comparatively less. In general the average observed difference in calculations (Table 5-2) was 17% with a standard

deviation of 14%, which was considered as an acceptable difference for this study.

5.7. Evaluation of Parameters Affecting Service Life in Corrosion Model

The corrosion deterioration in bridge decks primarily depends on the amount of chloride ingress. The chloride ingress in concrete depends on many parameters such as clear cover, diffusion coefficient, surface concentration. Therefore, it was important to assess the effect of these parameters on the corrosion deterioration and identify the critical parameters or properties that can be approximated as constant and parameters that need to be considered as variables in the model.

In order to evaluate these parameters, a tool or program that gives the ability to easily change the mixture proportions and can predict the service life influenced by the variation was required. Therefore, Life365^{TM} was selected as the software to assist in the assessment of these parameters. The selection of Life365^{TM} was based on following considerations,

1. This model is easy to use and it provides easy options to change the mixture proportions.
2. This is one of a few chloride diffusion models that evaluate the effect of temperature and the variation in chloride concentration on the diffusion rate of ions.
3. The model is unique in allowing the user to assess the performance of sealers, based in efficiency factors, which are based on testing.
4. Temperature and driving chloride content profiles are defined for various situations in almost every major centre in North America, based on real world chloride data supplied by many local organizations.

Life365^{TM} was developed to predict service life of reinforced concrete structures exposed to chlorides. This section deals with the utilization and the applications of software in consequence with the development of this model.

The assessment of different parameters was based on the results obtained with Life365^{TM} simulations. Different parameters such as, diffusion coefficient (D), time to reach maximum surface concentration (t_{max}), clear cover on reinforcement, surface concentration for chlorides (C_s), corrosion initiation concentration or threshold concentration of chlorides (C_t) were varied as a input in the software for evaluation and their effect on the predicted service life was studied.

5.7.1. Effect of the Diffusion Coefficient (D) on Service Life

To compare the effect of diffusion coefficient on the predicted service life, various simulations of Life365^{TM} were prepared by varying the diffusion coefficient. The software calculates the diffusion coefficient based on the mixture proportions. Therefore, to evaluate the effect of diffusion coefficient it is necessary to understand how diffusion coefficient develops in concrete and how this software adapts itself for this development.

The software calculates diffusion coefficients for the concretes based on two relations, temperature and time dependence of D, respectively [Thomas, 2000]. The time dependence relation for diffusion coefficient takes into account the development due to hydration of concrete with time. D at any time *t* can be calculated as [Thomas, 2000] ,

$$D(t) = D_{ref} \times \left(\frac{t_{ref}}{t} \right)^{m} \qquad \text{Eq. 5-10}$$

where, D(*t*) is the diffusion coefficient at time t, D_{ref} is the diffusion coefficient at some reference time t_{ref} , and m is the hydration decay constant. It should be noted here that reference time of 28 days was used in the Equation 5-7.

Since the time of reference was used as 28 days for calculations, the diffusion coefficient at 28 days (D_{28}) was taken as D_{ref}. However, D_{28} is a function of water to cementatious material ratio (W/CM) and calculated as [Thomas, 2000],

$$D_{28} = 10^{(-12 + 2.40 \cdot w/cm)} \qquad \text{Eq. 5-11}$$

where w/cm is water to cementatious material ratio for concrete. Fig. 5-5 is the graphical representation of the relation between D_{28} and W/CM. This relationship is used in this software to calculate D_{28}. This relationship was developed based on a large number of database of bulk diffusion tests [Thomas, 2000].

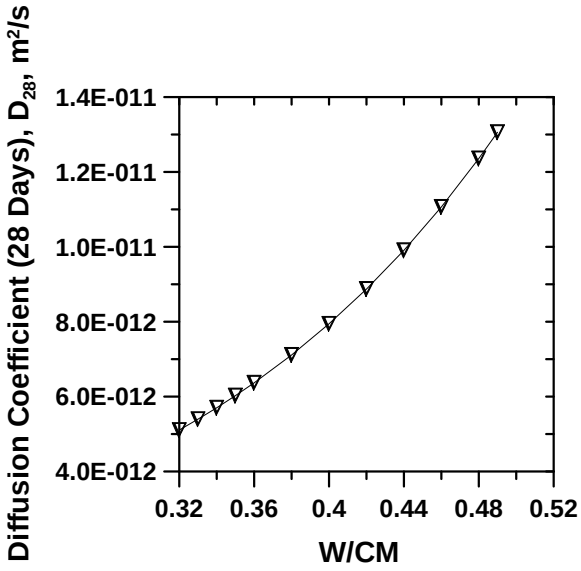

Fig. 5-5 Change in diffusion coefficient at 28 days (D_{28}) with variation in w/c

The parameter m in equation 5-10 accounts the effects of hydration process for plain portland cement. For plain portland cement, value of m is 0.2. This value of m is based on the data from University of Toronto and other published data [Thomas, 2000]. However, when cement is replaced by materials such as fly ash and slag, a modified relationship is used in the software so as to account the reduction in diffusivity due to the replacement of these materials. Therefore, the value of m is modified using the Equation 5-12

$$m = 0.2 + 0.4\left(\%FA/50 + \%SG/70\right) \qquad \text{Eq. 5-12}$$

where, %FA is the percentage of cement replaced by fly ash and %SG is the percentage of cement replaced by slag. Fig. 5-6 shows the effect of variation of m on the diffusion coefficient. Neither fly ash nor slag are assumed to effect the early age diffusion coefficient, D at 28 days [Thomas, 2000]. Therefore, in order to show the effect of m, the diffusion coefficient at 56 days has been presented in this figure. It should be noted here that, this software modifies m only up to the replacement levels of 50 % FA or 70 % SG. (i.e., $m \leq 0.6$).

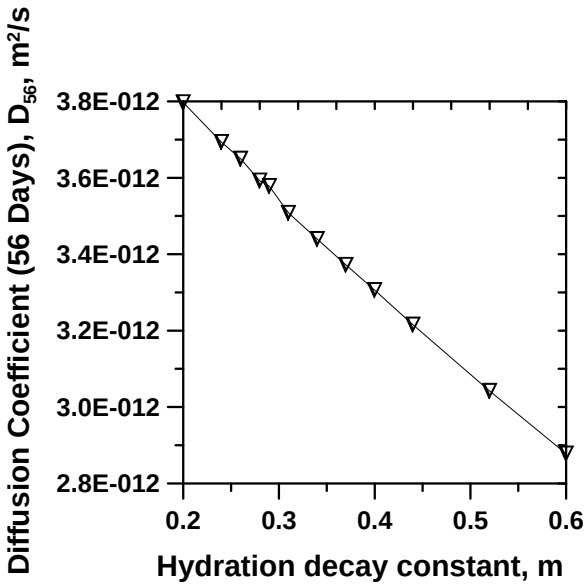

Fig. 5-6 Change in diffusion coefficient at 56 days with variation in hydration constant

When cement is replaced with silica fume, the values of D is modified by the software using the Equation 5-13 [Thomas, 2000].

$$D_{sf} = D_{PC} \cdot e^{-0.1646\,SF} \qquad \text{Eq. 5-13}$$

where, D_{sf} is the diffusion coefficient when cement is replaced by silica fume. D_{PC} is the diffusion coefficient of the concrete with portland cement and SF is the percentage of cement replaced by silica fume. Fig. 5-7 graphically shows the variation in diffusion coefficient as percent silica fume replaced was varied. It should be noted that this software assumes that silica fume will not have any effect on m and Equation 5-13 can be applied only up to replacement levels of 15 % silica fume.

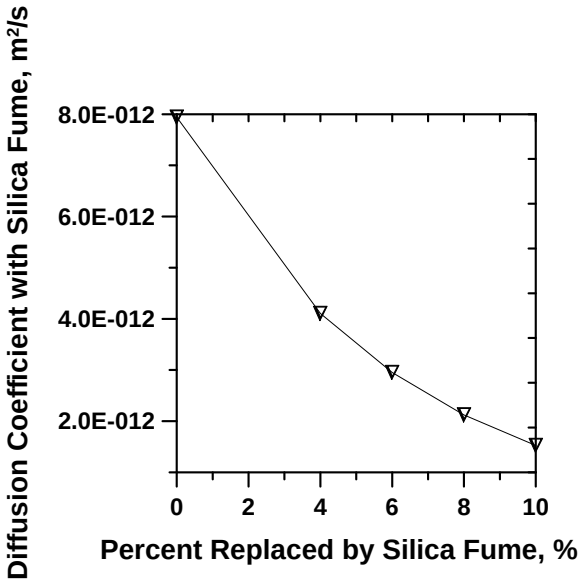

Fig. 5-7 Change in diffusion coefficient when cement replaced with silica (D_{sf}) for w/cm 0.42 with variation of amount of Silica fume replaced

The temperature dependent relationship for diffusion coefficient incorporates the change in diffusion coefficient due to change in temperature. This software has preloaded temperature profiles for cities in North America. In this study while calculating the D values, Indianapolis was selected as a location. Temperature details for this location, already available in software, were used for the calculations. The other constants values, t_{ref} = 28 days and T_{ref} = 293 K (20 °C), were used in Equation 5-14 for calculating the diffusion coefficient, [Thomas, 2000],

$$D(T) = D_{ref} \cdot \exp\left[\frac{U}{R} \cdot \left(\frac{1}{T_{ref}} - \frac{1}{T}\right)\right] \qquad \text{Eq. 5-14}$$

where, D(T) is the diffusion coefficient at time t and temperature T (°K), D_{ref} is the diffusion coefficient at some reference time (t_{ref}) and temperature (T_{ref} °K), U is the activation energy of the diffusion process (35000 J/mol), and R is the universal gas constant.

The effect of D on service life was studied using two sets of simulations. First set with concrete without fly ash, slag or silica fume and second set, with replacement of cement by fly ash, silica fume, slag or their combination (ex. replacement of 15% slag). In both the cases w/cm was varied in the range of 0.32 to 0.49 which resulted in basic variation in D, as per Equation 5-11. It should be noted that replacement of cement by fly ash effects the service life considerably for the same diffusion coefficient. Therefore diffusion coefficient variation based on mix proportion is one of the crucial parameter to be considered in this model.

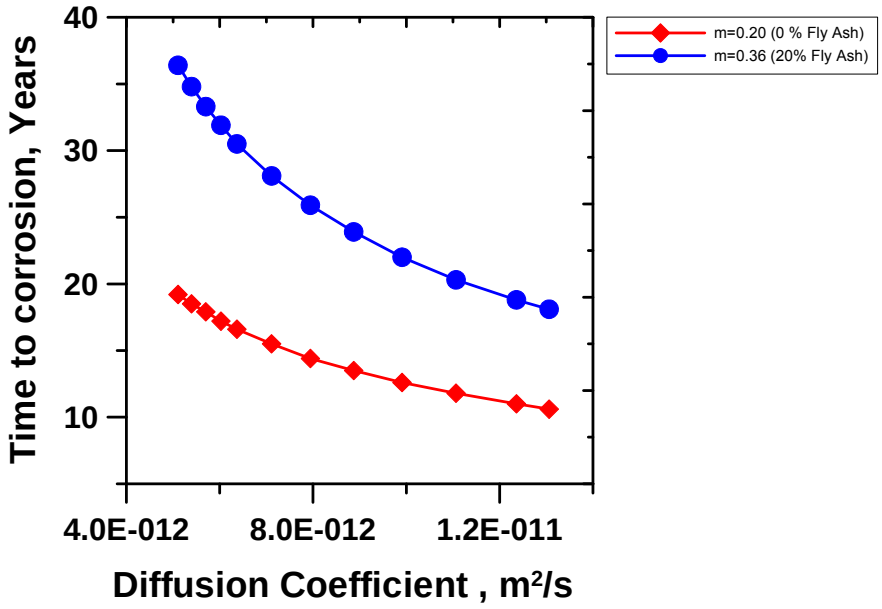

Fig. 5-8 Diffusion coefficient vs time to corrosion for concrete without fly ash (m=0.2) and with 20 % fly ash replacement (m=0.36) of cement respectively

5.7.2. Effect of Cover Variation on Service Life

To evaluate the effect of variation in cover depth on the time to corrosion, simulations were performed with clear cover of 2, 2.5, 3, 3.5 in. While performing this variation other parameters such as w/c, t_{max}, C_t, C_s, mixture proportions were kept constant. It can be seen from Fig. 5-9 that time to corrosion is linearly related to clear cover over the reinforcement. It can be clearly observed that as clear cover increases, time to corrosion increases accordingly.

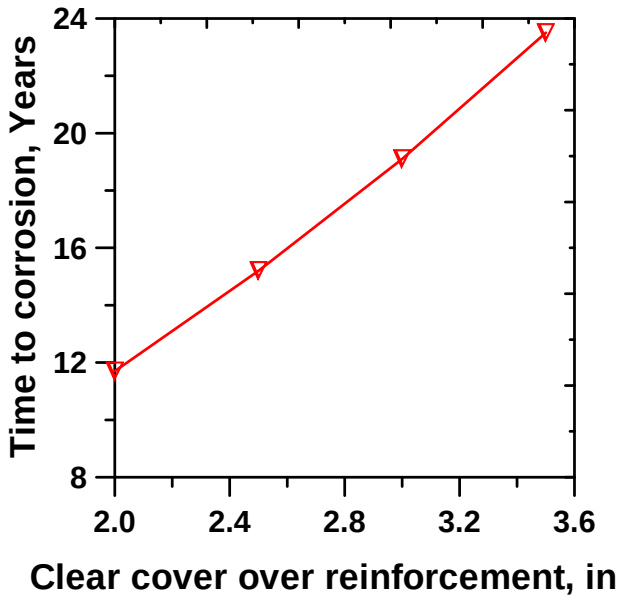

Fig. 5-9 Clear cover Vs time to corrosion

Therefore, it seems that the clear cover over reinforcement needs be included in the model as a crucial parameter. However, for a general case in the state of Indiana for concrete bridge deck, clear cover over the reinforcement is specified to be 2.5 in. As this study is concerned with Indiana bridge decks, the clear cover for single layer bridge deck was approximated to be a constant of 2.5" in this study. Therefore, the simulation for developing the model were performed with a constant clear cover over the reinforcement as 2.5 in. However, for the

case of bridge decks with an overlay, as per information provided by INDOT, a 1 in clear cover over the reinforcement in plain concrete was used.

5.7.3. Effect of Surface Concentration (C_s) Variation on Service Life

Chloride penetration into concrete is a critical issue in the process of corrosion of reinforcing steel bars [Xi and Bazant, 1999]. By far, the primary source of chlorides is the deicing salt used on bridge decks. The amount of deicing salt used varies in accordance with the weather conditions and traffic. As these change with the geographical location, the deicing salt usage change, and in consequence, source of chlorides vary.

Considering the influence of chlorides in the corrosion process it was necessary to evaluate the effect of variation in surface concentration of chlorides on service life of bridge decks. The Life365^{TM} simulations were performed by changing the Cs values, and the effect of variation in Cs was studied on the prediction of service life. It should be noted that other parameters were set to a constant value. It was observed that as the surface concentration increases the service life decreases [Fig. 5-10]. Therefore, it was necessary to consider the surface concentration of chlorides (Cs) as a crucial variable in the development of corrosion model.

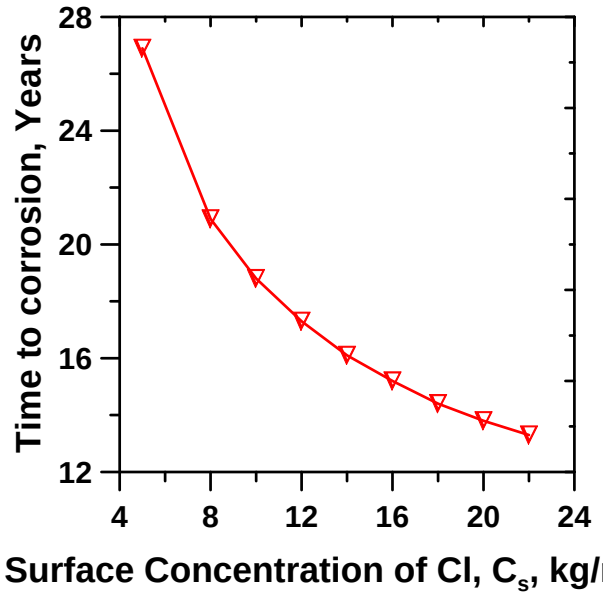

Fig. 5-10 Illustration of effect of variation in Cs on time to corrosion

5.7.4. Effect of Variation in Time to Reach Cs (t_{max}) on Service Life

The chlorides at the surface start accumulating on the surface, as more and more deicing salt is used, and the chloride concentration at the surface keeps on increasing. However, some of the salt gets washed away with time and, when the amount of salt washed out is approximately equal to amount of salt spread, the surface concentration of chlorides remains constant. The time required to reach this state is called as time to reach maximum concentration (t_{max}). In order to evaluate the effect of t_{max} on service life of bridge decks, Life365^{TM} simulations were prepared with other parameters set to constant. It should be noted here that in Life365^{TM} it is approximated that the chloride concentration increases linearly till it reaches a constant value. Fig. 5-11 shows the graphical representation of a typical chloride profile approximated in Life365^{TM}.

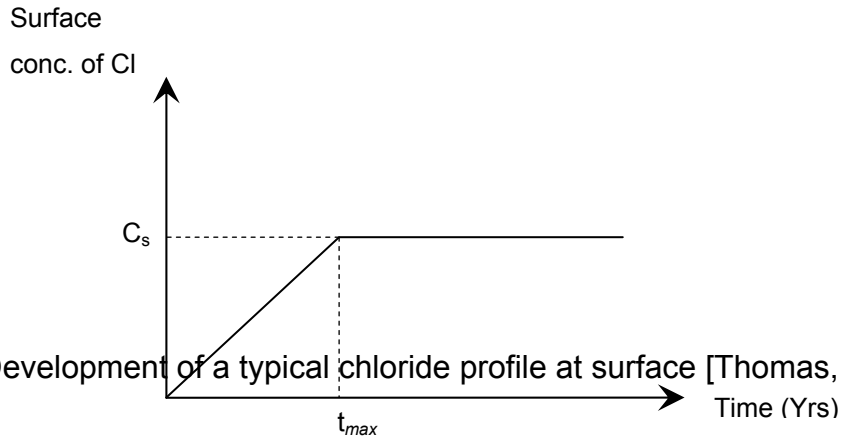

Fig. 5-11 Development of a typical chloride profile at surface [Thomas, 2000]

The software uses 19 years as a default t_{max} setting for the state of Indiana. Generally, the same setting is used for calculating the service life of bridge decks with single layer of concrete. It can observed from the Fig. 5-12 that service life increases as the t_{max} increases. However, it was observed that the slope for this increase was very small in case of bridge decks with single layer of concrete. Therefore it was concluded that change in service life with change in t_{max} is not significant. Thus for simplifying the calculations, in this study the t_{max} was assumed to be a constant value, 19 years.

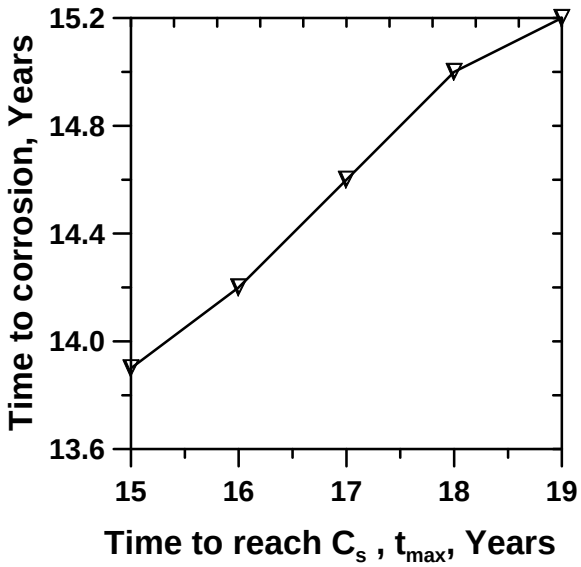

Fig. 5-12 change in time to corrosion for single layer concrete bridge deck with change in time to reach maximum surface concentration

5.7.5. Effect of Variation in Threshold Concentration on Service Life

Chloride concentration required to initiate the corrosion of reinforcement is called a threshold concentration (C_t) or critical concentration. This value is specific to reinforcement used. However, the threshold level can be increased by various protection techniques, such as epoxy coating, calcium nitrite inhibitor (CNI). It is obvious that as C_t increases the time required to reach equivalent concentration at the reinforcement increases and in consequence the service life increases. Therefore it was necessary to evaluate the effect of variation in C_t on the service life. In order to evaluate this parameter Life365^{TM} simulations were prepared with variation in C_t, while other parameters were set to constant values. The results of the simulations are presented in Fig. 5-13. The steep curve as seen in Fig. 5-13 shows the prominent influence of C_t on time to corrosion. However, as per the information provided by the INDOT, generally epoxy coated reinforcement is used in bridge decks in Indiana. Therefore, for the purpose of this study the C_t was set to a constant value of threshold concentration for epoxy coated

reinforcement. C_t = 1.2 kg/m^3 is the default value used by this software for an epoxy coated reinforcement. Also, 0.6 – 1.2 kg/m^3 is the range of C_t suggested in the literature [Kirkpatrick *et al.*, 2002a]. Therefore, in this study C_t was set to a constant value of 1.2 kg/m^3.

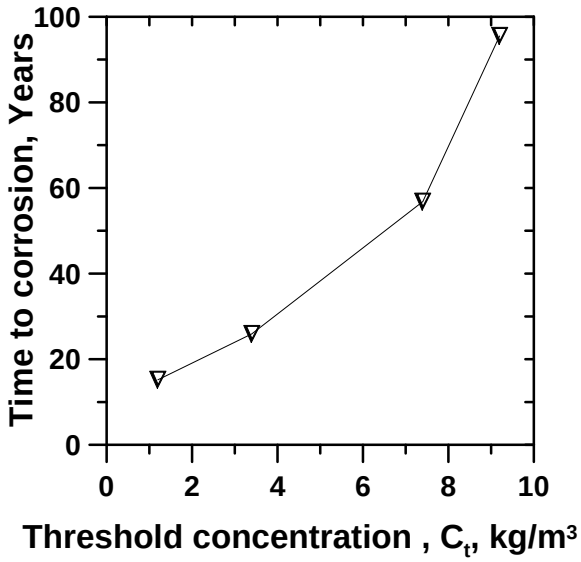

Fig. 5-13 Time to corrosion Vs threshold concentration

5.8. Development of Service Life Prediction Model for Corrosion

The corrosion model has been developed for bridge deck designed as a single layer and deck with an overlay of LMC concrete. When deck was considered as a single layer, four cases with different mixture proportions were considered in the model. These cases have been explained further in this section. In the case of dual layer bridge deck, a latex modified concrete overlay on plain concrete has been considered for development of model. As this case has different boundary conditions, modifications were performed in the process of development that was used for the single layer bridge deck model.

5.8.1. Development of a Corrosion Model for Concrete Bridge Deck

The chloride profile in concrete is assumed to be driven by diffusion mechanism. Therefore the service life prediction model was developed based on diffusion coefficient. For the case of a bridge deck designed as a single layer, the diffusion mechanism can described by Fick's second law shown in equation 5-15 [Crank, 1956].

$$\frac{dC}{dt} = D \cdot \frac{d^2C}{dx^2} \qquad \text{Eq. 5.15}$$

where, *C* is the chloride concentration, *D* is the apparent diffusion coefficient, *x* is the depth from exposed surface where concentration is calculated, and t is the time for which concentration is calculated.

Under the application of specific boundary conditions as discussed in literature review of this study, the solution of Fick's second law (equation 5-15) can be formulated as [Crank, 1956],

$$C_{(x,t)} = C_s\left(1 - erf\left(\frac{x}{2 \cdot \sqrt{D \cdot t}}\right)\right) \qquad \text{Eq. 5.16}$$

where, *t* is the time at the measurement, *D* is the diffusion coefficient of the specimen (sec/m^2), C_s is the surface concentration of chlorides. (kg/m^3), *x* is the depth at which $C_{(x,t)}$ is calculated, and $C_{(x,t)}$ (kg/m^3) is the concentration of chlorides at time *t* at depth x. Nevertheless, considering that the particular interest of this study is to find the service life, the equation 5-16 was solved for t [Schmit, 2005] as,

$$t = \frac{x^2}{4 \cdot D \cdot \left\{erf^{-1}\left[1 - \frac{C_{(x,t)}}{C_s}\right]\right\}^2} \qquad \text{Eq. 5.17}$$

Equation 5-17 enables the time to corrosion initiation to be determined by substituting the threshold concentration of chlorides (C_t) for reinforcement as $C_{(x,t)}$, surface concentration of bridge decks as Cs, and D as the diffusion coefficient of concrete. However, instead of calculating the time to corrosion numerically, in case of this study Life365^{TM} simulation results were used for calculating time to corrosion initiation. It can be clearly observed from equation 5-17 that, the diffusion coefficient is inversely proportional to the time to corrosion (equation 5-18).

$$t \propto \frac{1}{D} \qquad \text{Eq. 5-18}$$

Therefore, a linear relationship was developed between 1/D and time to corrosion from the results obtained with Life365^{TM} simulations, where constants of these relations were expressed as a function of surface concentration of chlorides and mixture proportions.

As discussed in the literature review section [2.3.1] of this study, the service life includes time for initiation of corrosion and propagation time (T_p + T_d). The propagation time is a function of type of reinforcement and the protection provided to it [Kirkpatrick *et al.*, 2002a; Thomas, 2000]. However, In case of this study, as suggested by Thomas in Life365^{TM}, propagation time was taken as 20 years. Therefore, by adding the propagation time to time to corrosion initiation, the service life of bridge decks was calculated.

It should be noted here that, in case of this study, D is always referred to diffusion coefficient at 28 days. For the ease in calculations, as discussed in section 5.7, the clear cover over the reinforcement was set constant to 2.5, C_t = 1.2 kg/m^3 , and t_{max} = 19 years. The w/c ratio was varied in the range of 0.32 to 0.49 (0.32, 0.33, 0.34, 0.35, 0.36, 0.38, 0.40, 0.42, 0.44, 0.46, 0.48, and 0.49)

and surface concentration in the range of 5-22 kg/m^3 (5, 8, 10, 12, 14, 16, 18, 20, and 22 kg/m^3).

In this model the relationship between the time to corrosion initiation and the diffusion coefficient (D) were developed for four cases depending upon the mixture proportion generally used in the field:

1. Concrete without any replacement of cement (m = 0.2)
2. Concrete with cement replaced by fly ash or slag (m > 0.2)
3. Concrete with cement replaced by silica fume
4. Concrete with cement replaced by fly ash and silica fume

5.8.1.1. Case 1: Concrete Without Any Replacement of Cement (m=0.2)

A relationship was developed for concrete with plain portland cement. Life365^{TM} simulations results were used to develop this relationship. The simulations were prepared with varying the surface concentration of chlorides, and variation in w/c. It should be noted that as only plain portland cement was used in this case, (m as a constant of value of 0.2). Considering the inverse relation [equation 5-18], time to corrosion results from simulations were plotted against 1/D. It was observed form Fig. 5-14, that time to corrosion was linearly related to 1/D. This was in support of the relation described in equation 5-18, and expressed in a typical form as,

$$t_1 = \frac{S_1}{D} + C_1 \qquad \text{Eq. 5-19}$$

where, S_1 is the slope of the linear function for case 1, D is the Diffusion coefficient, C_1 is the constant for the linear function for case 1, and t_1 is the time to corrosion initiation for case 1 (m=0.2).

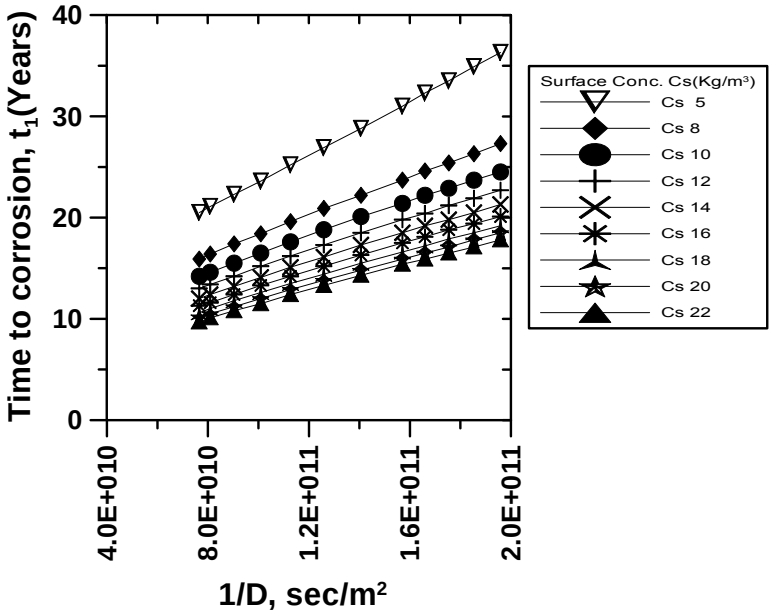

Fig. 5-14 Relationship between time to corrosion and 1/D for variation in Cs (Case1)

Furthermore, it was observed from the results that the linear relations vary their slopes and constants according to the Cs variation. Therefore, to develop the relationship between the slopes (S_1), constants (C_1) and Cs, the S_1 and C_1 were plotted against the Cs respectively (Fig. 5-15 and Fig. 5-16). It was observed from the respective graphs that power function fits the data set. These function were described as (equation 5-20 and 21),

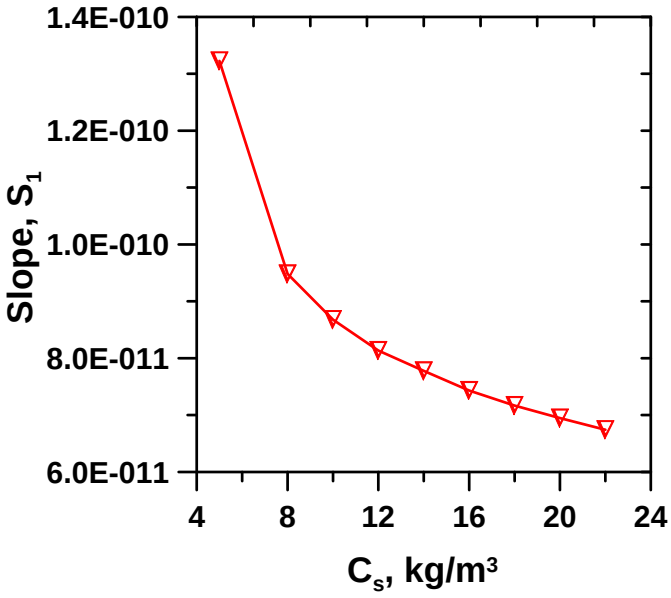

Fig. 5-15 Relationship between slope (S_1) of equation 5-16 and surface concentration of chlorides C_s

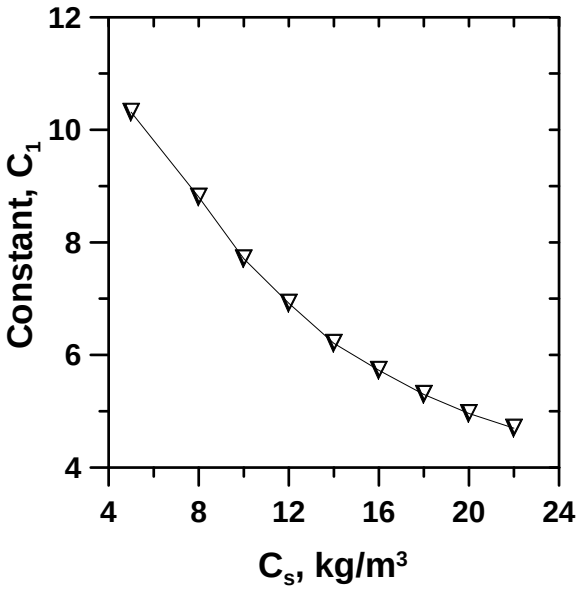

Fig. 5-16 Relationship between constant (C_1) of equation 5-16 and surface concentration of chlorides C_s

$$S_1 = 2.43E-10 \cdot C_s^{-0.427} \quad \text{Eq. 5-20}$$

$$C_1 = 26.785 \cdot C_s^{-0.5562} \quad \text{Eq. 5-21}$$

when S_1 and C_1 were back substituted in Equation 5-19, time to corrosion was expressed as a function of Cs and D (Equation 5-22).

$$t_1 = 2.43E-10 \cdot C_s^{-0.427} \cdot \frac{1}{D} + 26.785 \cdot C_s^{-0.5562} \quad \text{Eq. 5-22}$$

where, t_1 is the time to corrosion initiation for bridge deck with plain concrete. In order to find the service life, a propagation time of 20 years was added to t_1.

Case 2: Concrete With Cement Replaced by Fly ash or Slag (m>0.2)

When cement is replaced by fly ash or slag it impacts the rate of reduction in diffusion coefficient and hence the value of m [Thomas, 2000]. The value of m in that case is greater than 0.2 depending upon the amount of cement replaced and calculated as per equation 5-12. This ultimately affects the diffusion coefficient and increases the time to corrosion initiation. It should be noted here that in the simulations for this case the effect of fly ash or slag is numerically similar, it affects the value of m based on equation 5-12. Therefore, although the figures in this case represent the fly ash replacement, they actually represent case for a particular value of m which may be a result of fly ash or slag replacement. The Life365^{TM} can not simulate m greater than 0.6, and therefore for the development of model simulations with m up to 0.6 were performed. However, it should be noted here that value of m up to 0.6 value can account for practical as well as INDOT specified range of fly ash or slag replacement. The values of m for simulations were selected based on the values of m generally observed in field; and limitations placed by INDOT specification. In this case it was intended to develop a relationship for predicting the time to corrosion in concrete with cement replaced by fly ash or slag. For this, initially considering the inverse relation

between time to corrosion and diffusion coefficient [equation 5-18], time to corrosion obtained from simulations was plotted against 1/D. It was observed form Fig. 5-17, 16, 17, that similar to case 1 time to corrosion was linearly related to 1/D. The relation was expressed as,

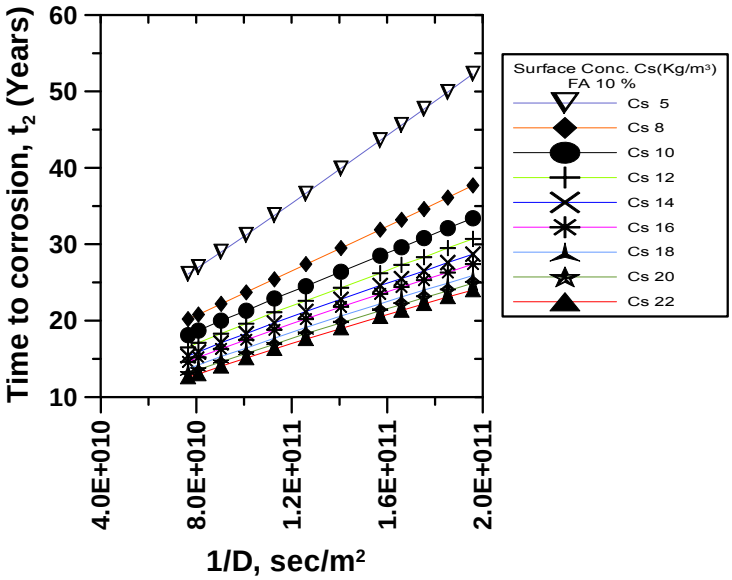

Fig. 5-17 Relationship between time to corrosion and 1/D for 10% FA replacement, m=0.28 (Case 2)

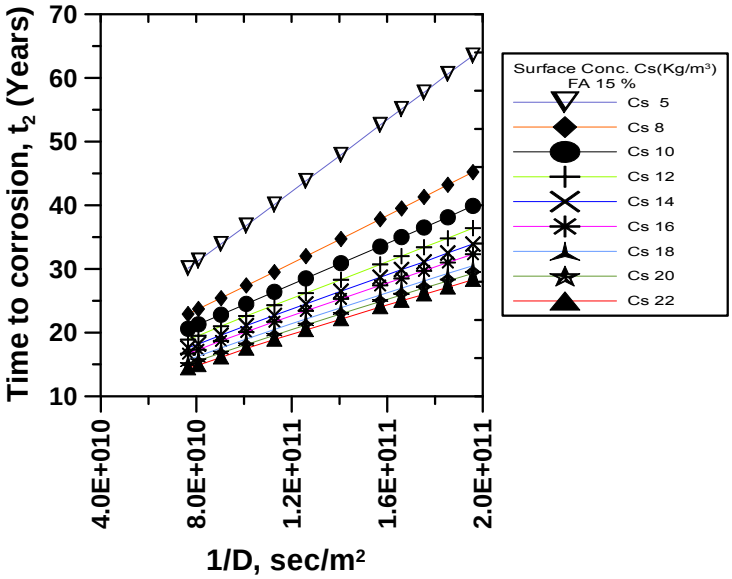

Fig. 5-18 Relationship between time to corrosion and 1/D for 15% FA replacement, m=0.32 (Case 2)

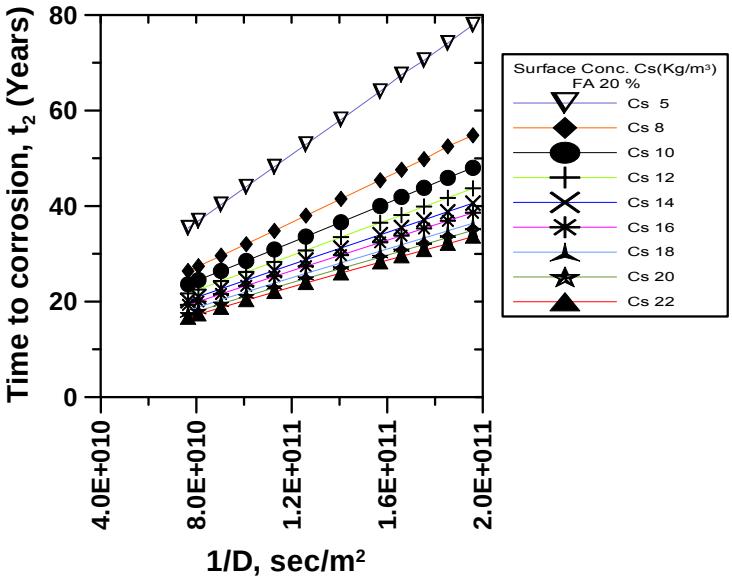

Fig. 5-19 Relationship between time to corrosion and 1/D for 20% FA replacement , m=0.36 (Case2)

$$t_2 = \frac{S_2}{D} + C_2$$ Eq. 5-23

where , S_2 is the slope of the linear function for case 2, D is the diffusion coefficient, C_2 is the constant for the linear function, and t_2 is the time to corrosion initiation for case 2 (m>0.2).

For case 2 it was observed that the slope and constant in Equation 5-23 were function of C_s and m. These functions were evaluated by preparing plots of Slope (S_2) and constant (C_2) against C_s for different values of m (Fig. 5-20 and Fig. 5-21). It was observed that power function fits to express slope as a function of C_s. However, it can be observed from Fig. 5-20 that the data in the practical range of salt application, i.e., 14 to 22 kg/m^3, fits the linear relationship better than power. Furthermore, considering that the salt application in the field will be most likely in the range of 14 to 22 kg/m^3, it was decided to use the linear relation between slope and surface concentration. Furthermore, it was observed that the constant C_2 was related to C_s with a linear equation (Equation 5-24 and Equation 5-25).

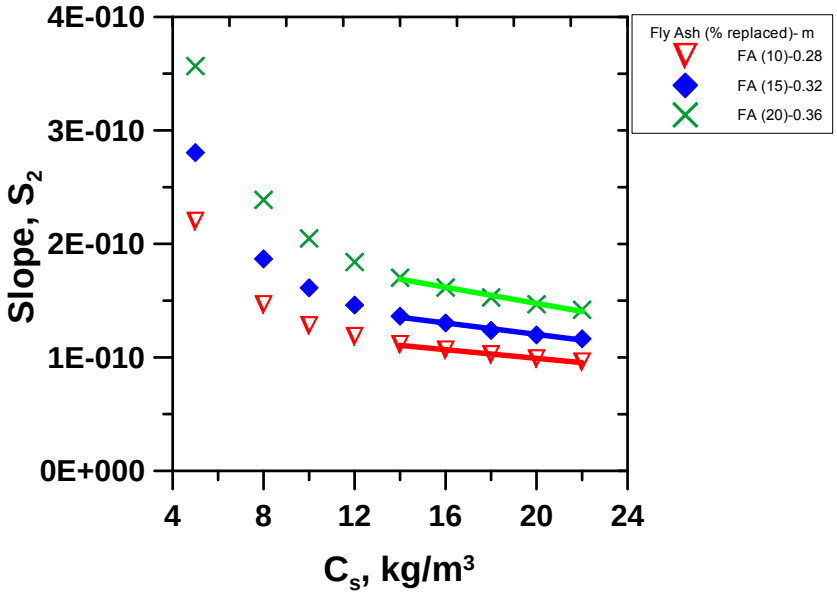

Fig. 5-20 Relationship between slope (S_2) of equation 5-20 and surface concentration of chlorides C_s

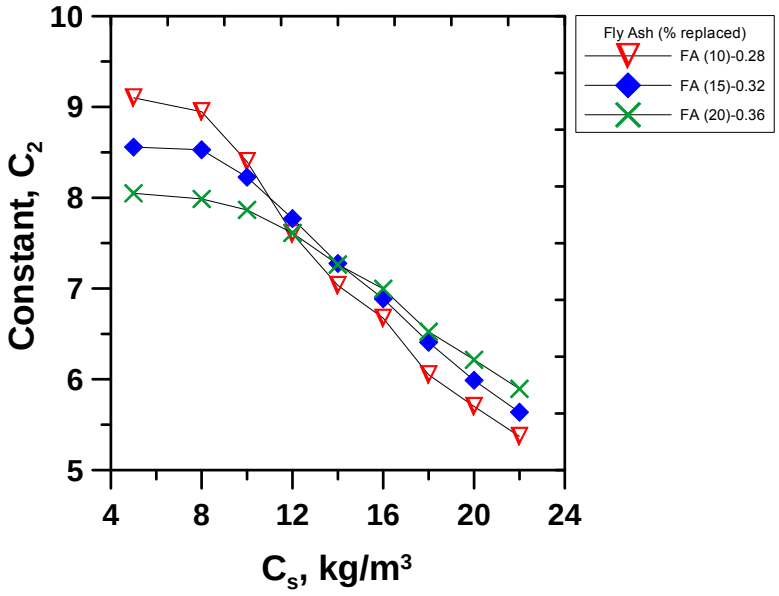

Fig. 5-21 Relationship between constant (C_2) of equation 5-20 and surface concentration of chlorides C_s

$$S_2 = B_{S2} - A_{S2} \cdot C_S \quad \text{Eq. 5-24}$$

$$C_2 = B_{C2} - A_{C2} \cdot C_S \quad \text{Eq. 5-25}$$

where, A_{s2}, B_{s2} are the constants used to define slope (S_2) and A_{c2}, B_{c2} for defining constants (C_2). It was observed that these constants were a function of m. Equations 5-26 to 5-29 show these constants as a function of m. These functions were evaluated using the graphs of these constant against m. The functions used here were selected on the basis of best fit determined using the highest R^2 value for the fit.

$$A_{S2} = 2.05E-11 \cdot (m) - 3.90E-12 \quad \text{Eq. 5-26}$$

$$B_{S2} = 1.02E-9(m) - 1.49E-10 \quad \text{Eq. 5-27}$$

$$A_{C2} = 0.6122 - 1.3188 \cdot (m) \quad \text{Eq. 5-28}$$

$$B_{C2} = 15.9200 - 18.9680 \cdot (m) \quad \text{Eq. 5-29}$$

when S_2 and C_2 were back substituted in Equation 5-23. Time to corrosion was expressed as a function of Cs, m and D (Equation 5-30) and in order to find the service life, propagation time of 20 years was added to t_2.

$$t_2 = [1.02E-9(m) - 1.49E-10] - [2.05E-11(m) - 3.90E-12] \cdot C_S \cdot \frac{1}{D} + [15.92 - 1896(m)] \cdot C_s - [0.6122 - 1.3188(m)] \quad \text{Eq. 5-30}$$

where, m is in the range of 0.2 to 0.6 ($0.2 < m \leq 0.6$).

Case 3: Concrete With Cement Replaced with Silica Fume

The addition of silica fume is known to produce significant reduction in diffusion coefficient of concrete [Thomas, 2000; Zhang and Gjorv, 1991]. Therefore, addition of silica fume was developed as a separate case in this model and

Life365^{TM} simulations were prepared with cement replaced by silica fume. The amount of silica fume replaced was varied as 6%, 8% and 10%. The variation of amount of silica replaced was based on the limits of INDOT specifications and amount generally used in field. The software takes care of the modifications in the diffusion coefficient based on equation 5-13. The results of time to corrosion from simulations were plotted against $1/D_{SF}$ (Fig. 5-22, Fig. 5-23, Fig. 5-24). The D_{SF} was calculated as per equation 5-15. It was observed that the time to corrosion was linearly related to inverse of diffusion coefficient (Equation 5-31). The relation was expressed as,

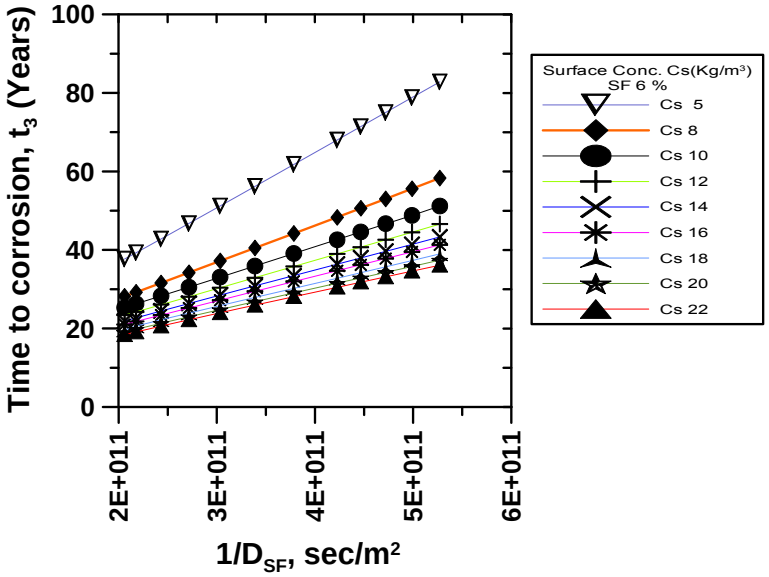

Fig. 5-22 Relationship between time to corrosion and $1/D_{SF}$ for 6% Silica Fume replaced (Case 3)

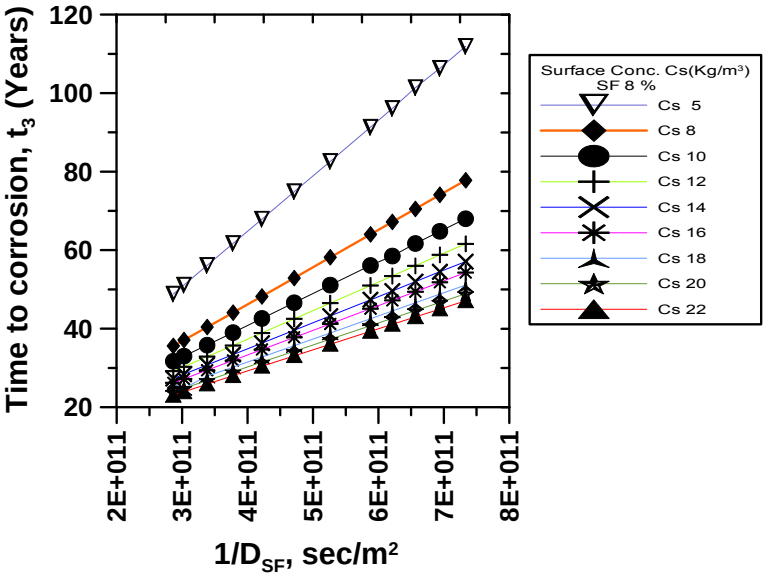

Fig. 5-23 Relationship between time to corrosion and $1/D_{SF}$ for 8% Silica Fume replaced (Case 3)

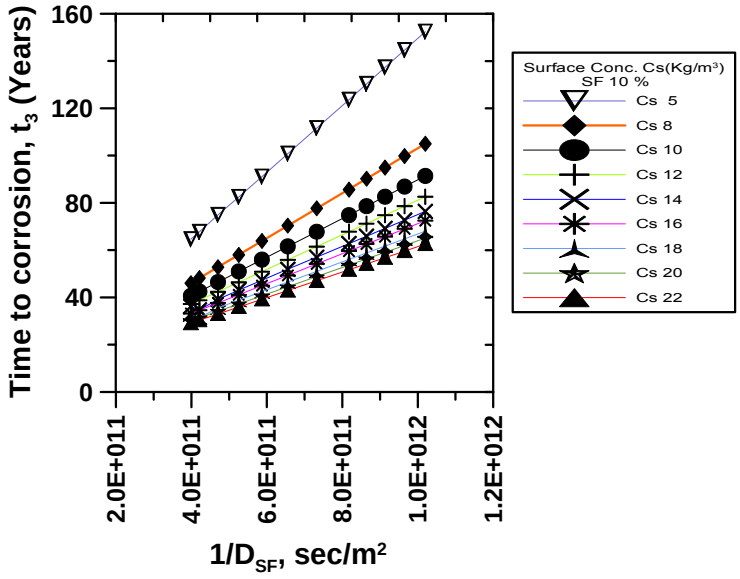

Fig. 5-24 Relationship between time to corrosion and $1/D_{SF}$ for 10% Silica Fume replaced (Case 3)

$$t_3 = \frac{S_3}{D_{SF}} + C_3 \qquad \text{Eq. 5-31}$$

where, S_3 is the slope of the linear function for case 3, D is the diffusion coefficient; C_3 is the constant for the linear function, and t_3 is the time to corrosion initiation for case 3.

It was observed that the slope and constant of linear relation (Equation 5-31) were a function of C_s. The relation between slope (S_3), constant (C_3) and C_s was evaluated by plotting the S_3 and C_3 against C_s (Fig. 5-25 and Fig. 5-26). It was observed from the graphs that the slope was related to C_s with power function. (Equation 5-32), while constant was related to C_s with an exponential function (Equation 5-33). However, as it can be observed from Fig. 5-26, the constant C_3 varies in the range of 8.8 to 7.2 years. For the range of salt application in Indiana, 14 to 22 kg/m^3, this variation is further reduced to 8.3 to 7.2 years for the entire range of silica fume replaced (6%, 8% and 10 %). This variation is approximately 1 year, and also very small compared to the predicted service life for similar concretes. Therefore, the constant C_3 was approximated as a constant value. The value of this constant was taken as the average value of constant for 6%, 8% and 10 % silica fume replacements.

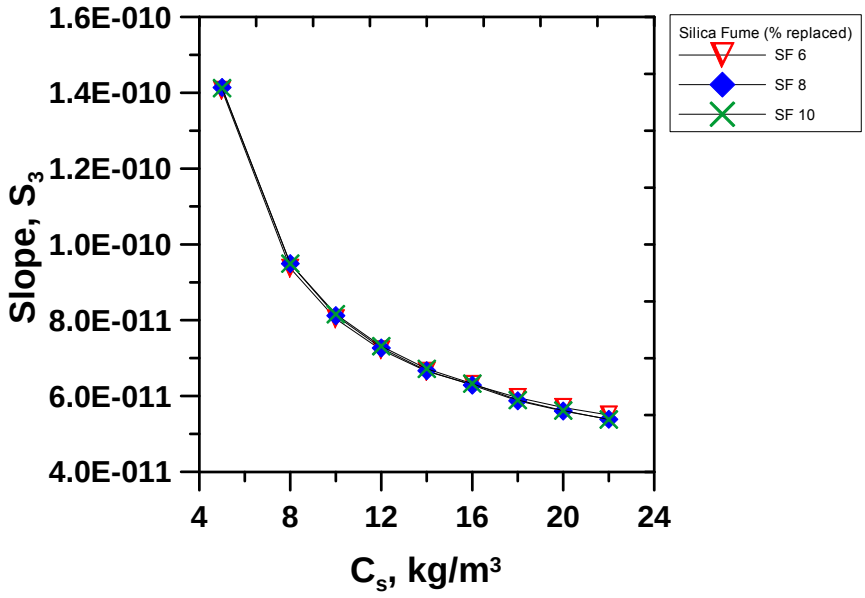

Fig. 5-25 Relationship between slope (S_3) of equation 5-28 and surface concentration of chlorides C_s

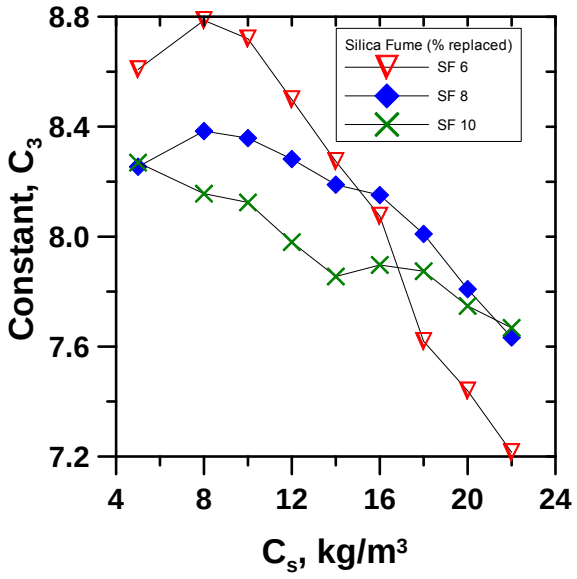

Fig. 5-26 Relationship between constant (C_3) of equation 5-28 and surface concentration of chlorides C_s

$$S_3 = 3.67E-10 \cdot C_S^{-0.639}$$ Eq. 5-32

$$C_3 = 8.07 \ years$$ Eq. 5-33

Finally, back substituting in Equation 5-30 we get.

$$t_3 = 3.67E-10 \cdot C_S^{-[0.639]} \cdot \frac{1}{D_{SF}} + 8.07$$ Eq. 5-34

Case 4: Concrete with Replacement of Cement by Fly Ash and Silica Fume

The addition of silica fume and fly ash both affects the diffusion coefficient of concrete. The effect is a combination of the effect observed separately as discussed before (case 3 and case 2). Simulations with Life365^{TM} were prepared to evaluate this effect on time to corrosion initiation. The simulations were prepared for three mixtures; replacement of silica fume 5%- fly ash 20%, silica fume 5% - fly ash 25%, and silica fume 7% - fly ash 25%. These proportions were selected based on the limitations of INDOT specification and proportions generally used in the field. The results obtained, time to corrosion for each case, were plotted against 1/D (Fig. 5-27, Fig. 5-28, Fig. 5-29). It was observed that there exists a linear relationship between time to corrosion and $1/D_{SF}$.

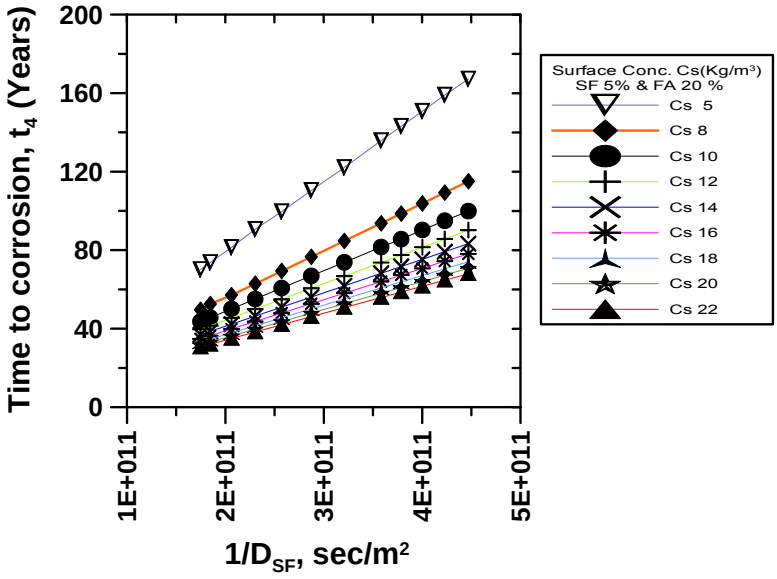

Fig. 5-27 Relationship between time to corrosion and $1/D_{SF}$ for SF 5% - FA 20% replacement (Case 4)

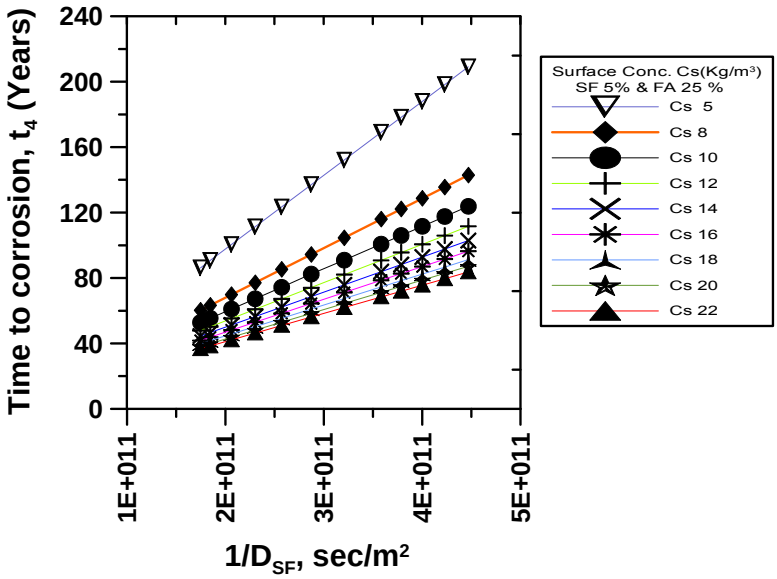

Fig. 5-28 Relationship between time to corrosion and $1/D_{SF}$ for SF 5% - FA 25% replacement (Case 4)

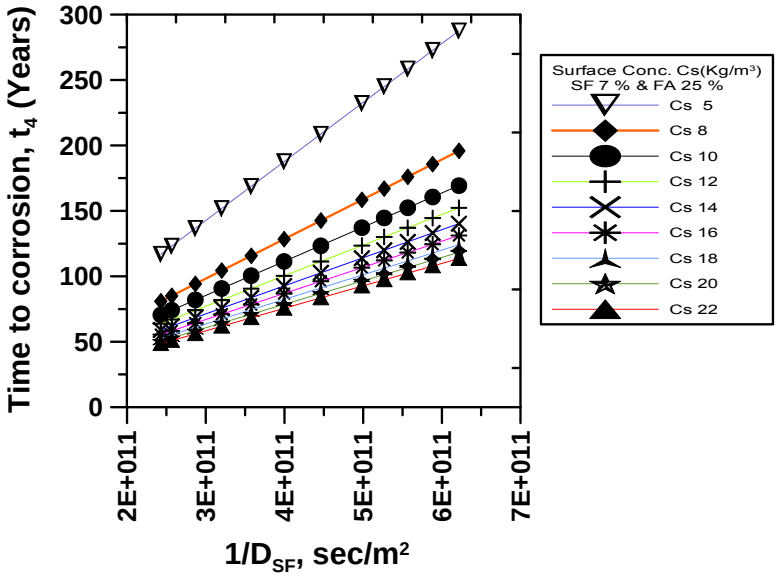

Fig. 5-29 Relationship between time to corrosion and $1/D_{SF}$ for case 3 - SF 7% - FA 25%

$$t_4 = \frac{S_4}{D_{SF}} + C_4 \qquad \text{Eq. 5-35}$$

where, S_4 is the slope of the linear function for case 4, D_{SF} is the diffusion coefficient calculated as per equation 5-15, C_4 is the constant for the linear function, and t_4 is the time to corrosion initiation for case 4.

It was observed that slope (S_4) and constant (C_4) of this relation (Equation 5-35) were dependent on C_s. This dependency was evaluated using the plots of S_4 and C_4 against C_s. It was observed from Fig. 5-30 and Fig. 5-31 that the slope was related to Cs with a power function, whereas constant with a linear relation (Equation 5-36 and 5-37)

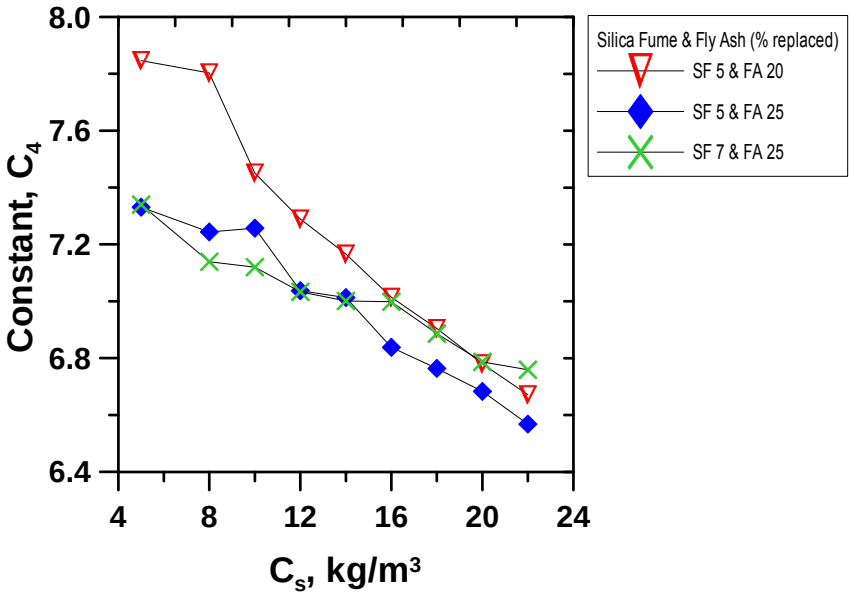

Fig. 5-30 Relationship between constant C_4 and C_s

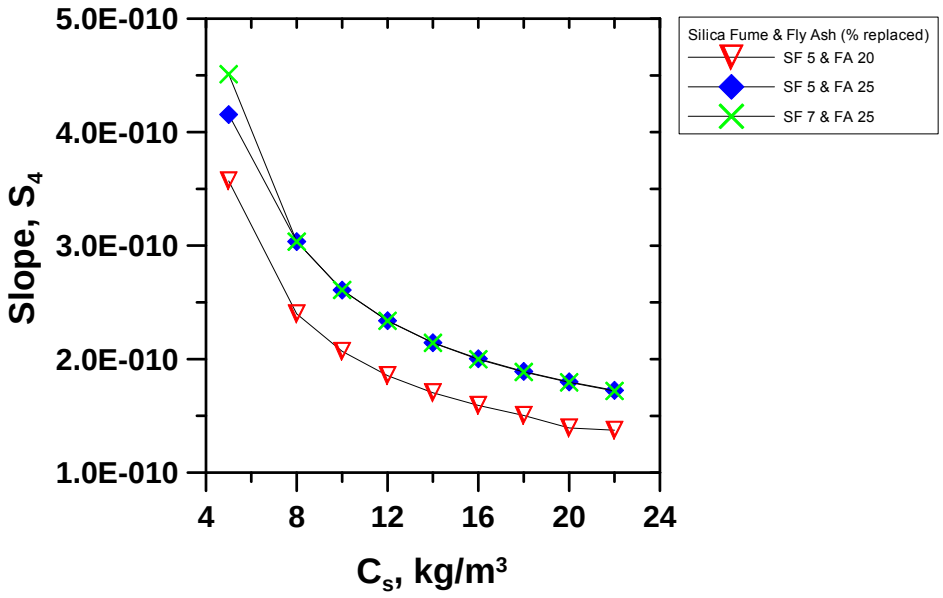

Fig. 5-31 Relationship between slope (S_4) of equation 5-35 and surface concentration of chlorides C_s

$$C_4 = B_{C4} - A_{C4} \cdot C_S \qquad \text{Eq. 5-36}$$

$$S_4 = A_{S4} \cdot C_S^{-0.63} \qquad \text{Eq. 5-37}$$

where, Cs is the surface concentration of salt. It was observed that A_{s4} changes according to amount of replacement. However, as it can be observed from Fig. 5-30, the constant C_4 varies in the range of 7.8 to 6.8 years. This variation is approximately 1 year, and very small compared to the predicted service life for similar concretes. Therefore, constant C_4 was approximated as a constant value. The value of this constant was taken as the average value of constant for the three combinations used in this case, which comes out to be 7 years. Furthermore, it was observed that in this case silica fume and fly ash were replaced together, which made it difficult to find the dependency of A_{s4} on these two independent variables. Therefore, instead of developing a relation, A_{s4} was calculated for each combination. When S_4 and C_4 were separately back substituted in relation for each combination (equation 5-38 – 5-40), the time to corrosion was expressed as a function of Cs and D_{SF}, and in order to predict the service life, propagation time of 20 years was added to t_4.

$$t_4(SF5, FA20) = \left[9.317E-10\right] \cdot C_S^{-[0.636]} \cdot \frac{1}{D_{SF}} + 7.0 \qquad \text{Eq. 5-38}$$

$$t_4(SF5, FA25) = \left[1.044E-9\right] \cdot C_S^{-[0.6]} \cdot \frac{1}{D_{SF}} + 7.0 \qquad \text{Eq. 5.39}$$

$$t_4(SF7, FA25) = \left[1.177E-9\right] \cdot C_S^{-[0.636]} \cdot \frac{1}{D_{SF}} + 7.0 \qquad \text{Eq. 5-40}$$

5.8.2. Development of Corrosion Model for Bridge Deck: Overlay on Plain Concrete

Latex-modified concrete (LMC) has proven to be a reliable method for not only the repair of existing deteriorated bridges and parking structures, but also for protection of new concrete decks [Kuhlmann, 1988]. INDOT has been also using the Latex-modified concrete for bridge decks. Therefore this case was included in the model.

This case, however, is quite different than the 8 in. concrete bridge decks. Since the material properties of LMC and plain concrete are different, the chloride ingress process is different in this case. Therefore, it was necessary to develop a model with a different modeling approach. As this was, in a way, a special case in the general practice; the model was developed for the specific geometry and materials details provided by Indiana Department of Transportation. In this section the model development has been described in three parts; problem description, boundary conditions and solution.

5.8.2.1. Problem Description

This model was developed for a particular case; and therefore, the details of geometry (as provided by INDOT) used in this problem have been discussed here. A 1.5 in overlay of LMC is used on a plain concrete pavement. The clear cover over the reinforcement is 1” from the interface of concrete and LMC. Fig. 5-32 shows the geometry details for the bridge deck, as provided by INDOT. The concentration of chlorides at the interface of LMC and concrete is denoted as C_I, whereas the chloride concentration at the reinforcement, as C_R. D_{LMC} and D_{PC} are the diffusion coefficient for LMC and concrete layer below respectively.

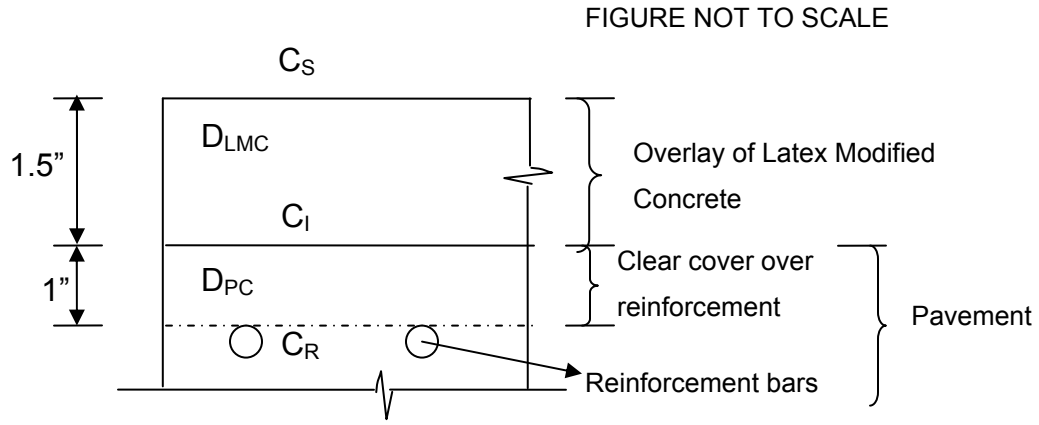

Fig. 5-32 The details of bridge deck where LMC overlay is used [INDOT].

5.8.2.2. Boundary Conditions

Material

Considering that different mixture proportions will be used for an overlay of LMC and concrete layer below, the material properties will be different for LMC and plain concrete. As discussed in literature review of this study, even for same w/c the LMC has lower diffusion coefficient than the plain concrete [$D_{LMC} < D_{PC}$]. The difference in diffusion coefficient voids the assumption of Fick’s second law; diffusion properties in the neighborhood of any point are same relative to all direction [Crank, 1956]. Therefore, the solution of Fick’s second law can not be directly applied in case of this problem. A modeling approach accounting for the difference in diffusion coefficient of LMC and concrete layer below have been described further in this section.

Chloride concentration

In order to predict the service life of bridge deck for corrosion, it is important to understand the chloride penetration in concrete. The chlorides at surface of LMC diffuse through the concrete until the chlorides reach the interface. After the chlorides reach the interface they start diffusing into the plain concrete below until they reach the reinforcement. It should be noted here that the diffusion rate in LMC is less than in plain concrete ($D_{LMC} < D_{PC}$).

The chloride profile that develops in concrete can be explained by considering the chloride concentrations at three locations; at the surface, interface of LMC and plain concrete, and at the reinforcement [Fig. 5-33]. The chlorides at the bridge surface increas as the chlorides from deicing salt accumulate at the surface. The chloride concentration at the surface (Cs) reaches the maximum concentration within t_{max} years as per the profile shown in Fig. 5-11. As chlorides at the surface start accumulating at the surface, some part of chlorides starts diffusing into the 1.5" LMC layer. The chloride concentration at the interface is negligible and practically considered as zero by the time chlorides from surface diffuse up to the depth of interface (i.e., 1.5"). The time taken by chlorides to reach the interface depends upon the diffusion coefficient of LMC. After chlorides reach the interface they start accumulating at the interface and simultaneously some part of chlorides start diffusing below in to plain concrete. The chlorides at interface build up very slowly and reach the concentration equal to surface concentration of chlorides. The time taken by chlorides at the interface to reach equivalent concentration as that of surface is denoted as $T_{max\text{-}int}$ [Fig. 5-33]. Simultaneously, the chlorides diffusing into concrete layer below reach to the reinforcement. As more and more chlorides diffuse into concrete, the chloride concentration at the reinforcement (C_R) starts increasing. When concentration at the reinforcement reaches threshold concentration (C_t=1.2 kg/m^3), the corrosion initiates at the reinforcement. It should be noted here that, as the diffusion coefficient is lower for the LMC than plain concrete, the

concentration at the interface is never higher than the concentration at the surface [$C_s \geq C_l$].

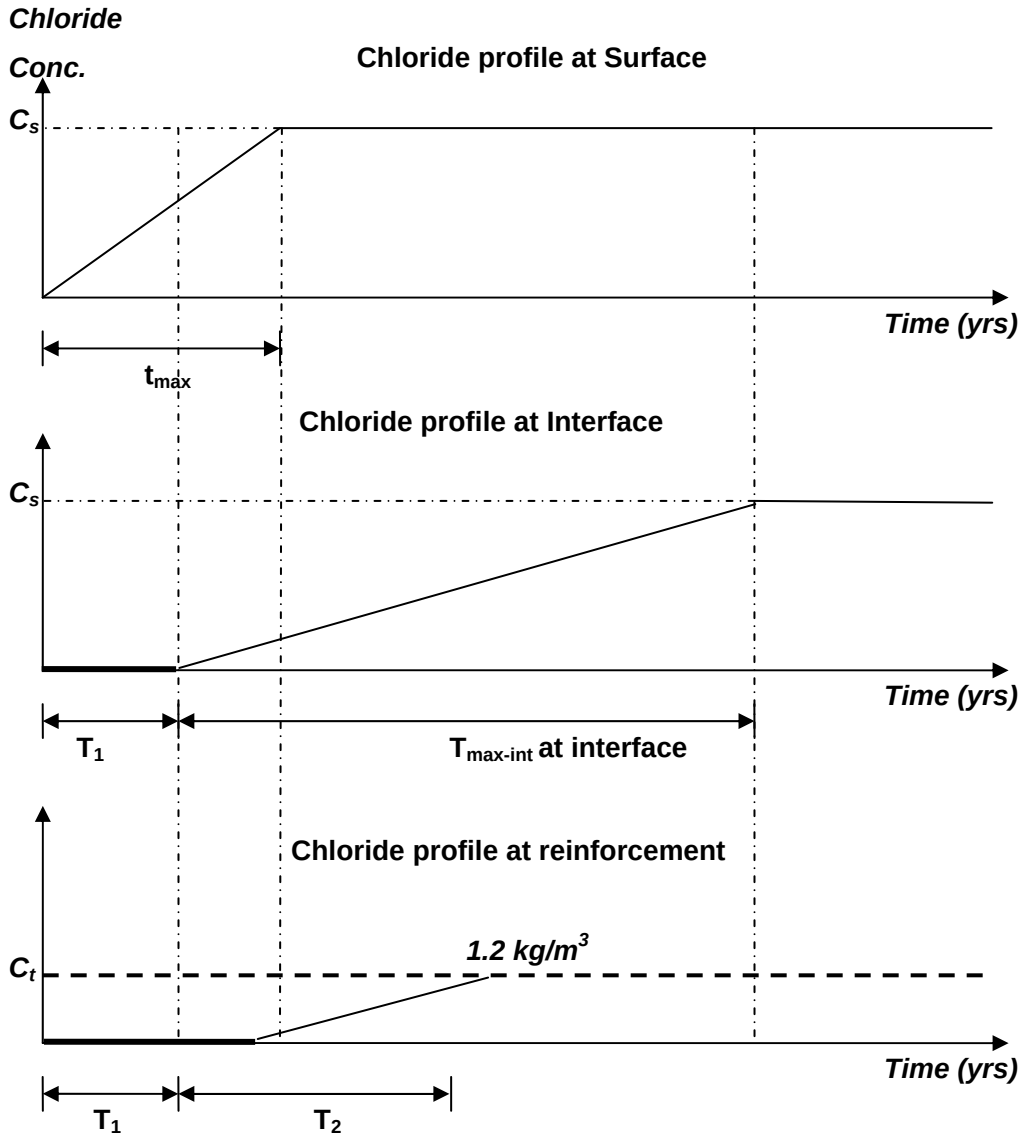

Fig. 5-33 Chloride profile at three locations in a dual layer system of bridge deck

Development of the Model

As discussed earlier in this section, the assumptions of Fick's law does not hold true in this case. Therefore, direct application of the Fick's solution was not

suitable and in order to develop the corrosion model it was necessary to solve the diffusion of chlorides through concrete with different diffusion coefficient. It was speculated that this numerical solution requires tedious calculations and will be time consuming. Nevertheless, another option available was to approximate the calculations of the service life by using Life365^{TM} simulations. As Life365^{TM} uses finite difference method to calculate the solution of diffusion in concrete, the model was developed based on Life365^{TM} simulations with some modification in the inputs. For modifying these simulations and calculations, the understanding of time dependent behavior of chlorides profile was important. The approximate time to corrosion initiation of bridge decks in this case was calculated in two parts.

One, the time required for surface chlorides to diffuse into concrete up to the interface of LMC and plain concrete, and second, the time required, after chlorides reach to interface, to reach the chloride concentration at the interface equal to threshold concentration. The time it takes for chlorides to diffuse through the LMC to reach the interface was denoted as T_1 [Fig. 5-33]. The time taken after chlorides reach interface to time when chloride concentration at the reinforcement reaches threshold concentration was denoted as T_2. Ultimately the service life can be calculated as,

$$Service\ Life = T_1 + T_2 + T_p \qquad \text{Eq. 5.41}$$

where, T_p is the propagation time approximated as 20 years. The development of relations for T_1, $T_{max\text{-}int}$ and T_2 has been explained further in the following section.

5.8.2.3. Development of Relations T_1 and T_{max}

Life365^{TM} simulations were prepared considering two surface concentrations (Cs equal to 10 and 20 kg/m^3 respectively). The diffusion coefficients were varied based on w/c. The chloride concentration at the 1.5 in depth was obtained as a function of time using the time dependent chloride profile developed using Life365^{TM} simulations. Fig. 5-34 shows the chloride concentration at 1.5 in depth from top surface concrete mixtures with different diffusion coefficients (D varied based on w/c). The surface concentration for the concrete shown in Fig. 5-34 was 10 kg/m^3. It was observed that power function was the best fit for these profiles. The time T_1 was calculated based on the time required to accumulate very small amount of chlorides (0.05 kg/m^3) at a depth 1.5 in (i.e., interface of concrete and LMC). It should be noted that the power function was used to calculate T_1.

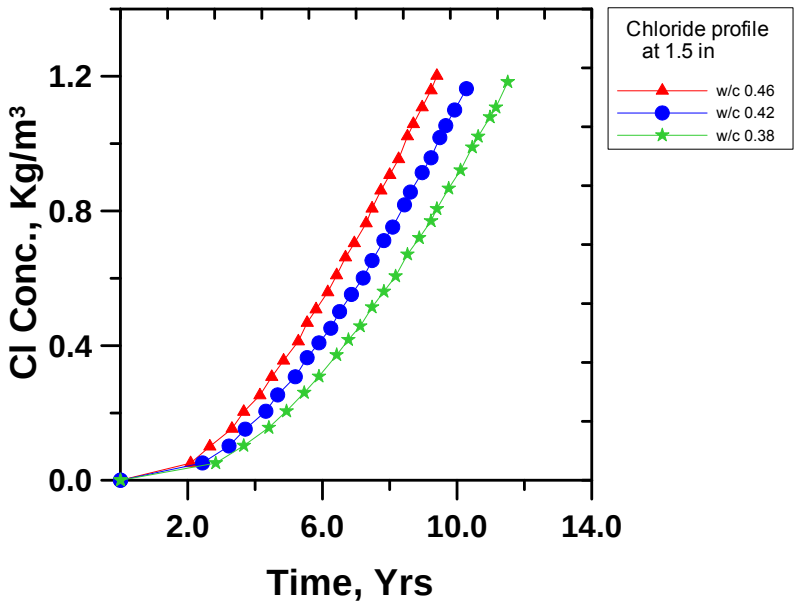

Fig. 5-34 A chloride profile at 1.5 in (interface of LMC and plain concrete), Cs (10 kg/m^3)

A very small variation in the T_1 was observed when the surface concentration was doubled [Fig. 5-35]. Therefore, T_1 was estimated to be independent of Cs, and expressed as a function of only D_{LMC},

$$T_1 = 9.83E-9 \cdot D_{LMC}^{-0.756} \qquad \text{Eq. 5.42}$$

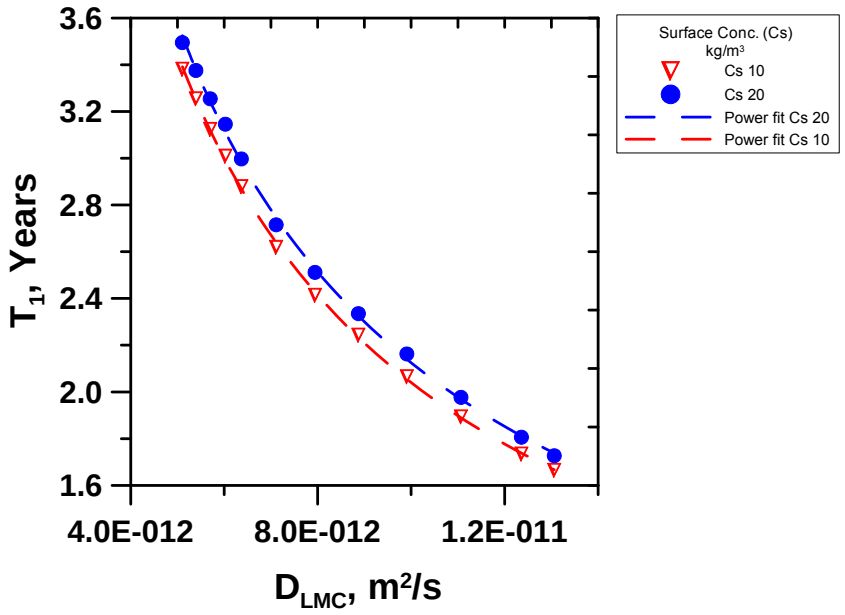

Fig. 5-35 The effect of Variation in Cs on the calculations of T_1

The time to reach chloride concentration equivalent to surface concentration at interface was calculated using the power fit to the chloride profile as shown in Fig. 5-34. However, the variation in the values of $T_{max\text{-}int}$ based on the variation in diffusion coefficient (varied based on w/c) and surface concentration was very small. Table 5-3 shows the variation. However, as it is expressed before, small variation of $T_{max\text{-}int}$ does not affect the time to corrosion initiation significantly [Fig. 5-12]. Therefore, $T_{max\text{-}int}$ was approximated as an average of all values obtained from calculations (values shown in Table 5-3).

$$T_{max-int} = Average\ of\ \ all\ T_{max-int}\ values \approx 32\ years \quad \text{Eq. 5.43}$$

Table 5-3 Variation of $T_{max\text{-}in}$

W/C	$T_{max\text{-}in}$ (Years)	
	Cs 10 kg/m^3	Cs 20 kg/m^3
0.32	33.6	40.6
0.33	32.8	39.1
0.34	32.2	38.1
0.35	31.4	36.7
0.36	30.7	36.6
0.38	29.9	36.3
0.40	28.7	34.5
0.42	27.5	33.2
0.44	26.7	31.9
0.46	26.0	31.6
0.48	25.3	31.4
0.49	24.9	31.3

It should be noted that, the use of Life365^{TM} simulations for developing these relations was based on two assumptions. One, it was assumed that the maximum chloride concentration at the interface can be at the most equal to surface concentration and will never be greater than surface concentration. Two, although the diffusion coefficient of LMC is less than plain concrete, the development of diffusion coefficient with time for LMC is similar to that of plain concrete.

5.8.2.4. Development of Relation for T_2

The chloride profile at the interface was used to calculate T_2. The chloride profile defined by $T_{max\text{-}int}$ and Cs was used to simulate plain concrete with clear cover 1 in. The time to corrosion initiation for these simulations was calculated as T_2. Since this case is similar to the plain concrete bridge deck corrosion model [5.8.1.1], a similar approach was used to develop relationship for this case. A relation between D_{PC} and T_2 was developed as,

$$T_2 = A_{D1} \cdot \frac{1}{D_{PC}} + B_{D1} \qquad \text{Eq. 5.44}$$

where A_{D1} and B_{D1} are constants, which were further found to be a function of Cs and expressed as,

$$A_{D1} = 8.06E-11 \cdot C_s^{-0.42} \qquad \text{Eq. 5.45}$$

$$B_{D1} = 42.134 \cdot C_s^{-0.81} \qquad \text{Eq. 5.46}$$

After back substituting A and B, equation 5-45 was expressed as,

$$T_2 = 8.06E-11 \cdot C_s^{-0.42} \cdot \frac{1}{D_{PC}} + 42.134 \cdot C_s^{-0.81} \qquad \text{Eq. 5.47}$$

Ultimately, the service life of a bridge deck with an overlay was simply calculated using equation 5-41,

$$Service\ Life\ (years) = 9.83E-9 \cdot D_{LMC}^{-0.756} + 8.06E-11 \cdot C_s^{-0.42} \cdot \frac{1}{D_{PC}} + 42.134 \cdot C_s^{-0.81} + 20 \qquad \text{Eq. 5.48}$$

5.9. Results of Corrosion Model

The final goal of this model was to establish a relationship between RCPT results and anticipated service life. Therefore, the results of this model have been presented in the graphical form of anticipated service life (T_{repair}) verses total charge passed in RCPT (Q). To obtain this graph, the relation between RCPT and diffusion (equation 5-6) was combined with the relationship between diffusion coefficient and time to corrosion. The service life (T_{repair}) was obtained by adding the propagation time of 20 years to time to corrosion. An example for each case has been presented using an assumed set of results for RCPT test.

5.9.1. Results & functioning of single layer bridge deck corrosion model

5.9.1.1. Case 1: Concrete without Any Replacement of Cement (m=0.2)

The calculations for the anticipated service life for a concrete with plain concrete have been presented here. The RCPT test result for the concrete was assumed to be 3200 coulombs. The concrete was assumed to be exposed to surface chloride concentration of 15 kg/m^3.

Using the equation 5.21 for t_1 and propagation time of 20 years

$$T_{repair} = t_1 + 20 \qquad \text{Eq. 5.49}$$
$$= 19 + 20$$
$$= 39 \ years$$

Same result has been shown in Fig. 5-36.

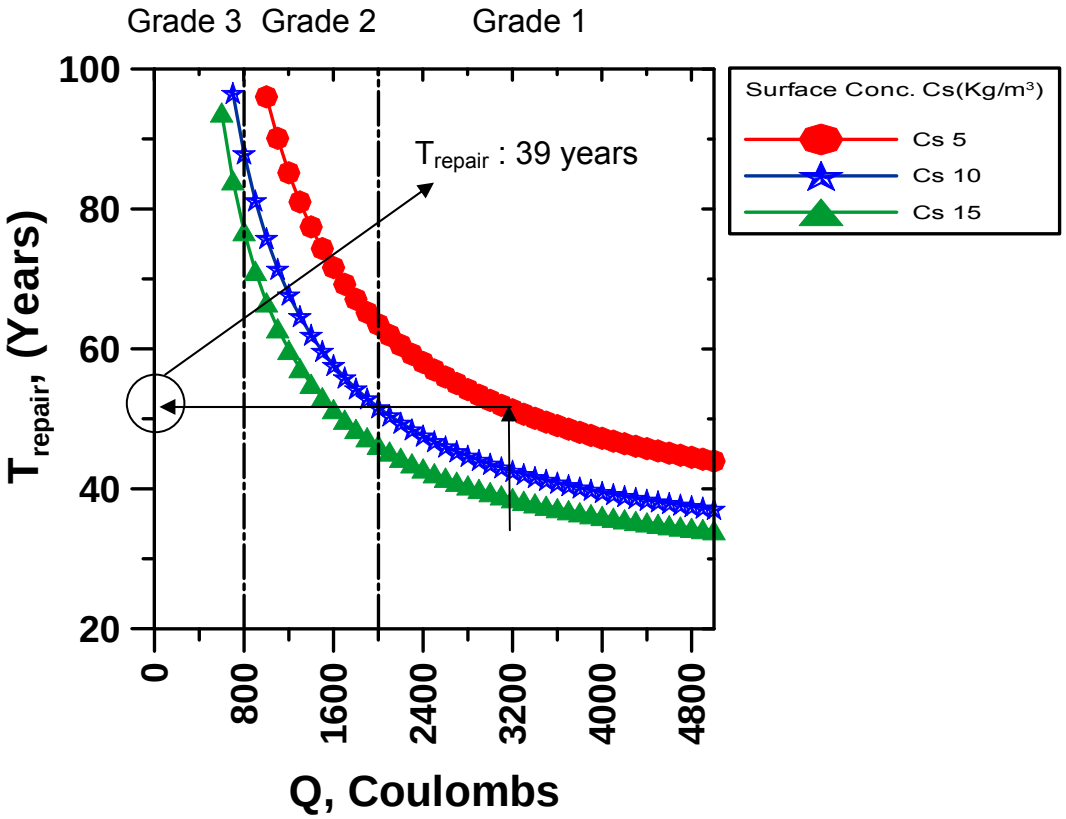

Fig. 5-36 Result of corrosion model for plain concrete

Case 2: Concrete with Cement Replaced by Fly Ash or Slag (m>0.2)

The T_{repair} for this case was a function of m. Therefore, in order to make the results more user friendly, the results have been presented in two steps. In first step, the service life for m=0.28 was calculated using the RCPT results. Then for the mix design with m other than 0.28 (i.e., different combinations of fly ash or slag) the T_{repair} obtained in the first step is multiplied with the multiplying factor (MF) for the respective m value. The multiplying factor was developed by simply dividing the T_{repair} for any other case (m value other than 0.28) with T_{repair} for m=0.28. This process is further illustrated with an example.

The calculations for the anticipated service life for a concrete with a replacement of 20% of the cement by fly ash has been presented here. The RCPT test result for the concrete was assumed to be 3200 coulombs. The concrete was assumed to be exposed to surface chloride concentration of 15 kg/m^3.

Fig. 5-37 shows the service life (T_{repair}) when cement is replaced by fly ash or slag for m=0.28. In order to find the solution for example data, first it was needed to obtain the service life using equation 5.26 & 5.27 for t_2 and propagation time of 20 years,

$$T_{repair} = t_2 + 20 \qquad \text{Eq. 5.50}$$
$$= 22 + 20$$
$$= 42 \ years$$

Same results has been shown in Fig. 5-37.

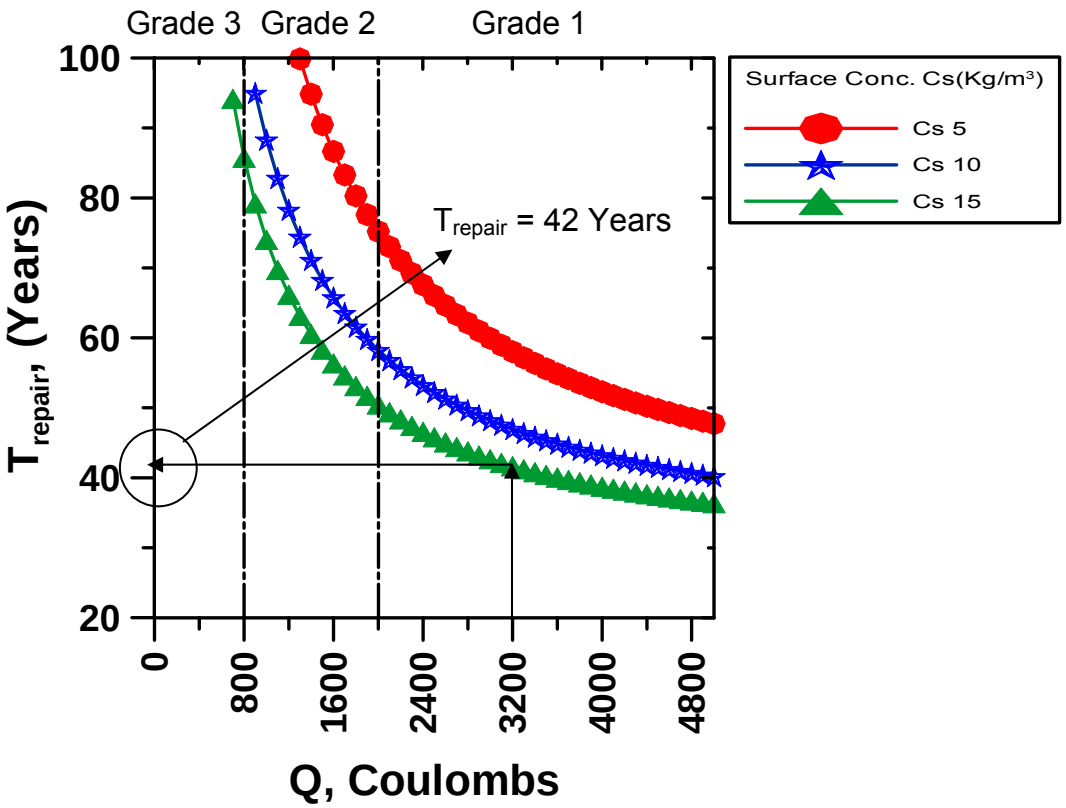

Fig. 5-37 Results of corrosion model for cement replaced by fly ash or slag (m>0.2)

The service life of bridge deck where 20 % fly ash is used can be calculated using the multiplication factor determined based on Fig. 5-38, and equal to 1.50,

Multiplication factor = 1.50

$$\textit{Service life} = \textit{Multiplication factor x } T_{reapir} \textit{ for } m = 0.28 \qquad \text{Eq. 5.51}$$

$$= 1.50 \times 44$$

$$= 66 \textit{ years}$$

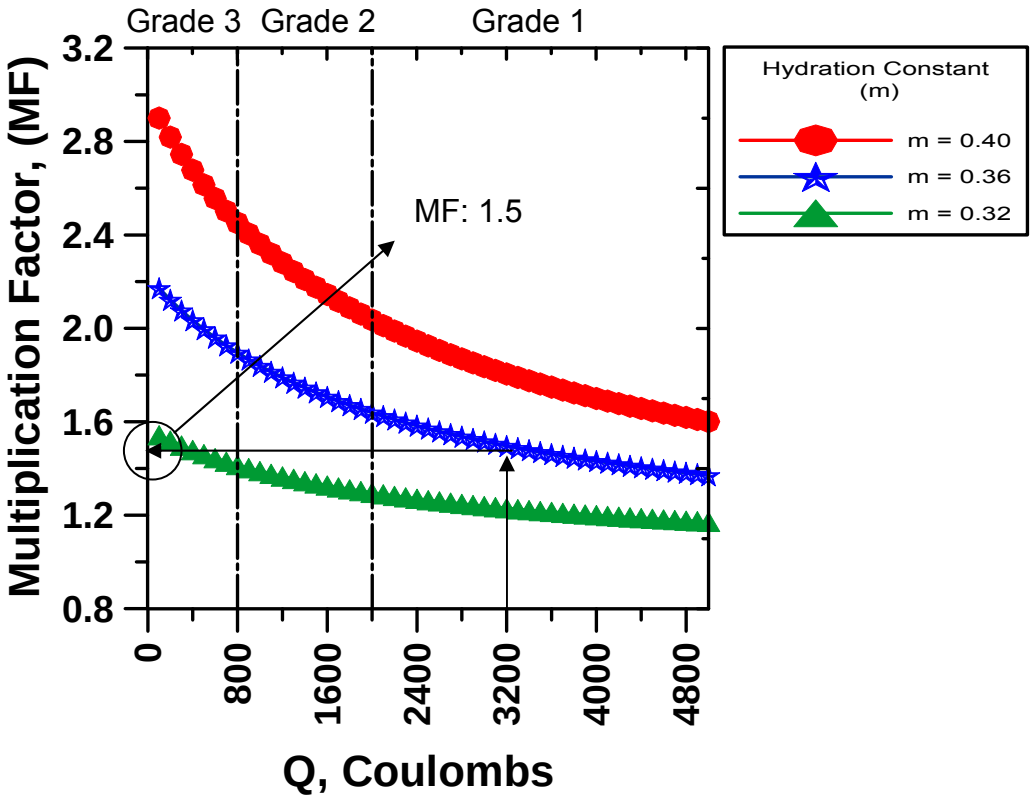

Fig. 5-38 Multiplication factor for corrosion model for cement replaced by fly ash or slag (m>0.2)

Case 3: Concrete with Cement Replaced with Silica Fume

The diffusion coefficient for concrete with cement replaced by silica fume varies with the amount of silica fume used [equation 5-13]. Therefore, T_{repair} varies when percent silica fume replaced is changed. Considering this, results have been presented for different amount of cement replaced by silica fume (6%, 8%, and 10 %). However, in order to make the results more user friendly, the results have been presented in two steps. In first step the service life for concrete with 6 % silica fume replacement was calculated using the RCPT results. Then for the mix design with different amount of silica fume replacement, T_{repair} obtained for 6

% silica fume replacement was multiplied with the multiplying factor (MF). The multiplying factor was developed by simply dividing the T_{repair} for any other case (more than 6% cement replaced by silica fume) with T_{repair} for 6% cement replaced with silica fume. This process is further illustrated with an example.

The calculations for the anticipated service life for a concrete with 8% replacement of cement by silica fume have been presented here. The RCPT test result for the concrete was assumed to be 3200 coulombs. The concrete was assumed to be exposed to surface chloride concentration of 15 kg/m^3.

First, the T_{repair} for concrete with 6% cement replaced by silica fume was calculated using equation 5.6 and 5.34 (for t_3) and propagation time of 20 years,

$$\begin{aligned} T_{repair} &= t_3 + 20 \\ &= 37.49 + 20 \\ &\approx 57 \ years \end{aligned}$$ Eq. 5.52

The same results has been shown in Fig. 5-39.

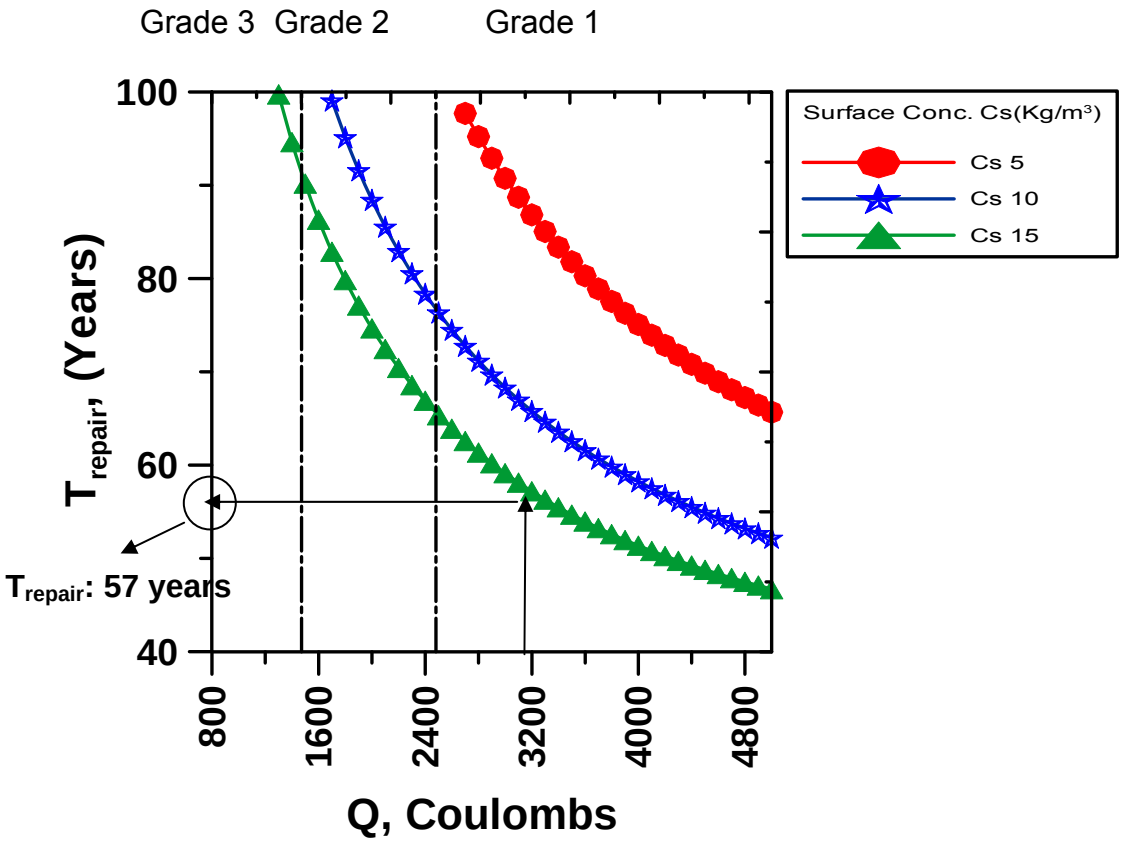

Fig. 5-39 Results of corrosion model for cement replaced by silica fume (SF %)

The service life of bridge deck where 8% cement is replaced with silica fume can be calculated using the multiplication factor. The multiplication factor for 8% cement replaced with silica fume can be determined using Fig. 5-38 as,

$$Multiplication\ factor = 1.23 \qquad \text{Eq. 5.53}$$

$$\begin{aligned} Service\ life &= Multiplication\ factor\ x\ T_{reapir}\ for\ 6\%\ silica\ fume \\ &= 1.23 \times 57 \\ &\approx 70\ years \end{aligned} \qquad \text{Eq. 5.54}$$

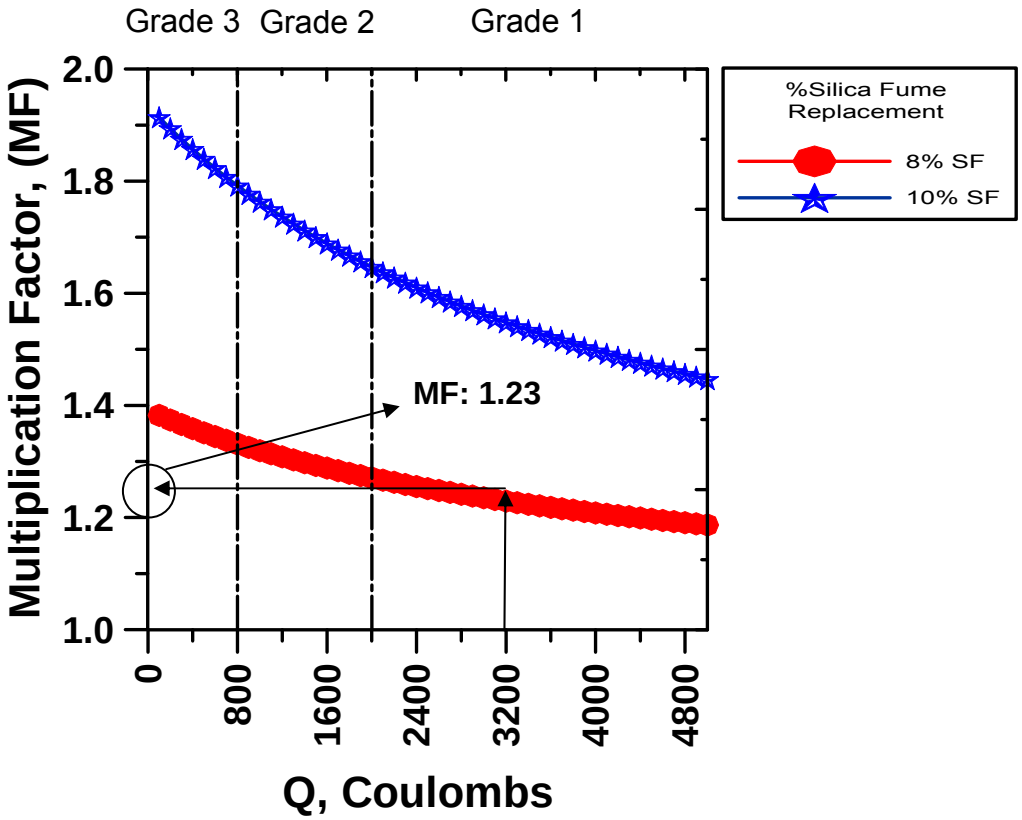

Fig. 5-40 Multiplication factor for corrosion model for concrete with more than 6 % cement replaced by silica fume

Case 4: Concrete with Replacement of Cement by Fly Ash and Silica Fume

The T_{repair} for this case is a function of amount of cement replaced by silica fume and fly ash. Therefore, in this case three graphs were prepared for three combinations. The T_{repair} for any combination can be simply obtained from selecting the appropriate graph for the combination and plotting the RCPT results on the graph. This process is further illustrated with an example.

The calculations for the anticipated service life for a concrete with 5% replacement of cement by silica fume and 20% replacement of cement with fly ash have been presented here. The RCPT test result for the concrete was

assumed to be 3200 coulombs. The concrete was assumed to be exposed to surface chloride concentration of 15 kg/m^3.

In order to find the solution for example data, the service life was needed and was obtained using equation 5.6 & 5.38 for t_4 and propagation time of 20 years,

$$T_{repair} = t_4 + 20 \qquad \text{Eq. 5.55}$$
$$= 34.81 + 20$$
$$\approx 55 \; years$$

Same results has been shown in Fig. 5-41.

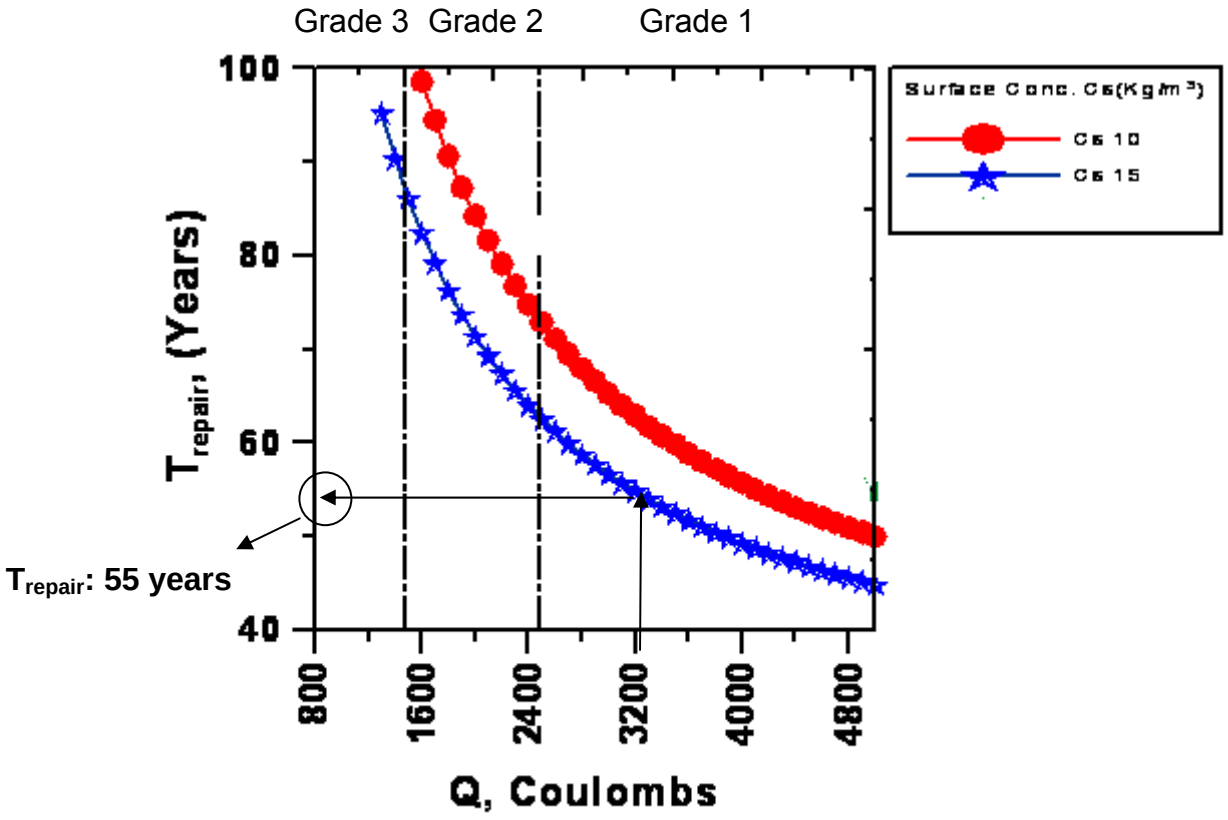

Fig. 5-41 Results of corrosion model for cement replaced by silica fume (SF 5 %) and Fly ash (FA 20 %)

5.9.2. Comparison of Results for Single Layer Bridge Deck Model

In order to check the realistic nature of the prediction, it was necessary to see that the developed model is producing rational results. Therefore, the results obtained with the model were compared with the results obtained from other studies. In this case results were compared in two stages. First, as the model was developed with the Life365^{TM} simulations, the predictions of developed model were compared with the predicted life from Life365^{TM}. In the second stage results were compared with the results obtained in a study performed for a SHRP project [Weyers *et al.*, 1993].

For comparing the results obtained with model to the Life365^{TM} software results, simulations with same input as used in model were performed. The absolute difference between both the prediction, expressed as a percentage of service life predicted by Life365^{TM} was defined as error in the model (Equation 5-49) .

$$Error = \frac{\textit{Prediction with Life365 - Prediction with Model}}{\textit{Prediction with Life365}} \times 100 \qquad \text{Eq. 5-56}$$

Table 5-4 shows the analysis of this error for 4 cases of the single layer bridge deck. It was observed that for first three cases the model predicts time to corrosion with a maximum error of 10%, whereas in case of case 4 it predicts with a maximum error of 15%.

Table 5-4 comparison of the results with Life365^{TM} results for single layer bridge deck

	Case 1	Case 2	Case 3	Case 4
	% Error	% Error	% Error	% Error
Mean	7.94	2.29	2.25	2.41
St. Deviation	1.73	2.00	1.76	2.61

In the second stage the results were compared with the results from a study performed by Weyers et al. [1993]. However, it was observed that the time and temperature dependent development of diffusion was not considered by Weyers et al. [1993]. Also, the surface salt concentration was assumed to be constant from the beginning of service life. These conditions were not same as that used in developed model. Therefore, direct comparison of results would have been inappropriate. For using the similar conditions it was necessary to set diffusion coefficient constant over the time, and in order to achieve that hydration constant (m) should be set to zero. However, considering the nature of model it was not possible to achieve such condition using the developed model. Therefore, in order to overcome this problem it was decided to use Life365^{TM} simulations to compare the results. It is understood here that since the developed model is in close agreement with the Life365^{TM} software, comparing results of Life365^{TM} will be a close approximation for comparing the results of this model. Therefore simulations were prepared with m set to zero and temperature set to constant value of 20 ° C. Also, the surface concentration was set to constant value from the beginning. For comparing the results two sets of calculations were prepared. First, with the calculations similar to as performed by Weyers et. al [1993] in SHRP S 360 project. Second, with results of simulations by Life365^{TM} for similar conditions. For both the cases, clear cover over the reinforcement was taken as 2.5 inches, threshold concentration for corrosion initiation as 1.2 kg/m^3, surface concentration of 5 kg/m^3 constant over time, epoxy coated steel in bridge deck as 2.5 % and constant diffusion coefficient (m=0). Table 5-5 shows the comparison of results from model and the SHRP S 360 study [Weyers et al., 1993]. The diffusion coefficient suggested by Weyers et. al. [1993] for different states was used here for calculations. The error was expressed as a absolute percentage of time to corrosion predicted by SHRP S 360,

$$Error = \frac{\text{Prediction with SHRP S 360 - Prediction with Life360}}{\text{Prediction with SHRP S 360}} \times 100 \qquad \text{Eq. 5-57}$$

This error was observed to be less than 2.5 % and the difference observed is on conservative side (i.e., Life365^{TM} predicts less service life). Therefore, it can be conferred that the Life365^{TM} results are in close agreement with SHRP S 360 [Weyers et al., 1993] results. And as developed model is in close agreement with Life365^{TM}, it will be in close agreement with SHRP S 360 [Weyers et al., 1993].

Table 5-5 Comparison of results obtained with Life365 and relationship developed by Weyers in SHRP S 360

D	Time to corrosion initiation (Yrs)		Difference	Error
10^{-12} m^2/s	SHRP S 360 (a)	Life365(b)	(b) – (a)	%
1.01	45.20	44.8	-0.40	0.88
1.43	32.29	31.6	-0.69	2.12
1.84	25.11	24.7	-0.41	1.64
2.25	20.55	20.1	-0.45	2.17
2.44	18.83	18.5	-0.33	1.77
2.66	17.38	17	-0.38	2.21
5.10	9.04	8.9	-0.14	1.55
6.75	6.85	6.7	-0.15	2.17

In this model the time and temperature dependent diffusion coefficient is used. This technique uses instantaneous diffusion coefficient based on value of m rather than using a constant value and this technique is considered to be more powerful approach [Stanish and Thomas, 2003]. Also, the surface concentration is assumed to vary with time as shown in Fig. 5-11. This is more realistic development of surface concentration in case of a bridge deck. Considering these modifications, the longer time to corrosion given by developed model can be justified.

5.9.3. Results for Overlay Bridge Deck Corrosion Model

The service life in this case was calculated in three parts; T_1, T_2, and propagation time. T_1 is a function of the diffusion coefficient of top layer and was calculated using equation 5-42. T_2 is a function of D_{PC} and Cs. The diffusion coefficient of plain concrete was calculated from its w/c using equation 5-11. Using this

diffusion coefficient and Cs, T_2 was calculated based on equation 5-47. Finally, service life was calculated by adding T_1, T_2, and propagation time of 20 years. This process is further illustrated with an example.

The calculations for the anticipated service life for a dual layer bridge deck have been presented here. The RCPT test result for LMC was assumed to be 300 coulombs. The w/c for concrete was assumed to be 0.42, and the bridge deck was assumed to be exposed to surface chloride concentration of 16 kg/m^3.

In order to find the service life for the above data, first the diffusion coefficient for LMC is obtained with equation 5.11 (Fig. 5-42).

D_{LMC} = 7.50E-12 m^2/s

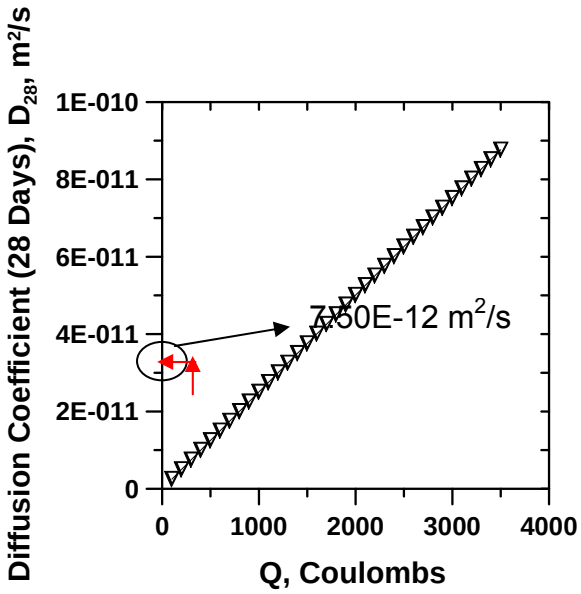

Fig. 5-42 Diffusion coefficient verses RCPT results (Q, coulombs)

From the D_{LMC}, the T_1 can be obtained using equation 5.42,

T_1 = 2.52 years

Same result has been shown in Fig. 5-43

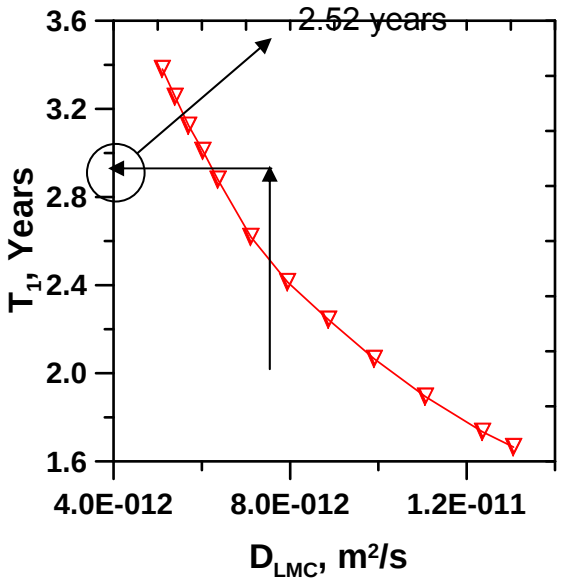

Fig. 5-43 T_1 verses diffusion coefficient of LMC layer

The D_{PC} is calculated using the equation 5-11, and $1/D_{PC}$ = 1.13E+11 m^2/s. Using the equation 5-48, T_2 is calculated for Cs 16 kg/m^3 as 7.28 years [Fig. 5-44]

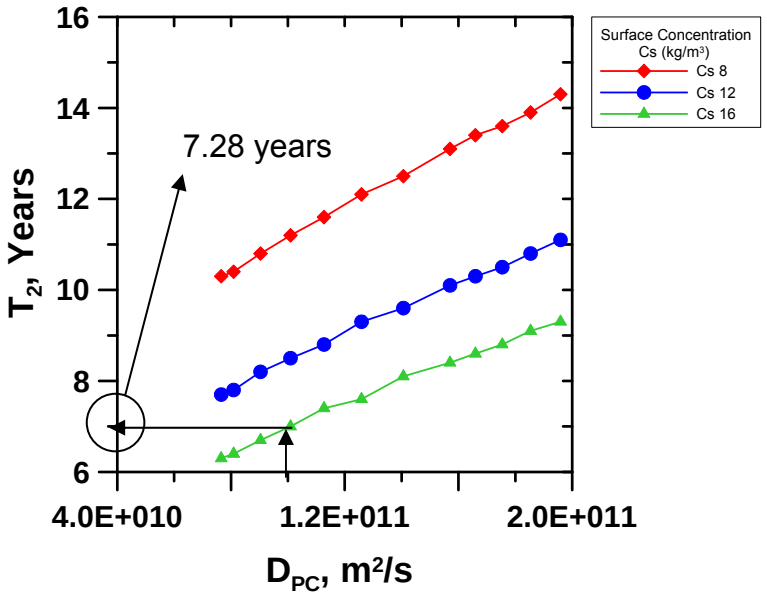

Fig. 5-44 T_2 Vs D_{PC} for variation in surface concentration

Therefore, finally, the service life was obtained using equation 5-49 as,

$$\begin{aligned} Service\ life &= 2.52 + 7.28 + 20 \\ &= 29.8\ years \end{aligned} \qquad \text{Eq. 5.58}$$

5.10. Summary and Conclusions

A model which relates the results of Rapid Chloride Permeability Test to anticipated service life of bridge deck has been described in this study. The relationship was developed in two major parts. First, the results of RCPT were related to the diffusion coefficient. Second, the diffusion coefficient was related to the anticipated service. The Nernst-Einstein equation was used to relate the RCPT results to the diffusion coefficient. The initial current was used in the Nernst-Einstein equation, and a correction factor of 0.75 was used to calculate the initial current from the total charge passed obtained from RCPT. Two bridge deck geometries were considered in this model. First, a concrete bridge deck and secondly, a concrete bridge deck with an overlay of latex-modified concrete.

In plain concrete geometry, four cases with different combinations of cement, silica fume and fly ash have been considered in this model. The results of this model have been compared with the results observed in the literature.

Based on the work performed in this study it was observed that:

- A simple model has been described which can predict the service life for chloride induced corrosion using the results of RCPT test. This model is based on the bridge deck geometries commonly observed in the state of Indiana. The results of the described model were compared to the results obtained with Life365^{TM} and results in a study performed by Weyers et al. [1993]. The comparison of the results indicate a good agreement with a less than 10% difference for considered cases.
- A simplified modeling approach has been presented in case of the concrete bridge deck with an overlay of LMC. However, the relationships described in this case were approximated for a specific case of bridge deck geometry as defined by INDOT. Based on the modeling approach used in study, it was observed that the overlay adds life to original concrete structure below by delaying the initial time (T_1) required for chlorides to reach the original structure, thereby provides a protective layer. Furthermore, it reduces the intensity of chlorides for the original structure by increasing the time to reach maximum surface concentration at the interface ($T_{max\text{-}int}$). It was observed that this initial time required is almost independent of the surface concentration of chlorides and depends entirely on the diffusion coefficient of the overlay. However, the bridge decks with a LMC overlay has not been addressed much in the published work. Therefore, direct comparison of the results could not be performed. It is recommended that further research should be aimed to validate this approach.

CHAPTER 6. DETERIORATION MODEL: FREEZE THAW MODEL

The objective of this chapter is to relate the material properties of concrete to its performance in a freeze thaw environment. A model was used to establish this relationship. Exposure conditions, specific to state of Indiana were used in this model. The model described in this chapter is based on the work performed by Fagerlund [2004].

This chapter begins with a description of boundary conditions used in this model to predict the service life of concrete in freeze thaw environment. Service life is described using a two part model that describes the time it takes for damage to initiate and the time it takes that damage to propagate. Section 6.1 describes this two part model. Section 6.2 and 6.3 describe the role of material properties such as porosity, critical saturation and sorptivity in the development of relationship used in this model. Section 6.4 summarizes the measurements typically observed in the literature for the different parameters used in this model. An attempt has been made to provide an assessment on how these parameters can be approximated for their application in the model. Typical calculations representing the use of this model have been illustrated in section 6.5. A comparison of results of the model predictions and predictions of CONCLIFE software or experimental data from literature is presented in section 6.6. Finally, the chapter ends with conclusions and suggestions for future work.

6.1. Service Life Under Freeze Thaw Deterioration

The service life of bridge decks can be defined as the time required for a structure to reach the user specified damage level. The damage level (D) can be

defined as either a loss of strength, degradation of stiffness (elastic modulus), or permanent expansion. It is observed that in case of freeze thaw deterioration the damage (D) is generally defined by the relative reduction in dynamic modulus of elasticity [Fagerlund, 2004],

$$D = \frac{\Delta E}{E_0} \qquad \text{Eq. 6.1}$$

where, ΔE is the reduction in the of dynamic modulus at the time of measurement and E_0 is the initial dynamic modulus (i.e., at 0^{th} freeze thaw cycle).

Service life can be divided in to two parts. First, the time required to initiate the freeze thaw damage ($Life_{init}$), and second, the time required to damage propagation ($Life_{sec}$).

$$Service\ life = Life_{init} + Life_{sec} \qquad \text{Eq. 6.2}$$

In this chapter a relationship has been developed for each of these two parts.

6.2. Development of Model for $Life_{init}$

The damage initiation part of this model was discussed in the literature review of this study [section 2.4.5]. In this work, a model was implemented to calculate the time required for damage initiation ($Life_{init}$). Several material properties were used in the development of this model.

6.2.1. Material Properties Related to damage initiation ($Life_{init}$)

Fagerlund [2004] showed that in order to calculate the time for damage initiation ($Life_{init}$) information is needed about porosity, sorptivity, critical saturation of concrete, and exposure conditions [Fig. 2-4]. Critical saturation, as described in section 2.4.3, is a material property itself [Fagerlund, 1999]. The variation in saturation of concrete can be calculated using the amount of water absorbed by concrete over time and volume of voids in concrete. The amount of water absorbed by concrete depends mainly on the sorptivity of concrete and the duration that the concrete is exposed to water. The details about sorptivity can be found in the literature review of this study [section 2.4.6]. The volume of voids in the concrete can be written as,

$$V_v = V_p + V_{air} \qquad \text{Eq. 6.3}$$

where, V_v is the total volume of voids in concrete, V_p is the volume of pores (capillary and gel) and V_{air} is the volume of entrained air.

6.2.2. Development of Actual Saturation in Concrete

The actual level of saturation in concrete varies with time based on the exposure history and the duration of wetting and drying events. The actual saturation of concrete at any given time (t) can be defined as,

$$S_{Act} = \frac{V_w}{V_v} \qquad \text{Eq. 6.4}$$

where V_w is the water in concrete at the time of measurement. The volume of voids may change with hydration; however, this change is relatively small for most mature concretes. Therefore, for this study the volume of voids measured

at 28 days has been assumed to remain constant with time. The water content in concrete (V_w) can be described as,

$$Vw = (Vw_{\text{int}}) + (Vw_{abs}) \quad \text{Eq. 6.5}$$

where, Vw_{int} is the initial water in concrete before concrete starts absorbing water through wetting events and Vw_{abs} is the water absorbed in wetting events. The initial water present in concrete only occupies a certain volume of capillary pores. Generally, capillary pores are not saturated in their initial condition. As concrete is exposed to water, it absorbs water. The porosity in the concrete begin to fill. Therefore, the absorbed water can be divided as,

$$Vw_{abs} = V_{abs-P} + V_{abs-air} \quad \text{Eq. 6.6}$$

where, V_{abs-p} is the absorbed water necessary to fill the capillary pores and $V_{abs-air}$ is the absorbed water necessary to fill the air void system.

The volume of water absorbed in a wetting event is dependent on the sorptivity of concrete and the duration of wetting event. It is well understood that the sorptivity changes over time [ASTM C 1585, 2004]. The time at which the sorptivity of concrete change is called as the nick point time. The sorptivity before nick point time (initial sorptivity) is higher than the sorptivity after nick point time (secondary sorptivity).

The absorbed water in any wetting event can be described as

$$Vw_{abs} = Vw_{IA} + Vw_{SA} \quad \text{Eq. 6.7}$$

where, the Vw_{IA} is the water absorbed during the initial sorptivity period (until nick point time) and Vw_{SA} is the water absorbed during the secondary sorptivity period (after nick point time).

Using the measurements of absorption with time, the water absorbed till nick point can be described as,

$$Vw_{IA} = \frac{A}{\rho}(I_n) \qquad \text{Eq. 6.8}$$

where, A (mm^2) is the area of the specimen exposed to water and ρ (g/mm^3) is the density of water. I_n is the initial absorption measured till nick point time. When the initial absorption (I_n) is expressed as a function of time and sorptivity [equation 2-5], Vw_{IA} can be explained as,

$$Vw_{IA} = \frac{A}{\rho} \cdot \left(S_i \sqrt{t_{nickpt}} + b\right) \qquad \text{Eq. 6.9}$$

where, b is the constant, and S_i is the initial sorptivity calculated from ASTM C 1585 [2004], and t_{nickpt} is the nick point time. Furthermore, for a unit area exposed to water and density of water equal to 1 g/mm^3, the volume of initial absorption can be obtained as,

$$Vw_{IA} = \left(S_i \sqrt{t_{nickpt}} + b\right) \qquad \text{Eq. 6.10}$$

where, S_i is measured in $mm/s^{0.5}$ and b is measured in mm. However, equation 6-10 only describes the water absorbed during first few hours (i.e., till t_{nickpt}) in a wetting event till nick point time. The total water present in concrete at the nick point can be obtained by adding the initial water.

$$Vw_{nickpt} = Vw_{\text{int}} + S_i\sqrt{t_{nickpt}} + b \qquad \text{Eq. 6.11}$$

where, Vw_{nickpt} is the total water content at nick point time. The sorptivity changes after the nick point. The water absorbed after nick point can be described as,

$$Vw_{SA} = \frac{A}{\rho} \cdot S_S\sqrt{t_s} \qquad \text{Eq. 6.12}$$

where, A (mm^2) is the area exposed to water and ρ (g/mm^3) is the density of water. S_s is the secondary sorptivity as calculated from ASTM C 1585 and t_s is the time period after nick point time. The t_s can be obtained as,

$$t_s = t_t - t_{nickpt} \qquad \text{Eq. 6.13}$$

where, t_t is the total duration of time (seconds) concrete is exposed to water. The total water in concrete at time t_t for unit area exposed to water of density 1 g/mm^3, can be described by adding the water present at nick point and water absorbed after nick point,

$$Vw = Vw_{\text{int}} + S_i\sqrt{t_{nickpt}} + b + S_s\sqrt{t_s} \qquad \text{Eq. 6.14}$$

Using equation 6-14 the total volume of water in concrete can be obtained at any time. Therefore, the saturation of concrete can be determined at any time of by dividing the water present in the system by total volume of pores (capillary and gel) and volume of entrained air. The saturation of concrete at any time can be expressed as,

$$S_{Act} = \frac{Vw_{\text{int}}}{V_p + V_{air}} + \frac{S_i\sqrt{t_{nickpt}} + b}{V_p + V_{air}} + \frac{Ss\sqrt{t_s}}{V_p + V_{air}}$$ Eq. 6.15

However, it should be noted that generally the volume of pores and air is expressed as a percentage of total volume. Therefore, for a unit area exposed to water, actual saturation can be described as,

$$S_{Act} = \frac{Vw_{\text{int}}}{\%\left(V_p + V_{air}\right)\cdot D} + \frac{S_i\sqrt{t_{nickpt}} + b}{\%\left(V_p + V_{air}\right)\cdot D} + \frac{Ss\sqrt{t_s}}{\%\left(V_p + V_{air}\right)\cdot D}$$ Eq. 6.16

where, D is the depth of concrete exposed to water and $\%(V_p+V_{air})$ is the total volume of voids expressed in percentage. Furthermore, equation 6-16 can be rewritten in terms of saturation as,

$$S_{Act} = S_b + e\sqrt{t_s}$$ Eq. 6.17

where, S_b is the saturation of concrete up to nick point time and e is the constant obtained from the secondary sorptivity and volume of total voids. Mathematically S_b and e are expressed as Equations 6-18 and 6-19.

$$e = \frac{Ss}{\%\left(V_p + V_{air}\right)D}$$ Eq. 6.18

$$S_b = S_{init} + \frac{S_i\sqrt{t_{nickpt}} + b}{\%\left(V_p + V_{air}\right)D}$$ Eq. 6.19

where, S_{init} is the initial saturation of concrete before it is exposed to water, and can be obtained as,

$$S_{\text{int}} = \frac{Vw_{\text{int}}}{\%\left(V_p + V_{air}\right) \cdot D}$$ Eq. 6.20

Equation 6-17 shows the development of actual saturation in concrete with time. However, Fagerlund [2004] showed that since the nick point time (t_{nickpt}) is normally short compared to the total water uptake time (t_t) ($t_{nickpt} << t_t$), and therefore, t_{nickpt} can be neglected ($t_s \sim t_t$). Therefore, actual saturation can be approximated as,

$$S_{Act} = S_b + e\sqrt{t_t}$$ Eq. 6.21

where, t_t is the total time of water exposure.

6.2.3. Potential Service Life

As it is discussed in section 2.4.5, the damage initiation starts when two conditions are met: 1) concrete exceeds critical saturation and 2) concrete experiences freezing (temperature < 0°C). To calculate the potential service life at uninterrupted water uptake (t_w), time required for concrete to reach critical saturation is calculated in this study [Fig. 6-1]

$$S_{Act}(t) = S_{CR}(t)$$ Eq. 6.22

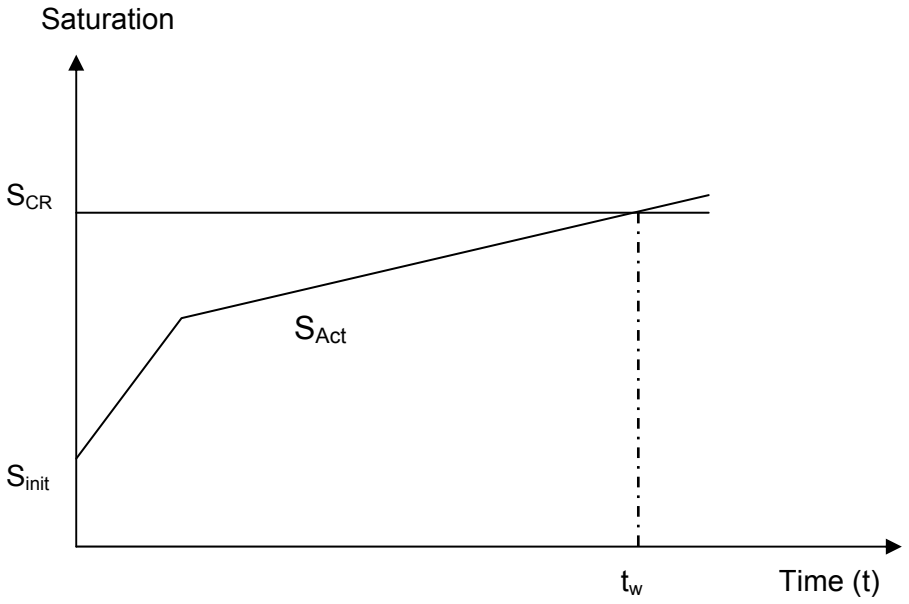

Fig. 6-1 Definition of the potential service life

Therefore, using this boundary condition, equation 6-21 can be rewritten as,

$$S_{CR} = S_b + e\sqrt{t_w} \qquad \text{Eq. 6.23}$$

Solving for time t_w, yields,

$$t_w = \left[\frac{S_{CR} - S_b}{e}\right]^2 \qquad \text{Eq. 6.24}$$

It should be noted here that the time t_w obtained would be the time of uninterrupted water uptake. However, in field conditions the concrete experiences alternate wetting and drying periods. Therefore, to calculate the time of damage initiation ($Life_{init}$), t_w should be transformed to equivalent time of water uptake in the field.

6.2.4. Equivalent Service Life

Fagerlund [1999] showed that when concrete is exposed to water, the water absorbed till nick point time contributes to the saturation of the capillary and gel pores, while the air void system remains empty. Furthermore, it is assumed that the capillary and gel pores of concrete are in a saturated condition at the nick point time, and water absorbed after nick point time contributes towards the saturation of air void system only.

$$Vw_{abs} = V_{abs-p} \; and \; V_{abs-air} = 0 \qquad for \; t \le t_{nickpt} \qquad \text{Eq. 6.25}$$

$$Vw_{abs} = V_{abs-air} \qquad for \; t_{nickpt} < t \le t_w \qquad \text{Eq. 6.26}$$

When a certain amount of air voids are saturated with water (S_{Air}) the concrete reaches its critical saturation. The saturation of air voids required to reach critical saturation is expressed as,

$$S_{Air} = S_{CR} - S_b \qquad \text{Eq. 6.27}$$

From equation 6-24, it can be observed that t_w is the time required to saturate S_{Air}. Therefore, the duration of wetting events that contribute to the saturation of air voids should be calculated. In order to calculate the time that contributes to saturation of air voids, each wetting event is considered individually. As the events that last more than nick point time contribute to saturation of air voids, with each event greater than nick point time, the saturation of air voids can be summed. The total duration of events required to increase the saturation of air voids by S_{Air} is considered as the equivalent service life or $Life_{init}$. It should be noted here that, for damage initiation, it is required that concrete reach S_{CR} and experience freezing. However, as this model assumes that the saturation of air voids accumulates with each wetting event and does not decrease with time,

once concrete has reached S_{CR}, the concrete will undergo freezing sometime in the same year. Therefore, the time of damage initiation ($Life_{init}$) is simply considered as time taken to reach S_{Air}. The total duration of wetting events that contributed towards the S_{Air} is calculated by adding all wetting events greater than nick point time over the year. The duration of each event over the year was calculated using the CONCTEMP program [Bentz, 2000]. Based on the total duration of events greater than nick point time the service life was calculated as,

$$Life_{init}\ (Years) = \left[\frac{t_w}{t_{w-nickpt}} \right] \qquad \text{Eq. 6.28}$$

where, $t_{w\text{-}nickpt}$ (hours) is the annual cumulative duration of all wetting events that lasted more than nick point time. It is assumed here that the drying or wetting due to events lasting less than nick point time only affect the capillary saturation (saturation up to S_b). The saturation of air voids is affected only by events that lasted more than nick point time.

6.3. Development of Model for damage propagation ($Life_{sec}$)

The time of damage propagation ($Life_{sec}$) can be defined as the time between the damage initiation and time when concrete reaches a defined level of damage. Within this period concrete is exposed to alternate drying and wetting periods. It is assumed that the moisture level in concrete is such that for each new freeze thaw cycle moisture level increases. For such conditions, Fagerlund [2004] showed that the water absorption can be defined as

$$S_{Act} = S_{CR} + \alpha\sqrt{\Delta N} \qquad \text{Eq. 6.29}$$

where, S_{Act} is the saturation after critical saturation, ΔN is the number of freeze thaw cycles that the concrete is exposed to after critical saturation, and α is the

coefficient that describes the gradual water uptake in air pores. However, following a simplified approach suggested by Fagerlund [2004], successive increase in cracking caused by each new cycle can be neglected. Therefore, it can be assumed that cracking caused right after concrete exceeds critical saturation remains constant over time and the increase in saturation with each cycle can be approximated as a constant. The actual saturation in concrete can be defined as [Fagerlund, 2004],

$$S_{Act} = S_{CR} + \Delta S \cdot \Delta N \qquad \text{Eq. 6.30}$$

where, ΔS is the increase in saturation per freeze thaw cycle and ΔN is the number of freeze thaw cycles after concrete has reached critical saturation.

When the actual saturation is greater than the critical degree of saturation, the damage in concrete can be expresses as [Fagerlund, 2004]

$$D = K_N \left(S_{Act} - S_{CR} \right) \qquad \text{Eq. 6.31}$$

where, K_N is the coefficient of fatigue and expressed as,

$$K_N = \frac{A \cdot \Delta N}{B + \Delta N} \qquad \text{Eq. 6.32}$$

where, A is the fatigue limit giving the maximum possible damage when ΔN reaches infinity and B is a coefficient [Fagerlund, 1999]. Fig. 6-2 shows the variation in the value of K_N as number of freeze thaw cycles increases. It should be noted that as the number of freeze thaw cycles increases, the K_N approaches the value of A. For instance, Fig. 6-2 shows the variation in K_N with number of freeze thaw cycles for a cement mortar specimen with A=1.2 and B=4 [Fagerlund, 1999]. It can be clearly observed from the figure that as number of

cycles is in the order of 60, K_N is approximately equal to the value of A. The A and B are individual for each concrete.

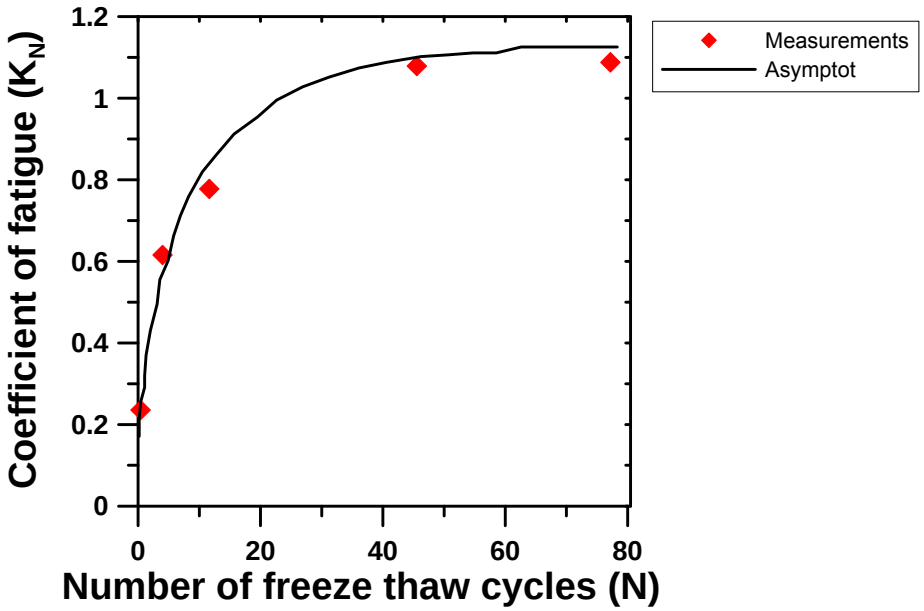

Fig. 6-2 Increase in the value of K_N as per number of freeze thaw cycles [Fagerlund, 2001]

Using equation 6-27 and 6-28 the damage in concrete can be defined as

$$D = \frac{A \cdot N}{B + N}(\Delta S \cdot \Delta N) \qquad \text{Eq. 6.33}$$

However, the number of freeze thaw cycles per year is generally considered to be a constant value and therefore N can be replaced by exposure time,

$$\Delta N \approx n \cdot t \qquad \text{Eq. 6.34}$$

where, n is the number of freeze thaw cycles per year and t is the exposure time (years) after damage initiation. Therefore damage can be expressed as,

$$D_t = \frac{A \cdot n \cdot t}{B + n \cdot t}(\Delta S \cdot n \cdot t) \qquad \text{Eq. 6.35}$$

where D_t is the damage at t years of exposure to freeze thaw environment.

Since the number of freeze thaw cycles per year is in the order of 50 (section 4.3.3), for long exposure times, the ΔN is approximately greater than 60. (equation 6-34). Therefore, K_N can be approximated as A [Fig. 6-2].

$$D = A(\Delta S \cdot n \cdot Life_{\text{sec}}) \qquad \text{Eq. 6.36}$$

Furthermore, as $Life_{sec}$ is defined by a certain level of damage, for a certain known damage level (D_s) $Life_{sec}$ can be obtained as,

$$Life_{\text{sec}} = \left[\frac{D_s}{A \cdot \Delta S}\right] \cdot \frac{1}{n} \qquad \text{Eq. 6.37}$$

It should be noted here that A and ΔS are individual for each concrete. In case of concretes, the values of order 12 have been observed frequently for A [Fagerlund, 2001].

However, ΔS for concrete should be calculated based on the actual measurements for damage and can be obtained as,

$$\Delta S = \left[\frac{D_o}{A \cdot t_0 \cdot n}\right] \qquad \text{Eq. 6.38}$$

where, D_0 is the measurement of damage at time t_0.

Ultimately, the service life can be expressed [using equation 6-28 and 6-37]

$$Service\ Life\ (Years) = \left[\frac{\left[\frac{S_{CR} - S_b}{e} \right]^2}{t_{w-nickpt}} \right] + \left[\frac{D_s}{A \cdot \Delta S} \right] \cdot \frac{1}{n} \qquad \text{Eq. 6.39}$$

6.4. Guidelines to Use the Freeze Thaw Model

It can be observed from the equation 6-35 that service life is dependent on many material properties. In order to use this model, these properties need to be measured with standard tests. However, the measurements typically observed in the literature for the different parameters used in this model has been summarized in this section. An attempt has been made to provide an assessment on how these parameters can be approximated for their application in the model. The wetting events for four cities in Indiana (Fort Wayne, South Bend, Indianapolis and Evansville) has been assessed. Based on this review, a set of values for material properties was selected to show an example calculation to explain the application of this model.

6.4.1. Critical Saturation

As it has been already discussed in literature review, critical saturation is unique for each concrete. Therefore, Scr should be measured for each concrete. However, based on characteristics of concrete and measurements observed in literature, it is possible to make some approximations that allow to select a value of critical saturation to be used in the model.

Fagerlund [2004] studied the critical saturation and following characteristics of Scr were observed,

- The freezing rate and freezing duration have some effect on the value of Scr. However, it was observed to be a marginal effect. Therefore, this effect can be neglected.
- The minimum temperature reached during freezing affects the value of Scr. However, the freezing temperature varies in concrete pores and it is difficult to account for this variation. Therefore, this effect can be neglected.
- The value of Scr changes with age of concrete. However, it was observed that Scr does not vary significantly after 28 days. Generally, concrete is exposed to freeze thaw after 28 days, and therefore, Scr measure at 28 days can be considered to remain constant over the life of concrete.
- The Scr was observed to vary in the range of 0.77 to 0.88 for different concretes [Fagerlund, 2004; Yang, 2004]. It should be noted that the concrete mixture proportion for these observations varied from w/c=0.40 to w/c=0.59 and entrained air in the range of 0.0 to 7.1 %. It should be noted however that generally for a typical concrete the value of critical saturation can be approximated between 0.80 to 0.85.

Furthermore, Yang [2004] observed a critical saturation of 0.85 for concrete with w/c of 0.42 and 6.6 % air. Therefore, based on the observations we chose to use 0.85 as typical value of critical saturation for the example calculations.

6.4.2. Porosity of Concrete

The porosity of concrete is a measure of capillary and gel pores, which affects the development of actual saturation. The porosity of concrete varies and should be measured for each concrete. However, an approximate value of porosity based on w/c can be suggested.

Using the mercury porosimetry Cook and Hover [1999] showed that porosity of cement paste varies according to w/c and curing period. However, it was observed from the measurements of Cook and Hover [1999] that the porosity for 28 days remains approximately constant after 28 days. Therefore, we chose to use the porosity for curing period of 28 days in the calculations. Fig. 6-3 shows the porosity as measured by MIP for cement pastes with different w/c and curing time of 28 days [Cook and Hover, 1999]. Using the measurements as shown in Fig. 6-3, porosity of cement paste with known w/c can be calculated. Based on these measurements porosity of 25 % for a cement paste with w/c of 0.42 was selected for the example calculations.

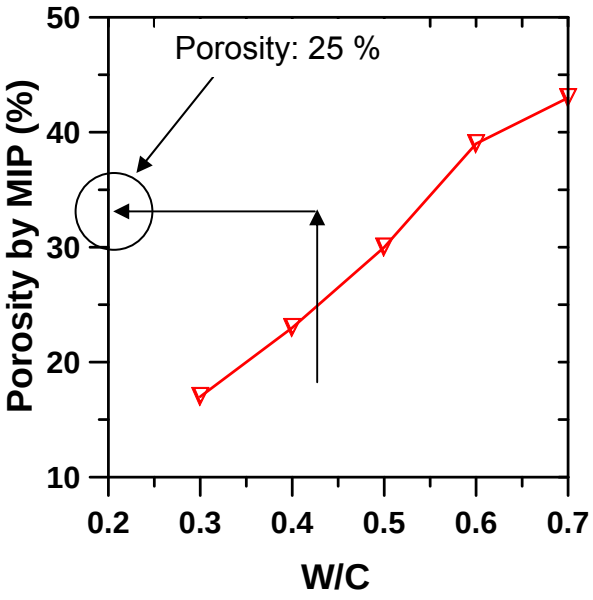

Fig. 6-3 Summary of porosity determined by MIP for cement pasts with different w/c ratio and curing time of 28 days [Cook and Hover, 1999]

The porosity calculated from Fig. 6-3 provides the volume of capillary and gel pores in cement paste. However, this volume needs to be converted to the

volume of capillary and gel pores in concrete. The volume of capillary pores of concrete can be obtained as,

$$Vp = P_{paste} \cdot V_{paste} + P_{Agg} \cdot V_{Agg} \qquad \text{Eq. 6.40}$$

where, V_p is the volume of capillary and gel pores in concrete, V_{paste} is the volume of paste in concrete and V_{Agg} is the volume of aggregates in concrete. The P_{paste} and P_{Agg} are the porosity of cement paste and aggregates, respectively. The V_p and V_{Agg} can be obtained from mixture proportions and will change for each concrete. However, considering a typical concrete mixture, 33% paste and 67% aggregates were selected as appropriate values for calculations. Furthermore, the porosity of aggregates is very small compared to the total porosity of concrete, and therefore, can be neglected while calculating the volume of capillary pores. Therefore, the volume of capillary pores can be obtained as

$$Vp = P_{paste} \cdot V_{paste} \qquad \text{Eq. 6.41}$$

Using the porosity of paste (25%) and fraction of paste as 33%, the volume of capillary pores was obtained as approximately 8% [Equation 6.41].

6.4.3. Initial Saturation

The initial saturation of concrete depends on the relative humidity of concrete. The initial saturation of concrete before the first wetting event, is of particular interest to this study. Therefore, the relative humidity before the wetting event was used to obtain the initial saturation. The relative humidity before each event can be obtained using the results of CONCTEMP program [Bentz, 2000] for each city. The average of RH just before each wetting events over the year was calculated for each selected location (Indianapolis, Fort Wayne, South Bend, and

Evansville) in the state on Indiana. Table 6-1 shows the average RH before wetting events for each location. A very small variation was observed in the values of RH, and therefore, the average RH at all locations (85%) was used to obtain the initial saturation. It should be noted however that, the external RH of concrete is assumed to be same as the internal RH of concrete.

Table 6-1 Average RH (%) before wetting event

City	Yearly average of RH before wetting events (%)
Fort Wayne	85
Indianapolis	86
South Bend	85
Evansville	84

The absorption isotherms are used to obtain the saturation of concrete from RH. However, the absorption isotherm are unique for each concrete. Therefore, absorption isotherms developed by various researchers were studied. The absorption isotherms developed by various authors for different concretes has been presented in Fig. 6-4 [Powers and Brownyard, 1948; Rajabipour and Weiss, 2006]. The saturation for 85% RH was obtained for each concrete as shown in Fig. 6-4.

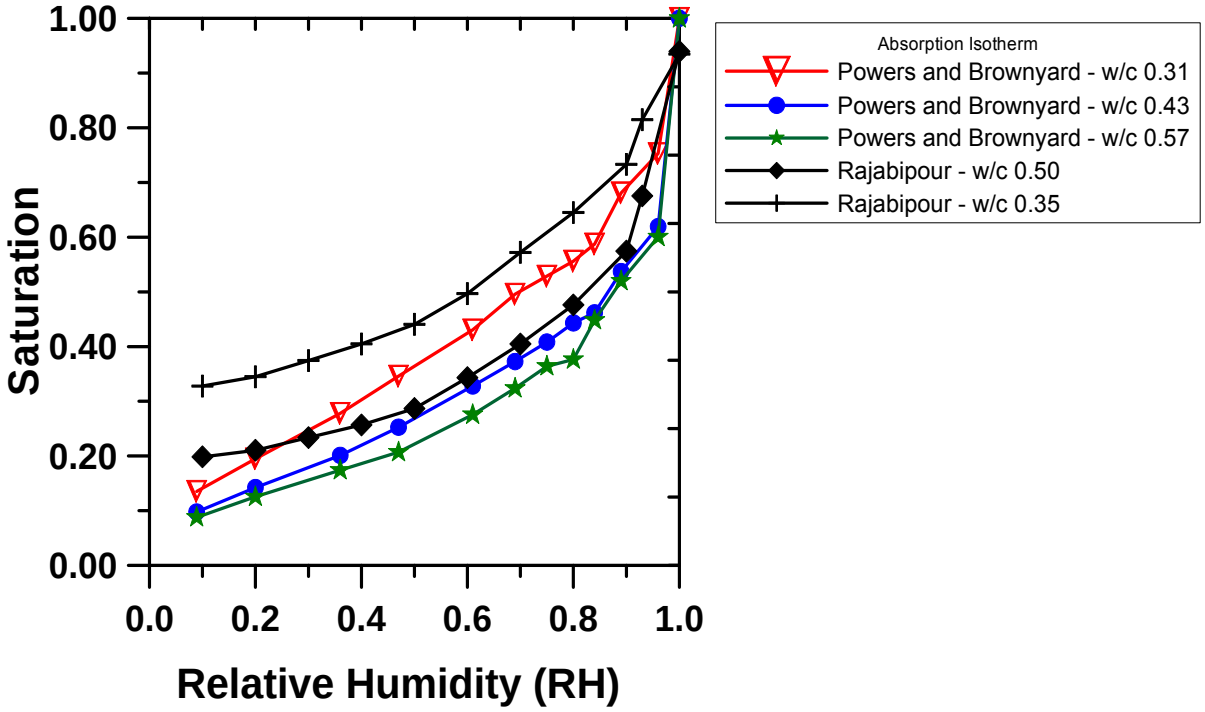

Fig. 6-4 Absorption isotherms developed by various researchers [Powers and Brownyard, 1948; Rajabipour and Weiss, 2006]

Table 6-2 shows the saturation measurements obtained for different concretes at 85% RH. It can be observed from the Table 6-2 that initial saturation for concrete at 85% RH would range between 0.48 to 0.70. It should be noted that based on the available data, it was difficult to obtain any relation between w/c and saturation at 85% RH. Therefore, it was decided to use the average value of saturation measurements obtained for different concretes as the initial saturation of concrete in the calculations of this model. Based on the values of saturation shown in Table 6-2 average value of 0.56 was selected.

Table 6-2 Saturation for 85 % RH, as obtained from Fig. 6-4.

W/C	Saturation at 85 % RH
0.31	0.61
0.35 + 5 % SF	0.70
0.43	0.49
0.50	0.52
0.57	0.48

6.4.4. Sorptivity

Sorptivity, being a material property, is unique for each concrete. As already discussed in literature review, sorptivity depends on many parameters such as entrained air, type and duration of curing, mixture proportions. Therefore, it is difficult to predict the sorptivity. However, measurements of sorptivity performed by other authors were studied and range of sorptivity measurements was selected for calculations.

Table 6-3 shows the range of initial sorptivity measured by different researchers. The measurements compiled in Table 6-3 are for different concrete mixtures with different curing conditions. However, the objective of this review was to identify the possible range of values of sorptivity. Therefore, based on the measurements observed in the literature, $1x10^{-3}$ to $10x10^{-3}$ $mm/s^{0.5}$ was selected as the typical range for calculations. It should be noted here that most of the measurements observed in the literature were for initial sorptivity. It should be noted however that, the secondary sorptivity is less than initial sorptivity [ASTM C 1585, 2004].

Table 6-3 Range of initial sorptivity observed in the literature

Range of initial sorptivity measurements $X10^{-3}$ mm/$s^{0.5}$	Reference
2.96 to 5.86	[Krishnan, 2002]
4.40 to 9.70	[Tasdemir, 2003]
5.00 to 10.00	[Nokken, 2002]
4.83 to 14. 26	[Claisse *et al.*, 1997]
0.48 to 1.56	[Yang, 2004]

6.4.5. Nick Point Time

Fagerlund showed that the capillary pores are saturated at the nick point time [Fagerlund, 1999]. As the time to saturate capillary pores varies for different concretes, a variation in nick point time is observed. The variation in the nick point time affects both, the value of saturation at nick point time and duration for saturation of air voids. As the nick point time increases the saturation at nick point increases [equation 6-20], and ultimately, S_{air} decreases [equation 6-27]. Furthermore, the duration after the nick point time contribute towards the saturation of air void system. Therefore, the greater the nick point time, the lesser the time contributed towards the saturation of air voids in any wetting event. This reduces the $t_{w\text{-}nickpt}$. Together, these factors affect the service life of concrete. The nick point has been measured from 6 hours to 10 hours in the literature [Bentz, 2002; Krishnan, 2002]. However, considering the scope of this study, the effect of variation in nick point time has not been studied, and nick point time of 6 hours, as suggested by ASTM C 1585 [2004] was selected for calculations.

6.4.6. Wetting Events for Cities in Indiana

Wetting events are used to predict the service life of bridge decks. However, wetting events vary based on the geographical location [Section 4.3.5]. In this study, four cities (Indianapolis, Fort Wayne, South Bend, and Evansville) were selected for the calculations. The wetting events for each city were obtained using the CONCTEMP program for bridge decks [Bentz, 2000]. However, the wetting events greater than nick point time were of interest to this study. As the nick point time of 6 hours was selected for calculations, cumulative duration of wetting events greater than 6 hours for each selected city in Indiana were obtained for the calculations [Fig. 6-5]. However, considering the possibility of variation in nick point time, cumulative duration of wetting events for different nick point time (8, 10, 12 hours) has been presented [Fig. 6-5].

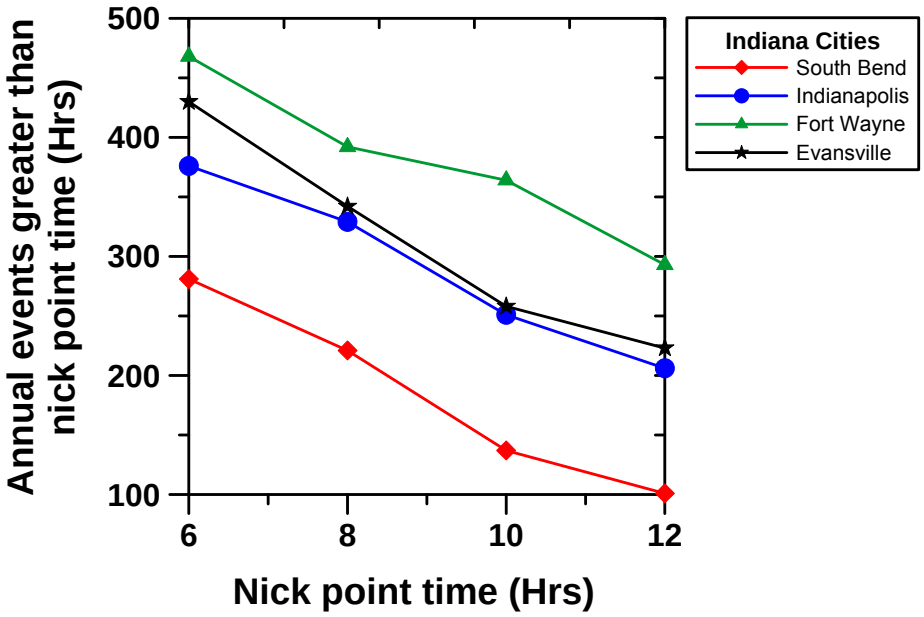

Fig. 6-5 Cumulative wetting duration of events that lasted more than nick point time (hours)

6.4.7. Increase in Damage with Number of Freeze Thaw Cycles

As discussed in section 6.3, the damage in concrete can be calculated as,

$$D = \left(A \cdot \Delta S \cdot n\right) \cdot Life_{\sec} \qquad \text{Eq. 6.42}$$

where, a value on the order of 12 is observed for A and n varies for each city. The ΔS should be calculated as per equation 6-38. However, this value varies for each concrete and exposure conditions. Therefore, ΔS has to be based on the actual damage measurements. Furthermore, this value could not be found in the literature nor could be measured for the purpose of this study. Therefore, a reasonable value of 1.4×10^{-4} was assumed. It should be noted that A and n being already approximated, the value of ΔS is a crucial parameter that decides the rate of increase of damage in the concrete.

6.5. Results for Freeze Thaw Model

The objective of this section is to present typical calculations as performed in this model for predicting service life. As discussed in section 6.4 the values of material properties were selected and service life at four locations in Indiana was calculated based on the equations described in section 6.2 and 6.3. The summary of material properties and other required inputs is presented in Table 6-4.

Table 6-4 Summary of material properties and inputs.

Material Property/Inputs	Value
Critical Saturation	0.85
Initial Saturation	0.56
Initial Sorptivity	$2x10^{-3}$ mm/$s^{0.5}$
Secondary Sorptivity	$1x10^{-3}$ mm/$s^{0.5}$
Porosity	8.0% the total volume of concrete
Entrained Air	6.5% of the total volume of concrete
Constant b	5.5 mm
Nick Point Time	6 hours
Depth of Bridge deck	0.2 m
Cumulative duration of wetting events greater than 6 hours ($t_{w\text{-}nickpt}$) [Fig. 6-5]	
South Bend	281 Hours
Indianapolis	376 Hours
Fort Wayne	468 Hours
Evansville	430 Hours
Damage level for service life (D_s)	0.60
A	12
ΔS	$1.4x10^{-4}$
Yearly number of freeze thaw cycles [(AFCCC), 1967-1996]	
South Bend	54 Cycles
Indianapolis	57 Cycles
Fort Wayne	56 Cycles
Evansville	48 Cycles

6.5.1. Calculation of $Life_{init}$

Substituting the values as shown in Table 6-4 and using equation 6-20 the saturation at nick point (S_b) was calculated as,

$$S_b = 0.56 + \frac{2.00E-6\sqrt{21600}+5.5E-3}{\%(8+6.5)0.20} = 0.76 \qquad \text{Eq. 6.43}$$

The same result has been shown in Fig. 6-6

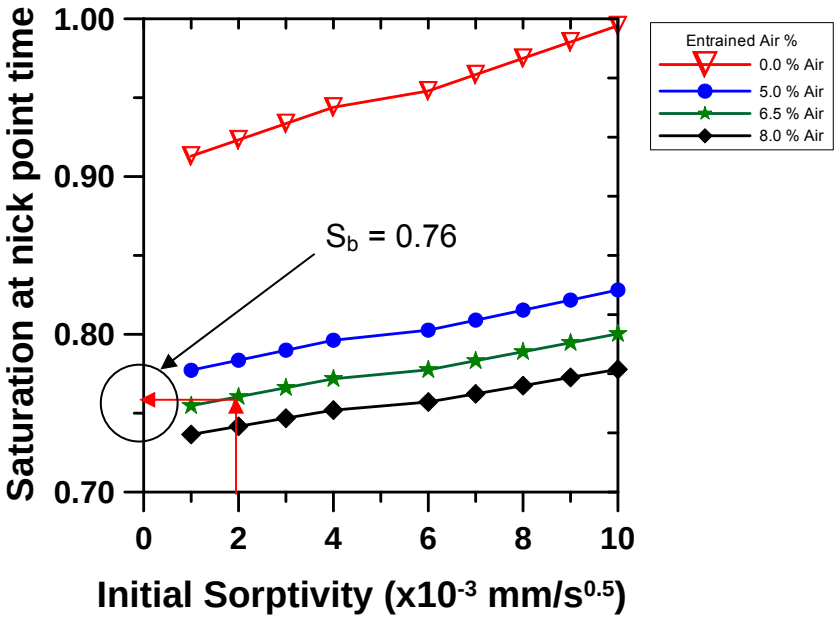

Fig. 6-6 Results for saturation at Nick point time from Initial Saturation

Using the value of secondary sorptivity, the constant e, as discussed in equation 6-18, was calculated based on equation 6-19

$$e = \frac{1.00E-06}{\%(8+6.5)0.20} = 6.25E-05\ mm/s^{0.5} \qquad \text{Eq. 6.44}$$

The time t_w was calculated using equation 6-24

$$t_w = \left[\frac{0.85 - 0.76}{6.25E - 05}\right]^2 = 1892\ Hrs \qquad \text{Eq. 6.45}$$

The same results has been shown in Fig. 6-7

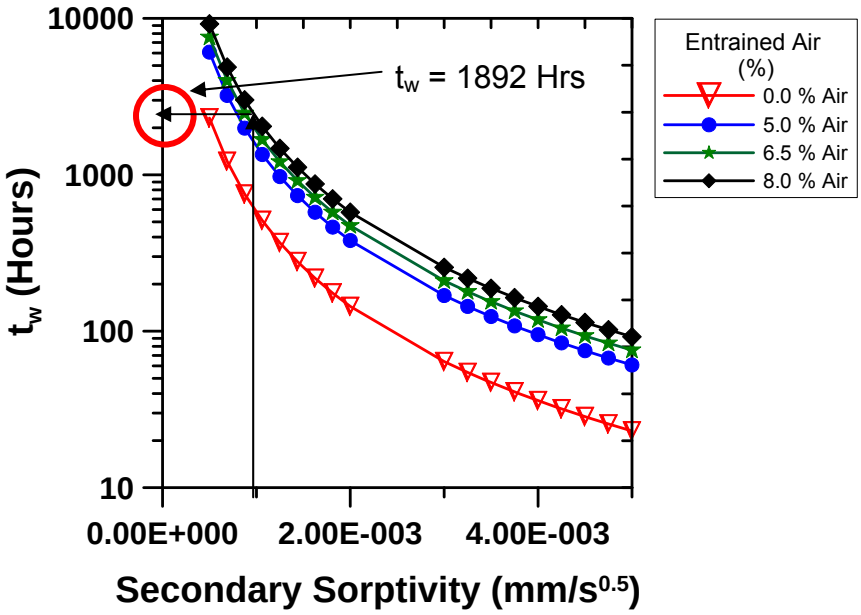

Fig. 6-7 Results for t_w from secondary sorptivity [For S_b=0.76]

The t_w obtained is the potential service life as discussed in section 6.2.3 and should be converted to equivalent service life as discussed in section 6.2.4. Therefore, using the equation 6-26 and $t_{w\text{-}nickpt}$ for each city as shown in Table 6-4, the $Life_{init}$ was calculated as,

$$Life_{init}\ (Years) = \left[\frac{1892}{281}\right] = 6.70\ years\ \ for\ South\ Bend \qquad \text{Eq. 6.46}$$

$$Life_{init}\ (Years) = \left[\frac{1892}{376}\right] = 5.03\ years\ \ for\ Indianapolis \quad \text{Eq. 6.47}$$

$$Life_{init}\ (Years) = \left[\frac{1892}{468}\right] = 4.04\ years\ \ for\ Fort\ Wayne \quad \text{Eq. 6.48}$$

$$Life_{init}\ (Years) = \left[\frac{1892}{430}\right] = 4.40\ years\ \ for\ Evansville \quad \text{Eq. 6.49}$$

6.5.2. Calculation for $Life_{sec}$

The $Life_{sec}$ is defined by the damage level of 0.6 in this case. Therefore, using the equation 6-37 time required to reach this level of damage ($Life_{sec}$) was calculated as,

$$Life_{\sec} = \left[\frac{0.60}{12 \cdot 1.4E - 4}\right] \cdot \frac{1}{54} = 6.61\ years\ \ for\ South\ Bend \quad \text{Eq. 6.50}$$

$$Life_{\sec} = \left[\frac{0.60}{12 \cdot 1.4E - 4}\right] \cdot \frac{1}{57} = 6.26\ years\ \ for\ Indianapolis \quad \text{Eq. 6.51}$$

$$Life_{\sec} = \left[\frac{0.60}{12 \cdot 1.4E - 4}\right] \cdot \frac{1}{56} = 6.37\ years\ \ for\ Fort\ Wayne \quad \text{Eq. 6.52}$$

$$Life_{\sec} = \left[\frac{0.60}{12 \cdot 1.4E - 4}\right] \cdot \frac{1}{48} = 7.44\ years\ \ for\ Evansville \quad \text{Eq. 6.53}$$

Ultimately, the predicted service life (both $Life_{init}$ and $Life_{sec}$) for cities in Indiana as calculated above has been shown in Fig. 6-8. The data points on the x axis for zero damage represent the $Life_{init}$.

Fig. 6-8 Service life for different cities in Indiana

6.6. Comparison of Results with Experimental Observations

The service life of concrete exposed to freeze thaw was calculated in two parts, $Life_{init}$ and $Life_{sec}$ respectively. The results of each part were compared to experimental data separately. The results of first part, predicted time to damage initiation ($Life_{init}$), were compared with the results of CONCLIFE, a software developed by NIST to predict service life in freeze thaw deterioration. In the case of second part, time required to reach defined level of damage after damage initiation in concrete ($Life_{sec}$), no published data could be found for the comparison. Therefore, it was difficult to compare the direct results of predictions for $Life_{sec}$. However, the modeling approach for the calculations of $Life_{sec}$ was

used to predict the relative dynamic modulus for the ASTM C 666 test results from literature [Sellevold et al., 1997]. The predicted relative dynamic modulus was compared with the relative dynamic modulus measured by Sellevold et al. [1997]. The objective of this comparison was to see the effectiveness of the modeling approach.

6.6.1. Comparison of Results for damage initiation ($Life_{init}$)

Table 6-5 shows the material properties used in calculating the time to damage initiation in concrete by CONCLIFE and the model developed in this study. CONCLIFE can be used for few major cities in the country, however no Indiana cities are included in the software. Therefore, three cities, Seattle, WA, Baltimore, MD and Providence, RI were selected for the comparison of the model results. The annual wetting events for these cities were calculated using the CONCTEMP program [Bentz, 2000]. The total duration of wetting events that lasted more than nick point time (7 Hrs) was calculated. It should be noted that, the values of nick point time, sorptivity, air content and porosity are taken same as presented in CONCLIFE manual [Bentz and Ehlen, 2002]

Table 6-5 Summary of material properties and inputs

Material Property/Inputs	Value
Critical Saturation	0.85
Initial Saturation	0.56
Initial Sorptivity	0.35×10^{-3} mm/s$^{0.5}$
Secondary Sorptivity	1.15×10^{-3} mm/s$^{0.5}$
Porosity	14% the total volume of concrete
Entrained Air	2% of the total volume of concrete
Constant b	5.46 mm
Nick point time	7 hours
Depth of Bridge deck	0.2 m
Cumulative duration of wetting events greater than 7 hours, calculated with CONCTEMP	
Seattle, WA	871 Hours
Baltimore, MD	454 Hours
Providence, RI	497 Hours

Table 6-6 shows the comparison of results obtained from CONCLIFE and model developed in this study. The difference in the prediction is presented as the percentage of service life predicted with CONCLIFE. From the comparison of the results, it can be observed that the developed model predicts $Life_{init}$ with a maximum difference of 18 %.

The difference observed in the prediction can be attributed to the fact that, the described model uses an average value initial saturation for all locations. Furthermore, this value used for initial saturation is an average of approximate values observed in the literature [section 6.4.3]. The variation in the value of

initial saturation affects the service life prediction, therefore, it is possible that the approximations in the value of initial saturation is responsible for the difference observed in the prediction.

Table 6-6 Results obtained with developed model and CONCLIFE

City	Prediction by CONCLIFE (Yrs) (A)	Prediction by developed model (Yrs) (B)	Difference [(A-B)/A]*100
Seattle, WA	3.00	3.54	18 %
Baltimore, MD	8.00	6.79	15 %
Providence, RI	6.00	6.20	3 %

6.6.2. Comparison of the Results for $Life_{sec}$

This model uses Equation 6-37 to calculate the time required to proceed to a defined level of damage from damage initiation ($Life_{sec}$). However, published data could not be found to compare the results for $Life_{sec}$ obtained with the model developed in this study. Therefore, the modeling approach was compared with the results from ASTM C 666. It should be noted that ASTM C 666 simulates a severe freeze thaw condition.

Measurements from an ASTM C 666 test was selected from literature [Sellevold et al., 1997]. Sellevold et al. [1997] measured the freeze thaw response of a concrete with a w/c of 0.3, 8% silica fume, a binder volume of 32%, and air in hardened concrete of 1.5%. A 100x100x350 (mm) specimen was cured in water for 4 months after demoulding and then wrapped in heavy foil until testing. A freezing cycle was applied between 4° and -18° C. The dynamic modulus and

mass change were recorded as a function of the number of freeze thaw cycles that were applied [Table 6-7].

Table 6-7 Change in dynamic modulus and mass as a function of number of freeze thaw cycles [Sellevold et al., 1997].

No. of FT cycles	E/E_0	Mass change (g)
0	100	8812
35	100	8818
60	99	8821
100	95	8837
132	84	8848
167	56	8864
202	44	8879

The data from Table 6-6 was used to compare the results obtained with the modeling approach and the experimental measurements. In all, two comparisons were carried out. First, based on the modeling approach, number of critical cycles (N_{cr}) was calculated. Generally, the number of critical cycles is defined as the cycle after which the relative dynamic modulus starts degrading (i.e., damage initiates). The N_{cr} calculated with modeling approach was compared with the N_{cr} obtained with the typical analysis of the measurements as suggested by Fagerlund [2004]. In the second comparison, the relative dynamic modulus was predicted using the modeling approach and the predicted values were compared with the relative dynamic modulus measured in the test.

6.6.2.1. Comparison of Number of Critical Freeze Thaw Cycles (N_{cr})

The critical freeze thaw cycle can be defined as the cycle from which the relative dynamic modulus starts decreasing in an ASTM C 666 test. Generally, the N_{cr} can be identified with a significant decrease in the relative dynamic modulus for the test results.

According to the modeling approach, the N_{cr} can be calculated as,

$$N_{CR} = \left[\frac{S_{CR} - S_0}{\Delta S} \right] \quad \text{Eq. 6.54}$$

where, S_0 is the initial saturation before test and ΔS is the increase in saturation during each new freeze thaw cycle. The increase in saturation during each cycle was obtained as,

$$\Delta S = \left[\frac{\Delta m}{Vv} \right] \quad \text{Eq. 6.55}$$

where, Δm is the increase is mass per cycle and Vv is the total volume of voids. The total volume of voids was calculated by using the equation 6-3 and 6-41 as,

$$Vv = \left(\left[0.32 \cdot (17) + 1.5 \right] \% \right) \cdot \left[10 \cdot 10 \cdot 35 \right] \quad \text{Eq. 6.56}$$

where, using the w/c of 0.3, paste porosity of 17% (obtained from Fig. 6-3), and paste content of 32% was used to calculate the volume of pores.

As the damage in concrete starts, the change in mass of concrete is not only due to absorption of water. The change in mass after damage initiation also accounts for the mass loss due to spalling of concrete specimen. Therefore, the Δm for

initial freeze thaw cycles (up to 35 cycles) was used to calculate the increase in saturation. The ΔS was obtained as,

$$\Delta S = \frac{0.171}{[0.32 \cdot (17) + 1.5]\% \cdot [10 \cdot 10 \cdot 35]} = 0.0007 \qquad \text{Eq. 6.57}$$

The value of S_{cr} was approximated as 0.85 for the calculations. Based on the description of curing conditions provided [Sellevold et al., 1997], it was assumed the RH of concrete would be approximately above 95% RH or equivalent to capillary saturation. Therefore, based on Fig. 6-4 the initial saturation of approximately 0.80 was selected. With these values, the N_{CR} was calculated as,

$$N_{CR} = \left[\frac{0.85 - 0.80}{0.0007} \right] \approx 71\, cycles \qquad \text{Eq. 6.58}$$

The N_{CR} for the measurements from the ASTM C 666 test [Sellevold et al., 1997] was observed to be approximately 98 cycles [Fig. 6-9]. Based on the calculations, it can be observed that, the predicted N_{CR} using the modeling approach is in reasonable agreement with the N_{CR} observed for the ASTM C 666 test results [Sellevold et al., 1997]. It should be noted here that, the modeling approach uses approximate values for critical saturation and initial saturation which may be the reason for the observed difference.

6.6.2.2. Check for Prediction of Relative Dynamic Modulus

The damage in concrete can be calculated with equation 6-33. The number of critical cycles for the measurements shown in Table 6-7 was considered as 98 cycles. The concrete reaches critical saturation at the N_{cr} therefore number of cycles after critical saturation (ΔN) can be calculated as,

$$\Delta N = N - N_{CR} \quad \text{Eq. 6.59}$$

The damage in concrete exposed to freeze thaw cycles can be calculated with equation 6-33. However, for larger number of freeze thaw cycles after critical saturation (ΔN), K_N can be approximated as A, and therefore, damage at can be described as ,

$$D_N = A \cdot (\Delta S \cdot \Delta N) \quad \text{Eq. 6.60}$$

where, D_N is the damage at N^{th} Cycle. Using equation 6.60, the damage in ASTM C 666 test was predicted for the measurements recorded by Sellevold et al. [1999]. The ΔS calculated in equation 6-57 and 12 as a value of A was used for calculations. Based on the damage calculations the relative dynamic modulus was calculated as

$$\frac{E_N}{E_0} = 1 - D_N \quad \text{Eq. 6.61}$$

where, E_N is the dynamic modulus at N^{th} cycle, E_0 is the initial dynamic modulus (i.e., at 0^{th} cycle).

Fig. 6-9 shows the comparison of relative dynamic modulus obtained from calculations as per the modeling approach and test results as shown in Table 6-7. It should be noted here that, in case of the calculations using the modeling approach, the damage was assumed to be zero for cycles less than N_{CR}, and E/E_0 is equal to 100.

It can be observed from Fig. 6-9 that the relative dynamic modulus obtained as per the calculations of model shows reasonable agreement with the test results obtained by Sellevold et al. [1999].

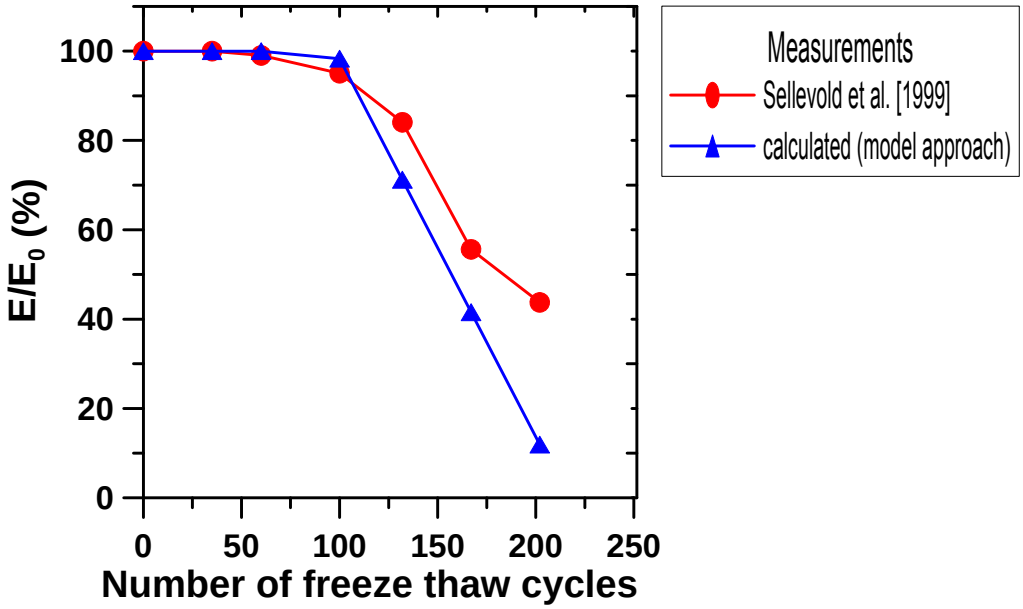

Fig. 6-9 Comparison of relative dynamic modulus calculations (modeling approach) and test results as obtained by Sellevold et al. [1999]

6.7. Summary and Conclusions

A model was implemented that relates material properties with service life for freeze thaw exposure. Service life prediction was divided into two parts. The first portion of this model describes the time to damage initiation or time to reach critical saturation ($Life_{init}$), and second portion of this model describes, the damage propagation phase ($Life_{sec}$). The freeze thaw resistance of concrete is dependent on different material properties such as critical saturation, porosity, sorptivity, and a fatigue coefficient. The saturation of concrete can be determined from the sorptivity, porosity, nick point time, and duration of wetting events. The duration of wetting events was calculated using the CONCTEMP program developed by Bentz [2000]. Only the wetting events responsible for the saturation of air void system were used for predicting the service life ($Life_{init}$). The increase in damage after concrete reached critical saturation was described using the fatigue coefficient and number of freeze thaw cycles. Based on the

literature review, approximate values of material properties were chosen to illustrate the calculations. The approach used in this model has been compared to the results of ASTM C 666 test from literature. The results of $Life_{init}$ has been compared with results of CONCLIFE.

Based on the work performed in this study it was observed that:

- The predicted relative dynamic modulus was observed to be in agreement with the experimental measurements [Sellevold et al., 1997]. Therefore, this approach could be considered as an approach for the preliminary prediction of service life with respect to freeze thaw exposure.
- The model was observed to predict the time to critical saturation ($Life_{init}$) that was similar to CONCLIFE predictions (< 18% difference). This difference can be attributed to the fact that the developed model uses an average value of initial saturation for all locations. Furthermore, the initial saturation used in the model calculations is based on the average of different measurements observed in the literature. As the variation in initial saturation affects the service life prediction of this model, the approximations in determining the initial saturation can be responsible for the difference observed in the results of model and CONCLIFE.
- It can be observed from the comparison of the results obtained with the model and experimental data that the value of initial saturation plays an important role in the prediction of service life in freeze thaw environment. It is recommended that a further study should be performed to describe the initial saturation for field exposure conditions observed for bridge decks in Indiana. Furthermore, it is recommended that the model should be compared with the damage in bridge decks. As these measurements could not be found in publications, it is recommended that further work should be planned to achieve these measurements.

Finally, it can be concluded that, based on the approximations suggested in this work, the developed model can provide a preliminary prediction of service life assessment for concrete exposed to freeze thaw environment. However, based on the available resources any calibration of the model could not be performed, and further research is recommended for the development of this model.

CHAPTER 7. DETERIORATION MODELS - SHRINKAGE MODEL

7.1. Introduction

The purpose of this chapter is to describe the development of the model that is used to relate shrinkage of concrete with probability of cracking. The importance of a shrinkage model is highlighted in the section 7.1. In Section 7.2, a model that enables crack prediction is introduced and four main steps of the cracking prediction model are presented. In Section 7.3, the modeling approach is explained and the concept of predicting the likelihood of cracking using cracking potential parameter is introduced. Since the probability of cracking in concrete element is time-dependant, the analysis needs to be time-dependant as well. To achieve this goal, modeling is conducted using time-dependant equations (as introduced in the Section 7.4). The basis of shrinkage-based design are explained in the Section 7.5 and the analysis of concrete with different strength gaining characteristic is presented. The probability of cracking is assessed using Monte Carlo simulation and a Load and Resistance Factor Design method which are described in Section 7.6. The results of relating probability of cracking in a restrained concrete bridge deck with the amount if shrinkage that the concrete members undergoes is presented in Section 7.7. Finally, Section 7.8 provides a summary and conclusions.

7.2. Introduction to the Shrinkage-Based Model

In practice, concrete is usually restrained from moving freely. For example, a bridge deck is restrained by girders and a concrete pavement is restrained by

tied sections and subgrade. This restraint can result in the development of residual stresses inside the concrete. If the magnitude of stresses exceed the material's resistance (i.e., tensile strength) cracking can occur. To analyze the potential for cracking in concrete, it is essential to analyze the degree of restraint and the amount of shrinkage that can occur within a concrete member.

Shrinkage of concrete can be measured according to ASTM C157, where prism specimens are stored in a condition that ensures 50 ± 4% RH and 23 ± 2°C (air storage). These conditions are not the typical environmental conditions that concrete bridge decks are subjected to throughout their service life. As such, there is a need to develop an approach that would allow an accurate assessment of shrinkage in the structure. This information can be further used to calculate the probability of cracking.

In order to assess the probability of cracking of a concrete member a four step model was used in this study. Figure 7-1 shows the flowchart of the four steps followed in the modeling approach. In the first step, the shrinkage model is used to estimate the shrinkage of concrete. In the second step, results from the shrinkage measurements are related to a cracking potential (Section 7.3). In the third step, the cracking potential is used to calculate the probability of cracking in the concrete element. For this purpose, a Load and Resistance Factor Design approach is used (Section 7.4). Finally, the probability of cracking is related back to measurable properties – shrinkage test results.

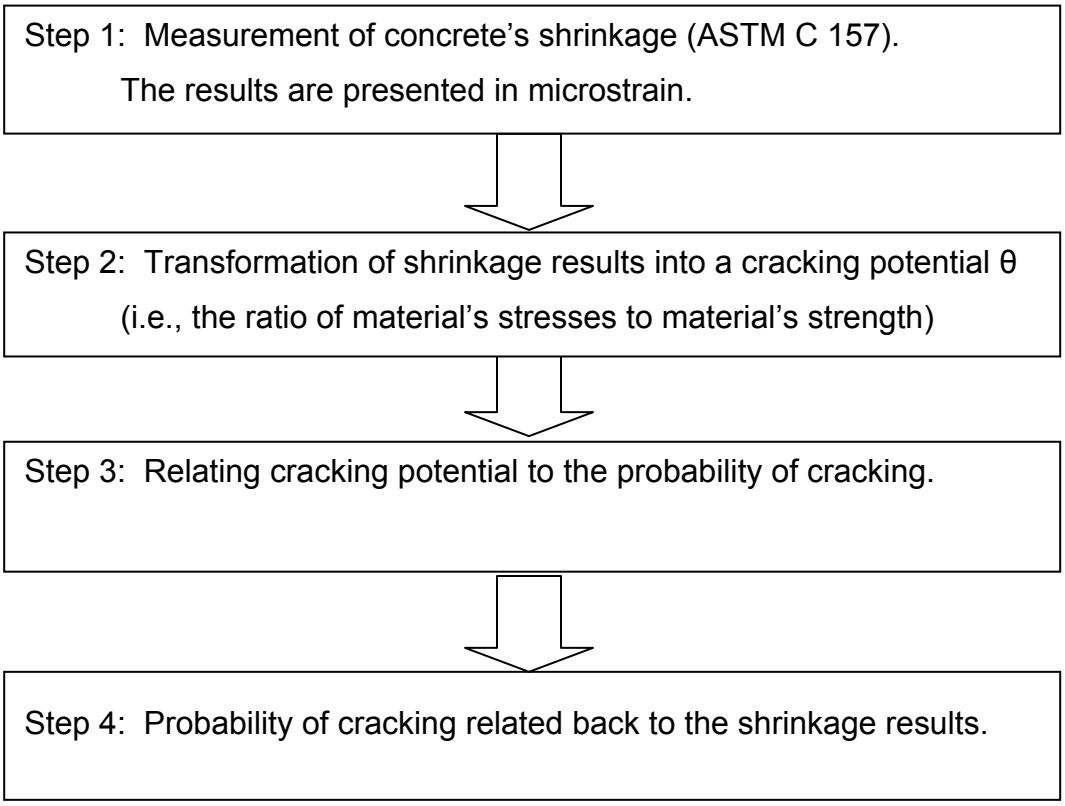

Fig. 7-1 Flow chart for shrinkage model

7.3. Development of the Model for Predicting Probability of Cracking

One of the objectives of this research is to relate the properties of concrete and the exposure conditions to the service life of bridge decks in the state of Indiana.

Shrinkage cracking can be thought to occur when the residual stresses that develop when shrinkage is prevented exceed the cracking resistance of the material (Figure 7-2). Determining whether cracks may develop in a concrete, however, is complicated since both the stress development and strength are time-dependent. Tensile strength, similar to other material properties, develops over time and increases with the progress of hydration. Residual stresses

development, on the other hand, occurs in response to shrinkage and moisture loss, which is a slow, diffusion-controlled process. It should be noted that the residual stress that develops in concrete as a result of restraint can not be computed directly using the product of the free shrinkage and elastic modulus (i.e., Hooke's Law) since the concrete experiences stress relaxation (creep). This phenomenon is schematically presented in the Figure 7-2 and shows that a considerable amount of shrinkage stress is relaxed by the creep effect.

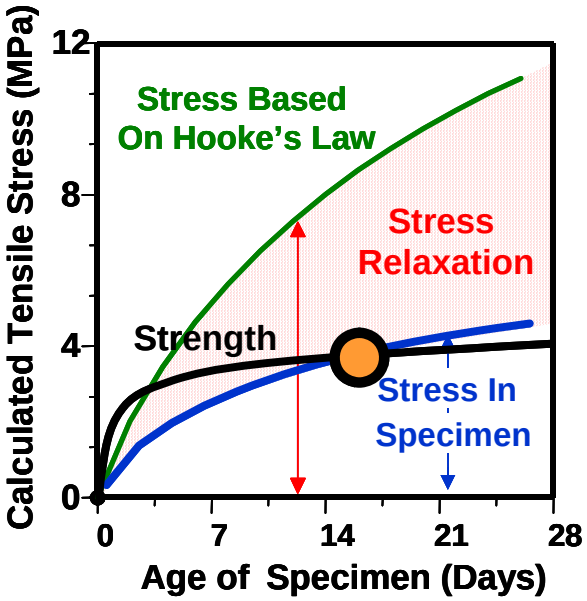

Fig. 7-2 Stress and strength development in restrained shrinkage specimens [Weiss 1997]

The potential for shrinkage cracking to occur in concrete depends on several time-dependent factors including material stiffness, shrinkage rate, magnitude of shrinkage, stress relaxation, and material toughness. A model has been formulated to estimate the potential for restrained shrinkage cracking in concrete elements [Weiss, 1997, Weiss, 1999]. This model allows on the assessment of the time-dependant stresses and strength development in restrained concrete element. The ratio of the stress and strength, or parameter known as cracking potential, can be further used to assess probability of cracking. Although this

model is relatively basic and assumes uniform shrinkage throughout the element, previous research showed a favorable comparison between the model predictions and experimental observations [Shah et al., 1998]. Other models have been developed to predict shrinkage cracking as well as to consider the potential for thermal cracking [Schindler, 2004, Schlangen, 2004]. This approach has been used to illustrate implications associated with the use of higher strength concrete, to simulate the behavior of structures with imperfect restraint, and to illustrate the role of reducing the magnitude and rate of free shrinkage [Shah et al., 1998, Parameswaran, 2004].

Stress development in a restrained concrete element can be estimated using Equation 1 [Weiss, 1997]:

$$\varepsilon_{Permit}(t) = \int_0^t \left[\left(\frac{1}{E_\sigma(\xi)} + \frac{1}{E_c}\phi(t,\xi) \right) \frac{d\sigma(\xi)}{d\xi} + \alpha(\xi) \right] \cdot d\xi \qquad \text{Eq. 7-1}$$

where, $\varepsilon_{Permit}(t)$ is the total strain that is permitted to develop in the actual restrained concrete (i.e., for complete restraint $\varepsilon(t)$ =0 which will be assumed in this work), $E_\sigma(\xi)$ is the time dependent elastic modules, E_C is a reference elastic modulus (i.e., a 28 day value), $\phi(t,\xi)$ is the creep coefficient, and $\alpha(\xi)$ is the differential shrinkage with respect to time (t).

$$\varepsilon_{Tot-Shr}(t) = \int_0^t \alpha(\xi) \cdot d\xi \qquad \text{Eq. 7-2}$$

Using this approach enables the influence of material properties (i.e., shrinkage and elastic modulus) to be related to the residual stress that develops in the concrete.

The likelihood of early-age cracking is predicted by comparing the residual stresses that develop in the restrained concrete with a materials' resistance to cracking (e.g., strength). While equation 7-1 can be used to compute the residual tensile stress, the tensile strength can be approximated with a time dependant function as described by Radlinska et al. [2005]. To predict the likelihood of cracking, a parameter called cracking potential, $\theta_{CR}(t)$, has been defined as the ratio of residual stress ($\sigma(t)$) and tensile strength ($f'_t(t)$), as shown in equation 7-3:

$$\theta_{CR}(t) = \frac{\sigma(t)}{f'_t(t)} \qquad \text{Eq. 7-3}$$

In theory, a cracking potential higher than 1 denotes the time of cracking (intersection of the curves on Figure 7-2, but laboratory experiments show that cracking can also be observed for lower values, i.e., beginning as low as 0.7 [van Breugel and Lokhorst, 2001, Hossain and Weiss, 2004, Schießl and Rucker, 2005]. This scatter can be explained by inherent material variability [Radlinska et al., 2005].

A single input in the model results in a deterministic solution which means that the time of cracking is determined by a discrete point of time. This may be misleading, however, as variability exists in both: the residual stress and the tensile strength development. The influence of variability on the predicted time of cracking is conceptually illustrated in the Figure 7-3:

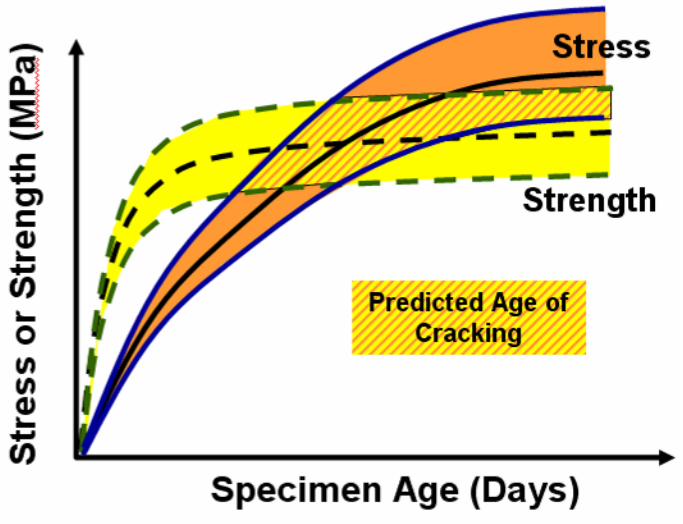

Fig. 7-3 A conceptual illustration of the role of variability on the predicted age of cracking [Weiss, 1999]

The variability can come from many sources including variations in the material properties (i.e., elastic modulus (E), creep/stress relaxation (ϕ), shrinkage (ε_{Sh}), and tensile strength or fracture resistance (f'_t)), variations in the environmental conditions (temperature or relative humidity), or variations in the degree to which the structure is restrained. While each of these variables can be thought to have some inherent variability, it is difficult to immediately determine which property may be the most significant. As a result, a probabilistic approach may have benefits in that it can quantify the extent of variability that may exist in cracking predictions. The following section describes the formulation of the problem together with simulations results allowing the assessment of how variability influences the predicted age of cracking.

7.4. Estimating Time-Dependant Properties of Concrete

Time-dependant properties of concrete can be described using equations developed by McIntosh [McIntosh, 1956], where time-dependent modulus of elasticity is as described by equation 7-4:

$$E_c(t) = E_\infty \frac{C_1(t - t_s)}{1 + C_1(t - t_s)}$$ Eq. 7-4

where E_∞ is the theoretical maximum elastic modulus that would develop at a very late age, C_1 is a material constant that describes the rate of elastic modulus development, t is the age of the specimen, and t_s is the time of initial set. Similarly, the formulation for the time-dependent tensile strength is given by equation 7-5:

$$f_{(t)} = f_{ten-\infty} \frac{C_2(t - t_s)}{1 + C_2(t - t_s)}$$ Eq. 7-5

where $f_{ten-\infty}$ is the theoretical maximum tensile strength that would develop at a very late age and C_2 is a material constant that describes the rate of tensile strength development. It should be noted that this formulation should remain somewhat flexible and as a result the constant is intentionally selected to be independent of the constant used in the equation for elastic modulus.

This work assumes concrete bridge decks undergoes drying shrinkage process and as such, an equation developed by Bazant [1989] can be applied, where the magnitude of drying shrinkage is related to the difference between internal and ambient humidity conditions:

$$\varepsilon_{Shr-Dry}(t) = \varepsilon_{SH-\infty}\left(RH_{INT}^3 - RH_{AMB}^3\right)$$ Eq. 7-6

where $\varepsilon_{Shr\text{-}Dry}$ is a parameter that describes materials drying shrinkage, $\varepsilon_{Shr\text{-}Dry}$ denotes ultimate shrinkage, RH_{INT} and RH_{AMB} are parameters that describe the internal relative humidity and relative humidity of the environment, respectively. The internal relative humidity will be taken as 100 % (RH_{INT} = 1), however it should be noted that salts may reduce internal RH [Sant,]. The ambient relative

humidity will be given value of 50% (RH_{INT} = 0.5) for many of the cases described here. It can be written that:

$$\varepsilon_{Shr-RH_x}\left(1-RH_x^3\right)=\varepsilon_{SH-RH_{50}}\left(1-0.5^3\right) \quad \text{Eq. 7-7}$$

where $\varepsilon_{Shr\text{-}RHx}$ denotes shrinkage at any given relative humidity and RH_x denotes corresponding relative humidity conditions. This equation can be further written as follows:

$$\varepsilon_{Shr-RH_x}=\frac{\varepsilon_{SH-RH_{50}}\left(1-0.5^3\right)}{\left(1-RH_{RH_x}^3\right)} \quad \text{Eq. 7-8}$$

In order to describe moisture loss and shrinkage as a function of time, an additional term needs to be added to Equation 7-6 and finally equation describing shrinkage takes form:

$$\varepsilon_{Shr-Dry}(t)=\varepsilon_{SH-\infty}\left(RH_{INT}^3-RH_{AMB}^3\right)\tanh\left(\sqrt{\frac{t-t_{dry}}{C_4}}\right) \quad \text{Eq. 7-9}$$

where C_4 is constant that accounts for the time-dependent nature of the shrinkage and t_{dry} denotes the time when drying was initiated [Bazant, 1989].

7.5. Shrinkage-Based Design Approach

In order to relate the shrinkage that concrete experiences at a given relative humidity a model to assess the potential for cracking has been used [Radlinska et al., 2005]. A plot relating the shrinkage and relative humidity was developed, as presented in the Figure 7-4, showing maximum allowable shrinkage before cracking potential $\theta_{CR}(t)$, described with equation 7-3 and defined as the ratio of residual stress ($\sigma(t)$) and tensile strength ($f'_t(t)$), reaches the value of one.

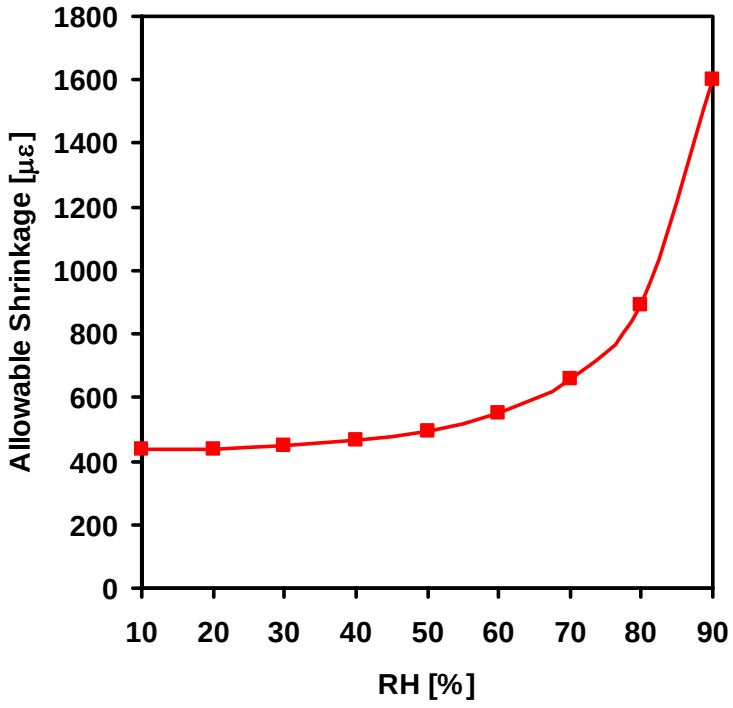

Fig. 7-4 The amount of shrinkage that can develop at a given relative humidity to reach maximum allowable stresses (lower than tensile strength)

The model previously introduced was combined with the material property development equations described in the section 7.4 and used to simulate the restrained shrinkage response of concrete under various conditions. The time-steps used in the model were 0.1 day increments for the first 8 days, 0.2 day increments to 14 days, 0.5 day increments to 28 days, 1 day increment to 56 days, 2 day increments to 90 days, and finally 4 day increments up to 350 days. Table 7-1 provides a listing of the basic material inputs that were used in the simulations.

Table 7-1 Baseline model inputs used for simulations

f'_c	E_{28}	f_{ten}	RH_{AMB}	RH_{INT}	t_{set}	t_{dry}

[MPa]	[GPa]	[MPa]	[%]	[%]	[day]	[day]
40	29.9	5	50	100	0.25	1

Three different types of concrete were analyzed: normal strength concrete with compressive strength equal to 40 MPa and two types of concrete of the same ultimate strength, but the first one had a slow strength gain and the second had a more rapid strength gain with a higher early strength. Different rates of strength gain were modeled changing constants C_1 and C_4 in the equations 7-4 and 7-5 (Table 7-2). The strength-gain curves have been presented in the Figure 7-5.

Table 7-2 Modeling constants and obtained ultimate shrinkage value

	C_1	C_2	C_3	C_4	ε_{shr}
'Base' (normal concrete)	2	0.3	15	30	625
'Fast' (fast strength gaining concrete)	22	0.3	15	10	600
'Slow' (slow strength gaining concrete)	0.5	0.3	15	200	1000

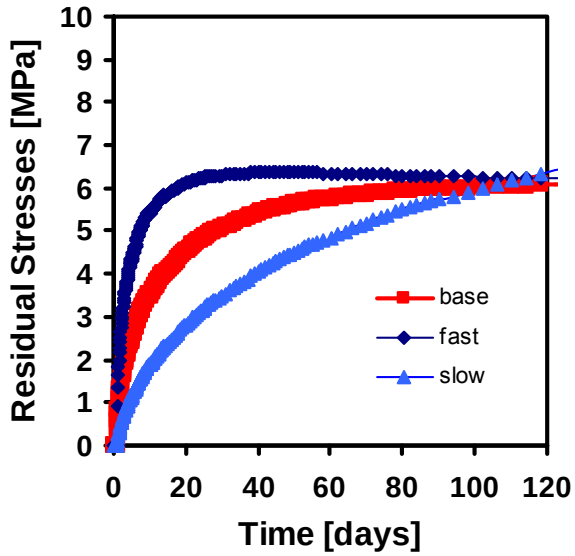

Fig. 7-5 Stress development for three different concrete models ('base' – normal concrete, 'fast' – fast strength gain concrete, 'slow' – slow strength gain concrete)

7.6. Load and Resistance Factor Design (LRFD)

It has been previously shown that a LRFD (Load and Resistance Factor Design) approach can be used to predict the probability of cracking in restrained concrete elements [Radlinska and Weiss, 2006a, Radlinska and Weiss, 2006b]. The LRFD method allows the probability of events that have exceeded a material's resistance to be determined using a simplified approach. This enables the probability of cracking to be related to both the material properties and expected construction variability.

The model assumed that tensile strength of concrete (f'_t) describes the materials resistance (R) to cracking and the residual stresses (σ) that develop in concrete can be considered to act as the load (Q). Both the material resistance (R) and

the load (Q) can be treated as random variables described with probability distribution function, as shown in the Figure 7-6:

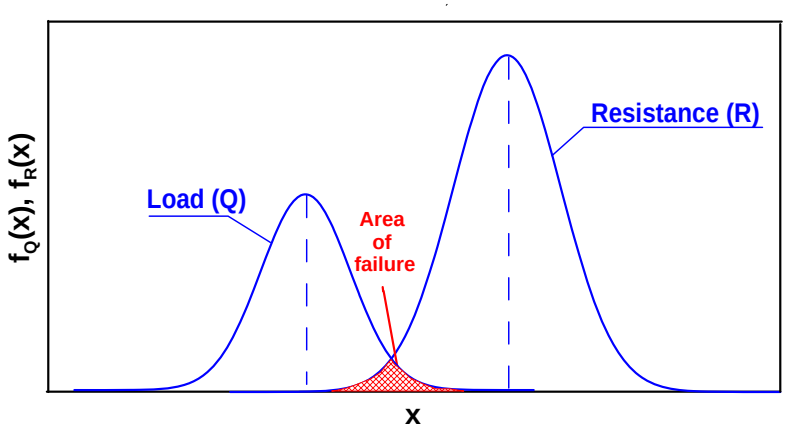

Fig. 7-6 Load (Q) and resistance (R) as the normally distributed variables

The area of failure (i.e., the area when the load (Q) exceeds the resistance (R)) may be approximated as the amount of overlap of two probability density functions: $f_Q(x)$ and $f_R(x)$ (it should be noted however it is not exactly equivalent to the overlap area [Melchers, 1987]). The area of overlap could be calculated using integration, but it is more convenient to deal with a single curve that consists of the logarithm of R divided by Q (or the inverse of the cracking potential: $1/\Phi$), as shown in Figure 7-7. In this case, the area of failure (i.e., the area where cracking can occur) is the region under the curve on the negative side of x-axis, marked with the cross-hatched region. Symbolically, the probability of cracking can be expressed as either the probability of resistance being lower or equal to load, as the difference between resistance and load being less than or equal to zero, or as the probability of the resistance to load ratio being less than or equal to one:

$$p_f = P(R \leq Q) = P(R - Q \leq 0) = P(R/Q \leq 1) \qquad \text{Eq. 7-10}$$

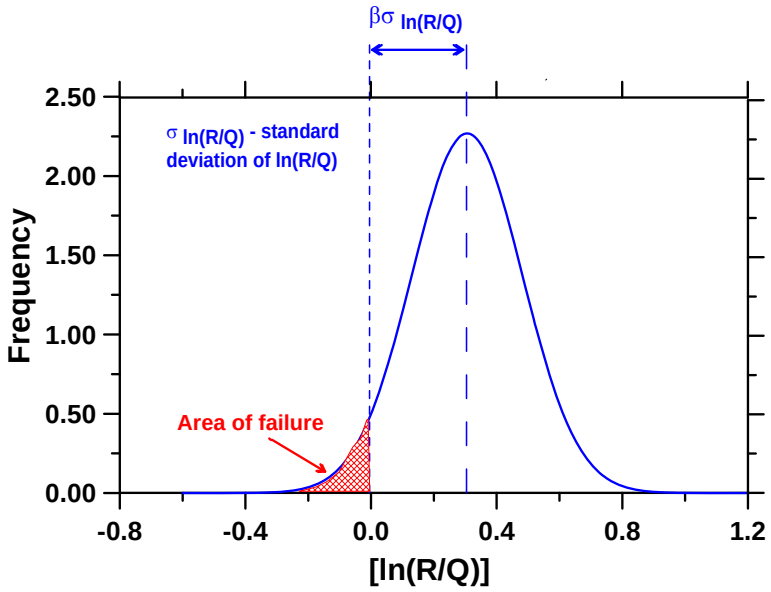

Fig. 7-7 The reliability index β

The LRFD approach enables the total variability of the system to be estimated through the calculation of the reliability index β (see Figure 7-7):

$$\beta = \frac{\mu_{\ln(R/Q)}}{SD_{\ln(R/Q)}} \qquad \text{Eq. 7-11}$$

where $\mu_{ln(R/Q)}$ is the mean value of the natural logarithm of R divided by Q and $SD_{ln(R/Q)}$ corresponds to the standard deviation of the natural logarithm of the R divided by Q.

Rather than describing the variability in each material property, a simplified approach can be used to approximate the total coefficient of variation (COV) using equation 7-12 [Salmon and Johnson, 1996]:

$$COV = \sqrt{COV_{\varepsilon}^2 + COV_E^2 + COV_{f'_t}^2} \qquad \text{Eq. 7-12}$$

where the single coefficients of variation under the square root are those of the shrinkage (ε), elastic modulus (E), and splitting tensile strength (f'_t). It can be assumed that the $SD_{ln(R/Q)}$ is equal to the total coefficient of variation [Salmon and Johnson, 1996]. In this work, all three parameters had a coefficient of variation equal to 10%, resulting in a total coefficient of variation that is equal to 0.1732.

Further, the probability of failure can be written as:

$$p_f = p(\ln(R/Q) < 0) = p\left(\frac{\ln(R/Q) - \mu_{\ln(R/Q)}}{SD_{\ln(R/Q)}} < \frac{-\mu_{\ln(R/Q)}}{SD_{\ln(R/Q)}}\right) = \quad \text{Eq. 7-13}$$

$$= p(Z < -\beta) = \Phi(-\beta)$$

where Z is the standard normal variable and Φ denotes the cumulative density function, i.e., probability that a variable has a value less than or equal to ln(R/Q) [Melchers, 1987]. The use of this approach to calculate the reliability index allows a rapid estimation of the cracking probability using commonly available standard normal distribution tables. For example, for the reliability index equal to -1.22, the probability of cracking would be:

$$p_f = \Phi(-\beta) = \Phi(1.22) = 0.8887 \quad \text{Eq. 7-14}$$

Deterministic analysis results in the time (day) when cracking can be expected to occur, however it does not provide information about the probability of such an event's occurrence. On the contrary, the Monte Carlo method gives precise and detailed information about the cracking risk at each age, but requires time-consuming computations. In this work, LRFD approach was used and allowed to relate probability of cracking with the shrinkage experienced in the system, and the results of the investigation are shown in the Figure 7-8. As can be noticed, slower strength gaining concrete has the lowest probability of cracking at the given magnitude of shrinkage. This is consistent with the idea that the slower

load application would provide a longer time for stress to relax and be relieved from the system.

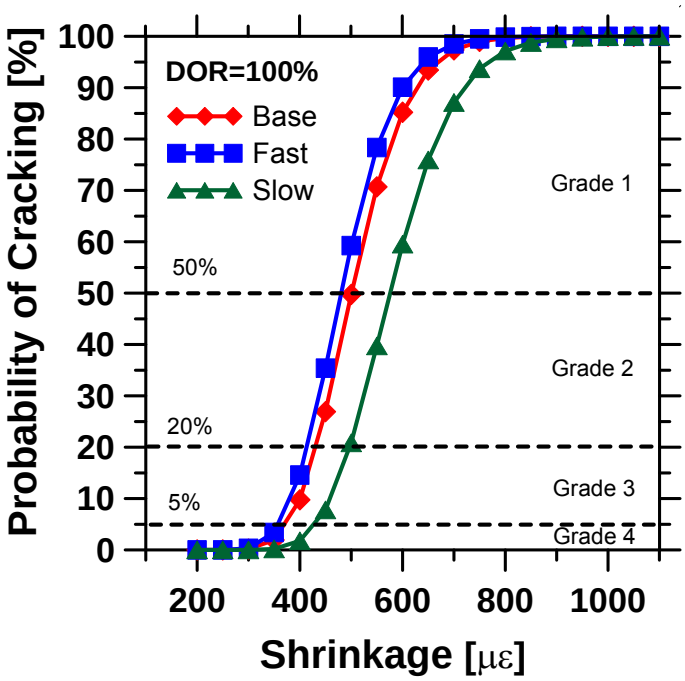

Fig. 7-8 Probability of cracking for different shrinkage values of three different concrete mixtures

7.7. Results of Shrinkage Model

The final goal of this model was to establish a relationship between shrinkage results and probability of cracking. The LRFD approach was used to relate the probability of shrinkage cracking to the long term shrinkage values. Based on the assessment of cracking probability (Figure 7-8) the following grades of concrete have been suggested:

- Grade 4 – for material experiencing less than 5% probability of cracking
- Grade 3 – for material experiencing less than 20% probability of cracking
- Grade 2 – for material experiencing less than 50% probability of cracking
- Grade 1 – for material experiencing more than 50% probability of cracking

It should be noted that this model assumes perfect restraint, however in reality lower degree of restraint is usually observed [Shah, 1998]. As such, additional simulations were performed for 80% and 60% degree of restraint, and results of those simulations have been presented in Figures 7-9 and 7-10, respectively. It can be noticed that the lower the degree of restraint corresponds to the lower probability of cracking.

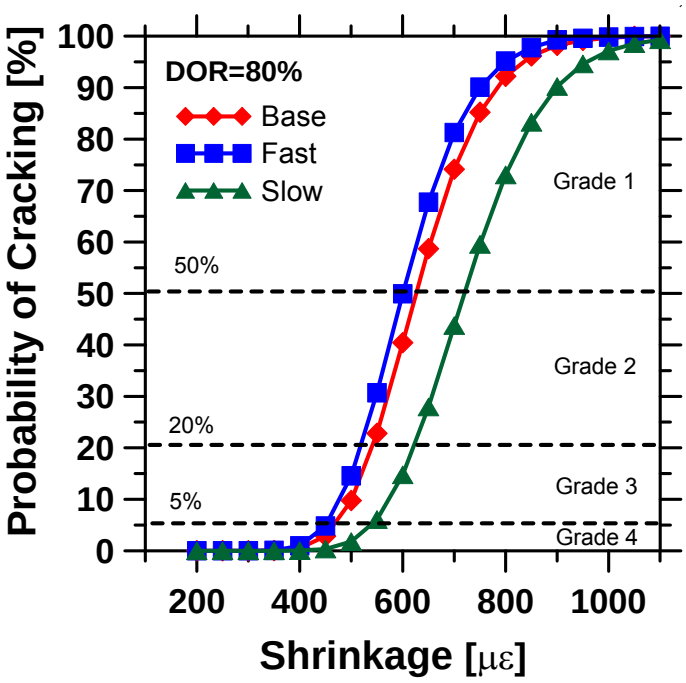

Fig. 7-9 Probability of cracking for different shrinkage values of three different concrete mixtures (DOR=80%)

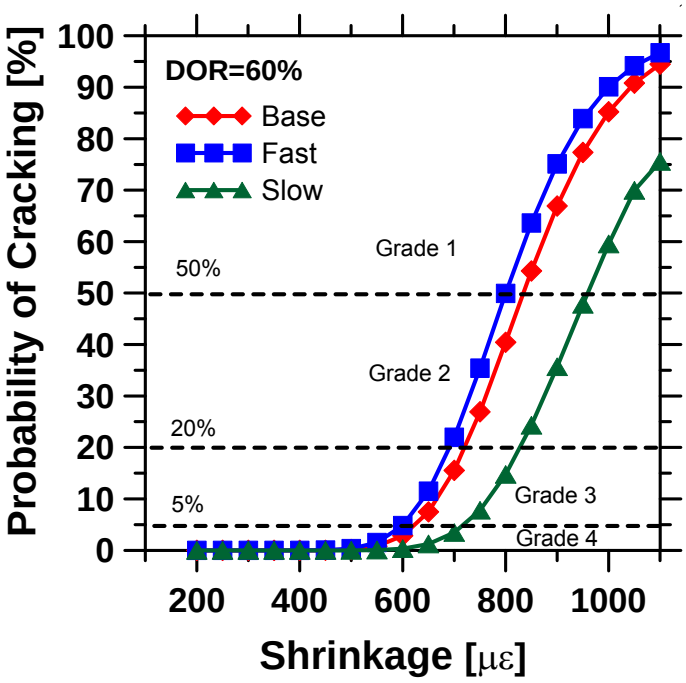

Fig. 7-10 Probability of cracking for different shrinkage values of three different concrete mixtures (DOR=60%)

7.8. Summary and Conclusions

A model has been presented that relates shrinkage in a restrained concrete element with the probability of cracking. The relationship was developed in two major parts. First, the amount of shrinkage in a concrete element was used to calculate the ratio of time dependent stress and strength, i.e., cracking potential. Second, reliability analysis was conducted and cracking potential was related to the probability of cracking. Three concrete types with different strength-gain characteristic were analyzed and separate curve relating the amount of shrinkage with probability of cracking was generated for each case.

Based on the work performed in this study it was observed that:

- A simple model can be used predict the probability of cracking in restrained concrete bridge desk. This model utilizes Load and Resistance

Factor Design Approach and allows on fast and accurate estimation of probability of cracking based on the shrinkage in a concrete member.

- A simplified modeling approach allowed on establishing performance grades for performance of bridge desks in the state of Indiana. Grade 4 corresponds to bridge deck for which probability of cracking is less than 5%, Grade 3 corresponds to bridge deck for which probability of cracking is less than 20%, Grade 2 corresponds to bridge deck for which probability of cracking is less than 50%, and Grade 1 corresponds to bridge deck for which probability of cracking is more than 50%.
- Further work is needed to modify the model so that degree of restraint could be implemented at the stage of the model definition. Additionally, only one scenario of the variability in the material properties was analyzed (10% coefficient of variation for elastic modulus, shrinkage coefficient and splitting tensile strength, respectively). It would be very beneficial to obtain additional information about the time dependant material properties changes, as the variability within one or more parameters changes.

CHAPTER 8. DISCUSSION

8.1. Introduction

Goodspeed et al. [1996] used four material parameters that describe durability and four material parameters that describe mechanical properties to specify the performance of High Performance Concrete (HPC). This report describes how material properties alone can not be used to entirely define the performance of concrete. The material parameters were reviewed in this work as they apply to bridge decks in Indiana. Three key distresses were investigated including chloride ingress, freezing and thawing, and shrinkage cracking. Using simulation procedures, performance grades were assigned as shown in Table 8-1. It can be seen that it may be possible to relate material properties, exposure condition, and anticipated performance of concrete. More research however is needed to further define these relationships, evaluate field performance, and implement new standards.

Table 8-1 An example of summary of grades for performance characteristic for plain concrete (Research is needed to confirm this estimates)

Corrosion Model				
	Grade 1	Grade 2	Grade 3	Grade 4
Service Life	25 Yrs	50 Yrs	75 Yrs	100 Yrs
Exposure Condition [kg/m^3]	Maximum Charge Passed, Q [coulombs]			
5	5000	3400	1500	900
10	5000	2300	1100	600
15	5000	1700	900	500
Freeze-Thaw Model				
	Grade 1	Grade 2	Grade 3	Grade 4
Service Life	25 Yrs	50 Yrs	75 Yrs	100 Yrs
Entrained Air [%]	Maximum Secondary Sorptivity [$\times 10^{-3}$ mm/s$^{0.5}$]			
0	0.30	0.20	0.15	0.10
5	0.50	0.30	0.25	0.20
6.5	0.55	0.30	0.25	0.23
8	0.60	0.35	0.30	0.25
10	0.70	0.40	0.35	0.30
Shrinkage Cracking Model				
Probability of cracking, x	Grade 1	Grade 2	Grade 3	Grade 4
	x > 50%	20% < x ≤ 50%	5% < x ≤ 20%	x ≤ 5%
Degree of Restraint [%]	Maximum Shrinkage [$\mu\varepsilon$]			
100	> 500	500	430	375
80	> 625	625	540	470
60	> 825	825	740	625

8.2. Conclusions

Based on the work performed in this study, the following conclusions can be made:

- The temperature, annual number of freeze thaw cycles, rainfall, and relative humidity have been classified using the data from Engineering Weather Data (EWD) [(AFCCC), 1967-1996]. Data for wetting events was obtained from the CONCTEMP program [Bentz, 2000] simulations. The variation in time to corrosion for bridge decks at various locations was assessed using the results of Life365^{TM} simulations. Contour maps were

prepared using the information described above for four major Indiana cities (Indianapolis, Fort Wayne, South Bend, Evansville) and 21 other major cities in surrounding states. A very small variation across the state of Indiana was observed for the case of temperature, relative humidity, annual freeze thaw cycles, and rainfall. Based on this variation alone, different exposure zones are not recommended. However, a variation was observed in the case of the time to corrosion and wetting events, and based on the observed variation, it is possible to divide the state of Indiana into two exposure zones. The first zone may include northern four districts (Laporte, Fort Wayne, Crawfordsville and Greenfield district), and the second zone may include remaining two districts (Vincennes and Seymour district).

- A service life prediction model for the chloride induced corrosion deterioration has been described in this work. The diffusion coefficient for concrete was related to result of the Rapid Chloride Permeability test (RCPT) with the application of Nernst-Einstein equation. The diffusion coefficient was further related to the performance of concrete bridge decks exposed to deicing salt. The initial charge was used in the application of Nernst-Einstein equation. A correction factor was used to convert the total charge passed, as determined in RCPT, to the initial charge. The surface concentration of chlorides, which accumulates with the use of deicing salt, was observed to have a significant effect on the chloride ingress, and ultimately on the performance of concrete. Therefore, surface concentration was used as a variable in the relation used to predict service life of bridge decks in this model. This model accounts for two geometries of bridge decks. First, a bridge deck with plain concrete. Second, a bridge deck where latex modified concrete is used as an overlay on plain concrete. In the case of a plain concrete bridge deck, four cases with different combinations of cement, silica fume and fly ash has been considered in this model. The results of this model were

observed to be in reasonable agreement with the results observed in the literature. It should however be noted that substantially more work is needed before this can be developed into a specification.

- A service life prediction model has been described in this work for concrete exposed to freezing and thawing. The service life was predicted in two parts. First, the time to damage initiation or time to reach critical saturation ($Life_{init}$) was predicted. Second, the time to proceed to a defined level of damage from damage initiation ($Life_{sec}$) was predicted. The model uses critical saturation, initial saturation, sorptivity, porosity, air content and time of exposure to water to predict service life in freezing and thawing. Based on the literature related to these properties, approximate values were chosen. It was observed that two exposure parameters affect the service life in freezing and thawing. First, the cumulative duration of wetting events greater than nick point time ($t_{w\text{-}nickpt}$) which affects the $Life_{init}$ and second, the number of annual freeze thaw cycles which affects the $Life_{sec}$. The predictions of $Life_{init}$ obtained with this model were compared to the CONCLIFE predictions, and difference of maximum 18% was observed. The modeling approach was used to predict the relative dynamic modulus for an ASTM C 666 test results [Sellevold et al., 1997]. It was observed that the modeling approach could predict the relative dynamic modulus with some agreement to the measured values. It should be noted, however, that a single set of result was used for the comparison and comparison with more result is recommended for a better comparison. In addition, substantially more work is needed to better understand freeze thaw from a fundamental aspect and to determine sorption and saturation properties.
- A service life prediction model relating shrinkage in concrete with probability of cracking has been described in this work. Shrinkage-based model was used to assess concrete bridge decks' susceptibility to cracking in four steps. Initially, information about the shrinkage that bridge

deck undergoes was needed (can be obtained using standard ASTM methods). Next, shrinkage results were used to calculate cracking potential, i.e., the ratio of material's stress to material's strength. This information was further used to assess probability of cracking (using Load and Resistance Factor Design approach). In the last step, probability of cracking was related back to the magnitude of shrinkage. It was observed that degree of restraint significantly affects probability of cracking and lower degree of restrain relates to the lower probability of cracking. Further research is needed to quantify the rate of material properties development and moisture gradients.

LIST OF REFERENCES

(AFCCC), A. F. C. C. C. (1967-1996). "Engineering Weather Data." National Climatic Data Center.

(NREL), N. R. E. L. (1961-1990). "Typical meteorological year (TMY) data sets."

ACI committee 116. (2005). "Cement and concrete terminology."

ACI committee 201. (1992). "Guide to durable concrete." *ACI 201.2R-92*, Detroit.

Aldea, C. M., Shane, J., Mason, T., and Shah, S. P. "Assessment of microstructural changes during Rapid Chloride Permeability Test using impedence spectroscopy measurements." *High Performance concrete*, 333-350.

Alonso, C., Andrade, C., Castellote, M., and Castro, P. (2000). "Chloride threshold values to depassivate reinforcing bars embedded in a standardized OPC mortar." *Cement and Concrete Research*, 30(7), 1047-1055.

Andrade, C. (1993). "Calculation of chloride diffusion coefficients in concrete from ionic migration measurements." *Cement and Concrete Research*, 23(3), 724-742.

ASTM C 672/C 672M. (2003). "Standard test method for scaling resistance of concrete surfaces exposed to deicing chemicals." C. C. 672M, ed.

ASTM C 1202. (1997). "Standard test method for electrical indication of concrete's ability to resist chloride ion penetration" AASHTO, C. 1202, ed., 2000, T 277.

ASTM C 1585. (2004). "Standard test method for measurement of rate of absorption of water by hydraulic cement concrete." C. 1585, ed.

Atis, C. D. (2002). "High volume fly ash abrasion resistant concrete." *Journal of Materials in Civil Engineering*, 14(3), 274-277.

Bazant, Z. P., “Mathematical Modeling of Creep and Shrinkage of Concrete,” John Wiley & Sons, Inc, 1989.

Ben-Dor, L., Heitner-Wirguin, C., and Diab, H. (1985). "Effect of ioninc polymers on the hydration of C_3S." *Cement and Concrete Research*, 15(4), 681-686.

Bentz, D. P. (2000). "A computer model to predict the surface temperature and time-of-wetness of concrete pavements and bridge decks." U. S. Department of Commerce.

Bentz, D. P., and Ehlen, M. A. (2002). "CONCLIFE, User's manual."

Bentz, D. P., Ehlen, M.A., Ferraris, C. F., Winpigler, J.A. (2002). "Service life prediction based on sorptivity for highway concrete exposed to sulfate attach and freeze-thaw conditions." Federal Highway Administration, Gaithersburg, MD.

van Breugel, K., Lokhorst, S.J., ‘Stress-based crack criterion as a basis for prevention of through-cracks in concrete structures at early ages’ RILEM Proceedings 23, International RILEM Conference on Early Age Cracking in Cementitious Systems - EAC'01, Edited by K. Kovler and A. Bentur (2001).

Browne, P. F., and Cady, P.D. . (1975). "Deicer scaling mechnisms in concrete." *American Concrete Institute, Detroit*, Publication SP-47, 101-119.

Cady, P. D., and Weyers, R. E. (1991). "Predicting service life of concrete bridge decks subjected to reinforcedment corrosion." *Corrosion Forms and Control for Infrastructure*(November), 328 - 338.

Claisse, P. A., Elsayad, H. I., and Shaaban, I. G. (1997). "Absorption and sorptivity of concrete cover." *Journal of Materials in Civil Engineering*, 9(3), 105-110.

Cook, R. A., and Hover, K. C. (1999). "Mercury porosimetry of hardened cement pastes." *Cement and Concrete Research*, 29(6), 933-943.

Crank, J. (1956). *The mathematics of diffusion*, Oxford at the Clarendon Press.

Envirochex. (2001). "Psychrometric Excel Functions, Linric Company." Linric Company.

Fagerlund, G. "On service life of concrete exposed to frost action." *International workshop in the resistance of concrete to scaling due to freezing in the presence of de-icing salts*, Sainte-Foy, Quebec, Canada, 273.

Fagerlund, G. "Modelling service life of concrete exposed to frost." *International conference on ion and mass transport in cement-based materials*, University of Toronto.

Fagerlund, G. (2001). "CONTECVET, A validated users manual for assessing the residual service life of concrete structures."

Fagerlund, G. (2004). "A service life model for international frost damage in concrete." Lund, Sweden.

Feldman, R. F., Chan, G. W., Brousseau, R. J., and Tumidajski, P. J. (1994). "Investigation of the rapid chloride permeability test." *ACI Materials Journal (American Concrete Institute)*, 91(3), 246-255.

FHWA. (2000). "Our nation's highways."

Foy, C., Pigeon, M., and Banthia, N. (1988). "Freeze-thaw durability and deicer salt scaling resistance of a 0.25 water-cement ratio concrete." *Cement and Concrete Research*, 18(4), 604-614.

Ghafoori, N., and Mathis, R. P. (1997). "Scaling resistance of concrete paving block surface exposed to deicing chemicals." *ACI Materials Journal*, 94(1), 32-38.

Gjorv, O. E., Baerland, T., and Ronning, H. R. (1990). "Abrasion resistance of high-strength concrete pavement." *Concrete International*, 12(1), 45-48.

Goodspeed, C. H., Vanikar, S., and Cook, R. (1996). "High-performance concrete defined for highway structures." Concrete International 62-67.

Graveen, C. (2000). "Nondestructive test methods to assess pavement quality for use in performance-related specification," Purdue University, West Lafayette.

Hall, C. (1989). "Water sorptivity of mortars and concretes: a review." *Magazine of Concrete Research*, 41(147), 51-61.

Hansen, M. R., Leming, M. L., Zia, P., and Ahmed, S. "Chloride permeability and AC impedence of high performance concrete." *High Perfromance Concrete in Sever Environment*, 121-145.

Hartt, W. H., Powers, R.G., Leroux, V. and Lysogorski, D.K. (2004). "A critical literature review of high-performance corrosion reinforcements in concrete

bridge Applications." Office of Infrastructure Research and Development Federal Highway Administration.

Hooton, R. D., Geiker, M. R., and Bentz, E. C. (2002). "Effects of curing on chloride ingress and implications on service life." *ACI Materials Journal*, 99(2), 201-206.

Hossain A., Weiss J., 'Assessing residual stress development and stress relaxation in restrained concrete ring specimens', Cement and Concrete Composites 26 (2004) 531-540.

INDOT, I. D. O. T. (2006). "Standard Specifications."

Jaiswal, S. S., Picka, J. D., Igusa, T., Karr, A. F., Shah, S. P., Ankenman, B. E., and Styer, P. (1998). "Experimental studies of the chloride permeability of concrete." National Institute of Statistical Sciences.

Julio-Betancourt, G. A., and Hooton, R. D. (2004). "Study of the Joule effect on rapid chloride permeability values and evaluation of related electrical properties of concretes." *Cement and Concrete Research*, 34(6), 1007-1015.

Kelham, S. (1988). "Water adsorption test for concrete." *Magazine of Concrete Research*, 40(143), 106-110.

Kirkpatrick, T. J., Weyers, R. E., Anderson-Cook, C. M., and Sprinkel, M. M. (2002a). "Probabilistic model for the chloride-induced corrosion service life of bridge decks." *Cement and Concrete Research*, 32(12), 1943-1960.

Kirkpatrick, T. J., Weyers, R. E., Sprinkel, M. M., and Anderson-Cook, C. M. (2002b). "Impact of specification changes on chloride-induced corrosion service life of bridge decks." *Cement and Concrete Research*, 32(8), 1189-1197.

Krishnan, A. (2002). "Durability of concrete containing fly ash or slag exposed to low temperatures at early ages," Purdue University, West Lafayette.

Kuhlmann, L. A. (1988). "Using styrene-butadiene latex in concrete overlays." *0361-1981*.

Kuhlmann, L. A., Foor, N. C. (1984). "Chloride permeability verses air content of Latex modified concrete." *Cement, Concrete, and Aggregates*, 6(1), 11-16.

Kurtz, M. A., and Constantiner, D. (2004). "Resistance to freezing and thawing cycles and scaling resistance of very high early strength concrete." *Cement, Concrete and Aggregates*, 26(2), 160-164.

Larbi, J. A., and Bijen, J. M. J. M. (1990). "Interaction of polymers with portland cement during hydration. A study of the chemistry of the pore solution of polymer-modified cement systems." *Cement and Concrete Research*, 20(1), 139-147.

Lewis, W. J., Lewis, G. (1990). "The influence of polymer Latex modifiers on the properties of concrete." *Composites*, 21(6), 487-494.

Liu, Z., and Beaudoin, J. J. (1999). "An assessment of the relative permeability of cement systems using AC impedance techniques." *Cement and Concrete Research*, 29(7), 1085-1090.

Lu, A. (2001). "Durability design of high performance concrete and its application in bridge decks," Purdue University, West Lafayette.

Lu, X. (1997). "Application of the Nernst-Einstein equation to concrete." *Cement and Concrete Research*, 27(2), 293-302.

McIntosh, J. D., “The Effects of Low-Temperature Curing on the Compressive Strength of Concrete,” Proceedings of the RILEM Symposium on Winter Concreting, 1956.

Melchers R.E., Structural reliability. Analysis and prediction, Baffins Lane, Chichester 1987.

Mindess, S., Young J.F., and Darwin, D. (2002). *Concrete*, Peaeson Education.

Naik, T. R., Singh, S. S., and Hossain, M. M. (1994). "Abrasion resistance of concrete as influenced by inclusion of fly ash." *Cement and Concrete Research*, 24(2), 303-312.

Napier, C. S., and Maruri, R. F. (2003). "High performance concrete survey results." FHWA.

Nokken, M., Hooton, R.D. (2002). "Dependence of rate of absorption on degree of saturation of concrete." *Cement Concrete and Aggregates*, 24(1).

Ohama, Y. D. (1995). *Handbook of polymer modified concrete and mortars-properties and process technology*.

Parameswaran, S. (2004) “Investigating the role of material properties and their variability in the selection of repair materials” MS Thesis, Purdue University, West Lafayette, USA.

Persson, B. (2003). "Internal frost resistance and salt frost scaling of self-compacting concrete." *Cement and Concrete Research*, 33(3), 373-379.

Powers, T. C. (1975). "Freezing effects in concrete." *American Concrete Institute, Detroit*, Publication SP-47, 1-11.

Powers, T. C., and Brownyard, T. L. (1948). "Studies of the physical properties of hardened portland cement paste."

Salmon G.C., and Johnson, J.E., Steel structures design and behavior, 3rd Edn, Harper and Row, New York 1996.

Radlinska A., Pease B., Weiss J., "A preliminary numerical investigation on the influence of material variability in the early-age cracking behavior of restrained concrete, Knud Højgaard Conference on Advanced Cement-Based Materials, Lyngby, Denmark, June 2005.

Radlinska A. and Weiss J. (2006) "Determining Early-Age Cracking Potential in Restrained Concrete Elements Using a Load and Resistance Factor Design (LRFD) Approach" Conference proceedings: Advances in Concrete through Science and Engineering, September 11-13, 2006, Quebec City, Canada.

Radlinska A. and Weiss J. (2006) "Quantifying Variability in Assessing the Risk of Early-Age Cracking in Restrained Concrete Elements" Eight International Symposium on Brittle Matrix Composites, 23-25 October, Warsaw, Poland.

Rajabipour, F., and Weiss, J. (2006). "Electrical conductivity of drying cement paste." *Materials and Structures/Materiaux et Constructions*, Submitted for Publication.

Shah, S. P., Weiss, W.J., and Yang, W., (1998) “Shrinkage Cracking-Can It Be Prevented?” Concrete International, Vol. 20, No. 4.

Schießl, P., Rucker P., (2005) ‘New results on early-age cracking risk of special concretes’ ACBM, Concrete Cracking Workshop, Evanston, IL.

Schindler, A.K., Ruiz J.M., Rasmussen R.O., Chang G.K., Wathne L.G. (2004) “Concrete pavement temperature prediction and case studies with the

FHWA HIPERPAVE models", Cement and Concrete Composites 26, 463-471.

Schlangen, HEJG, Koenders, EAB and van Breugel, K (2004) "Multi-scale modelling of crack formation in the concrete cover zone," Advances in cement and concrete, eds. Lange, D.A., Scrivener, K.L., and Marchand, J., Illinios at Urbana-Champaign: Engineering Conferences International, pp. 281-291.

Schmit, T. J. (2005). "A fundamental investigation on utilization error propagation, Monte Carlo simulation, and measurement interpretation techniques to design efficient in situ covercrete sensing system," Purdue University, West Lafayette.

Sellevold, E. J., Bakke, J. A., and Jacobsen, S. "High strength concrete without air entrainment: effect of rapid temperature cycling above and below." *International workshop on freeze thaw and de-icing resistance of concrete*, Lund, Sweden.

Snyder, K. A., Ferraris, C., Martys, N.S., Garboczi, E. J. . (2000). "Using impedance spectroscopy to assess the viability of the rapid chloride test for determining concrete conductivity." *Journal of Research of the National Institute of Standards and Technology*, 105, 497-509.

Sprinkel, M. M. (1999). "Very-early-strength latex-modified concrete overlay." *Transportation Research Record*(1668), 18-23.

Stanish, K., and Thomas, M. (2003). "The use of bulk diffusion tests to establish time-dependent concrete chloride diffusion coefficients." *Cement and Concrete Research*, 33(1), 55-62.

Stanish, K. D., Hooton, R. D., and Thomas, M. D. A. (1997). "Testing the chloride penetration resistance of concrete: A literature review." *FHWA Contract DTFH61-97-R-00022*.

Tasdemir, C. (2003). "Combined effects of mineral admixtures and curing conditions on the sorptivity coefficient of concrete." *Cement and Concrete Research*, 33(10), 1637-1642.

Thomas, M. D. A., Bentz, E. C. (2000). "Life-365 computer program for predicting the service life and life-cycle costs of reinforced concrete exposed to chlorides."

Tikalsky, P. J., Scanlon, A. "Defining the high performance concrete requirements for highway structures." *The Econimical Solution for Durable*

Bridges and Transportation Structures, PCI/FHWA/FIB International Symposium on High Performance Concrete, Orlando, Florida, U.S.A.

Tuutti, K. (1982). "Corrosion of steel in concrete." Stockholm.

Weiss, W. J., “Shrinkage Cracking in Restrained Concrete Slabs: Test Methods, Material Compositions, Shrinkage Reducing Admixtures and Theoretical Modeling,” MS Thesis, Northwestern University, Evanston, IL, 1997.

Weiss, W. J., “Prediction of Early-Age Shrinkage Cracking in Concrete Elements.” Ph.D. Dissertation, Northwestern University, Evanston, IL, 1999.

Weiss, W. J., Schiebl, A., Yang, W., , and Shah, S. P. "Shrinkage Cracking Potential, Permeability, and Strength for HPC: Influence of W/C, Silica Fume, Latex, and Shrinkage Reducing Admixtures." *International Symposium on High Performance and Reactive Powder Concrete*, Sherbrooke, Canada, 349-364.

Weyers, R. E., Prowell, B. D., Sprinkel, M. M., and Vorster, M. (1993). Strategic Highway Research Program.

Whiting, D., and Dziedzic, W. (1989). "Chloride permeabilities of rigid concrete bridge deck overlays." *Transportation Research Record*(1234), 24-29.

William, H. H., Rodney, G. P., Virginie, L., and Diane, K. L. (2004). "Critical literature review of high-performance corrosion reinforcements in concrete bridge applications."

Xi, Y., and Bazant, Z. P. (1999). "Modeling chloride penetration in saturated concrete." *Journal of Materials in Civil Engineering*, 11(1), 58-65.

Yang, Z. (2004). "Assessing cumulative damage in concrete and quatifying its influence on life cycle performance modeling," Purdue University, West Lafayette.

Zhang, M.-H., and Gjorv, O. E. (1991). "Effect of silica fume on pore structure and chloride diffusivity of low porosity cement pastes." *Cement and Concrete Research*, 21(6), 1006-1014.